Increasing energy storage in compliant tape-spring mechanisms

J.M. Verzendaal

Technische Universiteit Delft

TU Delft Delft University of Technology

Challenge the future

Increasing energy storage in compliant tape-spring mechanisms

by

J.M. Verzendaal

in partial fulfillment of the requirements for the degree of

Master of Science
in Mechanical Engineering

at the Delft University of Technology,
to be defended publicly on Friday May 29, 2020

Student number:	4299272	
Supervisor:	Ir. W. W. P. J. van de Sande,	TU Delft
	Ir. B. M. Wisse,	Laevo BV
Thesis committee:	Dr. ir. D. H. Plettenburg,	TU Delft, Chair
	Prof. dr. ir. J. L. Herder,	TU Delft

This thesis is confidential and cannot be made public until May 29, 2021.

An electronic version of this thesis is available at http://repository.tudelft.nl/.

The work in this thesis was performed within Laevo BV. Their cooperation is hereby gratefully acknowledged.

TU Delft Delft University of Technology

laevo exoskeletons

"Oh, the depth of the riches of the wisdom and knowledge of God!
(...)
For from him and through him and for him are all things.
To him be the glory forever! Amen."

— Romans 11:33,36, New International Version

Preface

I guess I am now at the end of the beginning! This thesis concludes my formal education at the TU Delft, at which I have followed with great interest and pleasure my study Mechanical Engineering. During my master BioMechanical Design, the interesting courses Precision Mechanism Design and Compliant Mechanisms made me choose a graduation project at the PME department, which is coming to an end in this thesis.

I want to express gratitude to my supervisor Werner for the insightful discussions, his valuable feedback and passion for tape-springs. I am also thankful for Dick and Just and their time and interest in my project, for Giuseppe who gave me valuable insights in modelling. Furthermore, I am thankful for Ali and the students of the ShellSkeletons research group for their enthusiasm and our fruitful discussions, as well as for showing interesting unrelated stuff.

Besides the university, Laevo was also a very welcoming and educational place. I want to thank my company supervisor Boudewijn for his time and feedback throughout my graduation. The comments from Mike, Bas, Jaromir, Suzanne and fellow students during our weekly student meetings were also very much appreciated, together with the necessary distraction with foosball and other games.

Last but not least, my gratitude goes out to my family and friends for supporting and stimulating me, and their patience to listen to me.

J.M. Verzendaal
Delft, May 2020

Contents

1

Introduction

Many mechanical systems require power to operate. Static balancing of the forces acting on the system can reduce the operating power. A common way of static balancing is to introduce springs to the system, that store and release energy of the system as strain energy. One essential feature for static balancing is obtaining the right force-deflection curve of the spring to compensate for undesired forces to get energy free motion, which in many systems largely comes down to balancing the static gravity load [1]. To achieve this, the force deflection behaviour of the balancing mechanism should have a specific behaviour counteracting the behaviour of gravity acting on the mechanism, resulting in a constant energy state in the system. Radaelli identified fifteen unique (nonlinear) force-displacement curves and corresponding energy graphs [2].

In figure 1.1, a pendulum and its force-deflection behaviour is shown as an example, as well as the required balancing force-deflection behaviour. The static gravity load is a function of θ, $-mgl\sin\theta$, so to balance this, a force generator with a force-deflection behaviour of $mgl\sin\theta$ is needed. This function has two requirements: it needs to (I) follow a sinus-curve ($\sin\theta$), and (II) have the right magnitude (mgl).

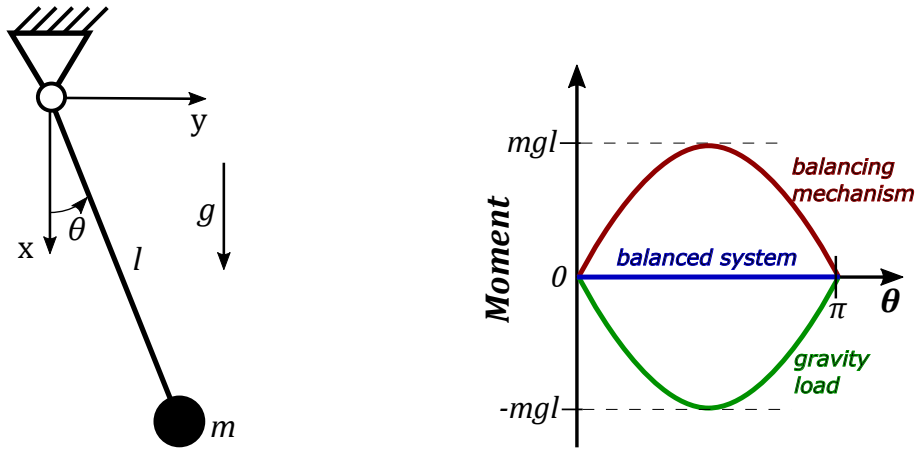

(a) Pendulum

(b) Force deflection pendulum

Figure 1.1: Balancing mechanism

A practical well-known example of a weight-balancing mechanism is the *Anglepoise* desk lamp [1]. In this design, balancing is achieved by traditional helical springs. More recently, compliant shell mechanisms have shown to be a valuable addition to balancing mechanisms and force generators [3–5]. Compliant shell mechanisms are defined by Radaelli as 'spatially curved thin-walled structures able to transfer or transform motion, force or energy through elastic deflection' [2]. A tape-spring, defined as a single-curved shell, is one of the basic possible shell geometries. Tape-springs can be

[1] https://www.anglepoise.com/

used for different applications, such as hinges in deployable space structures [6], as force generators in a folded tape-loop configuration [7] or in arm support systems [5]. When a tape-spring is folded, it exhibits first a high bending moment after which it buckles at a certain location along the length. At this buckling location, local flattening of the transverse curvature takes place, after which the bending moment reduces significantly. This buckling behaviour can be used as a design element in compliant shell mechanisms to achieve a specific force-deflection behaviour. Research on tailoring the shape of the force-deflection curve (requirement I) has been successfully done, however, the energy storage (requirement II) in a tape-spring is limiting for some applications [5]. In order to increase the possible applications of this shell geometry, the energy storage has to be enlarged.

The energy that can be stored in a tape-spring is limited by material yielding. In conventional springs, the energy storage can be increased by placing multiple springs in parallel. This method can be applied to tape-springs as well, however, since tape-springs have a complex three dimensional buckling behaviour the resulting behaviour might not be evident. The tape-springs can be placed on top of each other, resulting in a stack of tape-springs.

The practice of stacking tape-springs is mentioned briefly in literature, without being the main topic of research. Walker and Aglietti [8] tested multilayer tape-springs experimentally; Yang et al. [9] study a tape-spring hinge combining opposite and equal sense bended tape-spring in a single layer tape-spring and a double tape-spring configuration; Cook and Walker [10] mention a doubled tape-spring configuration; and lastly Lee et. al [11] study the attenuation of the deployment of a tape-spring hinge, by adding a shape memory alloy layer between two stacked tape-springs

These studies show the possibilities of stacking for energy increase. However, a clear concise overview of the potential of this approach is lacking. This brings us to the research objective of this thesis:

Increase the energy storage in tape-spring mechanisms by stacking multiple tape-springs

Regarding the boundary conditions, a planar approach is taken, such that a limited set is possible.

Thesis outline

This thesis consists of five chapters. Chapter 2 consists of a paper that presents a theoretical approach to stacking of tape-springs, and studies the potential of energy storage using analytical functions of tape-spring strain energy and deformation behaviour. The goal of this simplified approach is to understand the potential of energy increase through stacking, and subsequent material considerations, without taking practical considerations in account yet. This creates context for the next chapter, in which a more specific configuration is further worked out.

Chapter 3 consists of a paper with a simulation and experimental approach on energy increase in tape-springs, considering a specific configuration of boundary conditions, comparable to an arm support system. The goal of this paper is to verify the energy storage increase for a practical implementation of a stack of tape-springs. The strain energy distribution in the material and the resulting force-deflection behaviour is studied in a finite element shell model in MATLAB. The force-deflection behaviour of a stack of two tape-springs is experimentally validated, and compared to the force-deflection behaviour of the individual tape-springs.

Chapter 4 contains the general discussion of the findings for both the theoretical, as well as for the simulation and experimental approach to the stacking of tape-springs.

The main findings are highlighted in chapter 5. Some additional information on this thesis is added in the appendices.

2

Paper: Theoretical energy storage in stacks of translation-free folded tape-springs

Theoretical energy storage in stacks of translation-free folded tape-springs

Jan Maarten Verzendaal
Department of BioMechanical Engineering
Delft University of Technology
Delft, 2628 CD, The Netherlands

Abstract

Tape-springs are single, constant curved thin-walled structures, that exhibit interesting force-deflection behaviour when folded. This tape-spring behaviour can be tailored, enabling their use as specific force generators. However, energy storage in a single tape-spring is limited. This study uses a theoretical framework to investigate the potential for energy storage increase by stacking tape-springs, defined as the practice of placing tape-springs on top of each other in parallel. The energy storage in a unit volume is studied, and the energy storage for different materials is compared for single and stacked configurations.

The materials polycarobnate and spring steel are compared as example. It was found that in an ideal situation, with continuous increments in material thickness, an increase in energy storage of factor 5.59 is possible for polycarbonate and for spring steel an increase of factor 33.6. When considering discrete increments 88% and 79% of this ideal energy storage increase can be achieved, for polycarbonate and spring steel respectively.

A general material index is derived which can be used to determine the most suitable material to maximize energy storage. This index is derived for a single tape-spring and a stack of tape-springs. These two indices contradict each other, implying that materials such as polymers and elastomers are more suitable for maximizing energy in a single tape-spring, while spring steel is more suitable for maximizing the energy storage in a stack of tape-springs.

Nomenclature

α	subtended angle
ν	Poisson's ratio
σ_y	yield stress
θ	fold angle
c_m	material constant
D	flexural rigidity
E	Young's modulus
L	length tape-spring
R	radius tape-spring
$R^*, r(\beta)$	fold radius
s	length of the fold
t	thickness
U	potential strain energy

1 Introduction

Compliant mechanisms (CM) transfer of transform motion, force or energy through elastic deformation, having advantages over rigid-link mechanisms by increased precision, reliability, and reduced wear, weight and maintenance [1]. Planar CM are extensively investigated, while spatial CM are gaining interest. Compliant shell mechanisms are an example of such spatial CM, and are defined by Radaelli as "spatially curved thin-walled structures able to transfer or transform motion, force or energy through elastic deflection" [2].

A tape-spring can be considered as a basic shell element, having zero longitudinal and constant transverse curvature. The folding behaviour of a tape-spring is relatively well understood, very stiff before but compliant after buckling. A tape-spring can, for example, function as a hinge [3], deployable structure [4], or force generator in a folded tape-loop configuration [5].

A standard tape-spring has a constant fold radius and moment after buckling, and an analytic equation for the strain energy in the bent region is derived by Seffen [6]. A rod model to study the folding of tape-springs is proposed by Guinot et al. [7] and is used to study the buckling behavior of a tape-spring [8]. This knowledge can be used to tailor the force-deflection behaviour [5]. A drawback of tape-springs is the limited energy storage and subsequent force magnitude. For this shell geometry to be more useful as force generator (e.g. in human-assistive devices), the energy storage capacity needs to be increased.

Analogous with conventional helical springs that can be placed parallel to increase stiffness, tape-springs can be placed parallel as well. This study uses a theoretical framework to investigate the potential for energy storage increase by stacking, defined as the practice of placing tape-springs on top of each other. This is done by studying a unit volume, comparing the energy storage for different materials in single and stacked configurations.

Firstly, the theoretical equations of energy are introduced and the unit volume and its boundaries are described. Subsequently, the results of the comparison are shown. In the discussion of the acquired results, a generalization of material indices is made, which can be used to optimize for both stacked and single tape-spring configurations. This is followed by a description of assumptions and consequent limitations of the approach. Lastly, a brief summary and general conclusion are given.

2 Method

2.1 Equations of energy

The potential strain energy U for a fold in a tape spring without twist is given by

$$U = \frac{\alpha D}{2} \int_{-\theta/2}^{\theta/2} \left[\frac{R}{r(\beta)} + \frac{r(\beta)}{R} \pm 2v \right] d\beta \tag{1}$$

with subtended angle α, flexural rigidity $D = Et^3/12(1-v^2)$, fold angle θ, tape-spring radius R, and fold radius $r(\beta)$ [9, 10]. The plus-minus sign is for opposite or equal sense bending, respectively. This equation does not take the energy in the transition regions into account. According to De Jong [9], the fold radius $r(\beta)$ can be approximated with a constant radius R^* when the subtended angle α is larger than 100°, and with the assumption that $R^* = R$, for which a maximum difference in calculated energy is only 0.32%, the equation can be simplified to

$$U = D(1 \pm v)\alpha\theta \tag{2}$$

To prevent plastic deformation of the tape-spring, the radius and thickness should be limited, according to the following equation [9]

$$t < \frac{2\sigma_y(1+\nu)}{E\sqrt{3}} R \tag{3}$$

2.2 Case study - unit volume

To get an idea of the improvement in energy storage by stacking, a unit volume of unit width x is studied. In figure 1 a cross-section is shown of the unit volume. In this volume, two tape-springs are shown, both with a subtended angle α of 180°, sharing the same circle centre. The outer tape-spring is considered the first tape-spring of the stack. The next tape-springs are placed directly next to the previous tape-spring, so $R_{i+1} = R_i - t_i$. with R_i and t_i being the radius and thickness of tape-spring i, respectively. To simplify the approach, no contact or interplay between the individual layers is assumed, which is in line with the findings of Walker and Aglietti [11] and Lee et al. [12].

In this chapter, two different materials are studied and compared: spring steel (material number 1.4310), and polycarbonate. Both are considered to be good candidates for compliant shells, as steel does not suffer from creep and stress relaxation under normal conditions and polycarbonate has a high volumetric elastic energy storage density and is easily formed. The yield strength σ_y, Young's modulus E, and Poisson's ratio ν are:

Spring steel: $\sigma_y = 1400MPa$, $E = 210GPa$, $\nu = 0.3$
Polycarbonate $\sigma_y = 72.0MPa$, $E = 1.79GPa$, $\nu = 0.37$

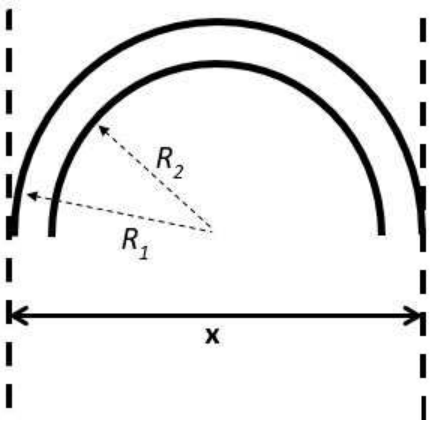

Fig. 1: Cross-section of unit volume with unit width x, containing two tape-springs with radii R_1 and R_2, and subtended angles $\alpha = 180°$

2.3 Length change

As the fold radius differs per layer, the tape-springs translate with respect to each other at the free sliding end of the tape-spring during bending, as shown in figure 2. The length of the fold s is defined as $s = \theta R^*$, resulting in a relative change in length $\Delta L = \Delta s = \theta(R_1^* - R_2^*)$. Using the assumption that the fold radius is equal to the tape-spring radius, and $R_{i+1} = R_i - t_i$, and substituting the maximum thickness as defined in equation 3, this gives

$$\begin{aligned} R_{i+1} = R_i - t_i &= R_i - \frac{2\sigma_y(1+\nu)}{E\sqrt{3}} R_i \\ &= R_i \left(1 - \frac{2\sigma_y(1+\nu)}{E\sqrt{3}} \right) = R_i(1-c_m), \end{aligned} \tag{4}$$

with material constant $c_m = \frac{2\sigma_y(1+\nu)}{E\sqrt{3}}$. Generally, it can be written as

$$R_n = R_i(1-c_m)^{n-i} \tag{5}$$

The relative length change between two adjacent layers i and $i+1$ is $\Delta L_{i,i+1} = \theta\left(R_i - R_i(1-c_m)\right) = \theta R_i\left(1-1(1-c_m)\right) = \theta R_i c_m$. Generalizing this, using $R_n = R_1(1-c_m)^{n-1}$, results in

$$\begin{aligned} \Delta L_{1,n} &= \theta\left(R_1 - R_1(1-c_m)^{n-1}\right) \\ &= \theta R_1\left(1 - 1(1-c_m)^{n-1}\right) \end{aligned} \tag{6}$$

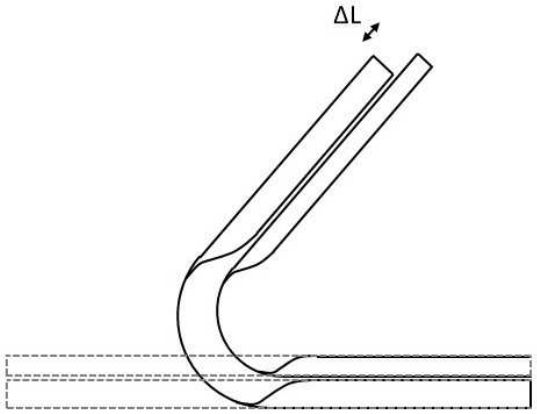

Fig. 2: Deformation of a stack of two tape-springs

Since the assumption that the fold radius is equal to the tape-spring radius does not hold with a maximum difference of 7% [9], there is an error in the calculation of the relative change in length. The relative change in length varies linearly with the change in radius. If the fold radius is 7% bigger than the tape-spring radius ($R^* = 1.07R$), this would result in 7% bigger length change ($\Delta L = \theta(R_1^* - R_2^*) = 1.07\theta(R_1 - R_2)$).

2.4 Energy storage

Equation 2 gives the potential strain energy in a tape-spring fold. Since the increase in stored energy is studied, the ratio of the stored energy in a stack of tape-springs and a single tape-spring is more interesting than the actual stored energy. Equation 2 describes only the strain energy in the fold, and not in the transition region. The energy in the transition region is a certain percentage of the total stored energy, which is dependent on subtended angle α [9]. By studying the ratio between a stack of tape-springs and a single tape-spring, both having a constant subtended angle $\alpha = 180°$ and the same fold angle θ, this problem is also eliminated. When stacking one material, the resulting ratio is

$$\begin{aligned} \frac{U_i}{U_j} &= \frac{D_i(1 \pm \nu_i)\alpha_i\theta_i}{D_j(1 \pm \nu_j)\alpha_j\theta_j} = \frac{D_i}{D_j} \\ &= \frac{E_i t_i^3}{12(1-\nu_i^2)} \frac{12(1-\nu_j^2)}{E_j t_j^3} = \left(\frac{t_i}{t_j}\right)^3 \end{aligned} \tag{7}$$

Using the maximum allowable thickness, as defined in equation 3, the thickness is proportional to the radius with the material constant c_m. Using this, and substituting equation 5 gives

$$\frac{U_i}{U_j} = \left(\frac{R_i}{R_j}\right)^3 = \left((1-c_m)^{i-j}\right)^3 \tag{8}$$

When calculating the maximum energy storage increase in a stack of tape-springs compared to a single tape-spring in the same volume, the sum is taken of the ratio defined in equation 8 with $i = 1, 2, ..., n$ and $j = 1$, for $n \to \infty$

$$\begin{aligned} \sum_{i=1}^{n\to\infty} \frac{U_i}{U_1} &= \sum_{i=1}^{n\to\infty} \left((1-c_m)^{i-1}\right)^3 \\ &= \frac{(1-c_m)^{3i} - 1}{(1-c_m)^3 - 1} \\ &= -\frac{1}{(1-c_m)^3 - 1} \quad \text{for } |1-c_m| < 1 \end{aligned} \tag{9}$$

This implies that materials with a small value for c_m can have a greater increase in energy storage when stacked relative to an unstacked configuration.

2.5 Ideal vs. discrete thicknesses

For equation 5, the thickness for each layer is maximized to the value before it starts yielding. This results in thicknesses that would not be readily available from stock. After studying the energy storage using these ideal thicknesses, the energy storage is also studied using sheet thicknesses which are available from stock. The discrete sheet thicknesses used are:

Spring steel: 0.05, 0.075, 0.10, 0.15, 0.20, 0.25, 0.30, 0.40, 0.50, 0.60, 0.70, 0.80, 0.90, 1.00, 1.10, 1.20, 1.30, 1.40, 1.50 [mm] [13];
Polycarbonate: 1, 2, 3, 4, 5, 6, 7, 8, 9, 10 [mm] [14, 15].

3 Results

In figure 3, the radius of each layer i of the stack, R_i, is shown, normalized with the radius of the outer tape-spring R_1. This plot follows the function $(1-c_m)^{i-1}$, as shown in equation 5. The radius of the polycarbonate tape-springs decrease faster, as the thickness of the layers are greater. This results in less possible layers per volume for polycarbonate.

In figure 4, both the energy storage in a single tape-spring and the total energy storage in a stack of tape-springs are shown, up to a stack of 25 tape-springs. The figure shows the energy storage for both spring steel and polycarbonate, for the optimal case with continuous thicknesses as well as for the realistic case with discrete steps in thicknesses. The initial radius R_1 is defined as $R_1 = 0.15716\ m$ such that the maximum thickness of polycarbonate according to equation 3 t_1 is exactly equal to $t_1 = 10mm$. This way the outer tape-spring maximizes its energy storage.

In figure 4, the following variables are used: U_i, U_{max}, and R_i. U_i indicates the strain energy in a single tape-spring with index i, which is numbered from the outside to the inside. The outer tape-spring of a stack, being the biggest and storing the most strain energy, is referred to as tape-spring 1 with strain energy U_1. U_{max} denotes the maximum strain energy that is stored in a single polycarbonate tape-spring. The total stored strain energy of a stack of tape-springs is achieved by summing all individual strain energies

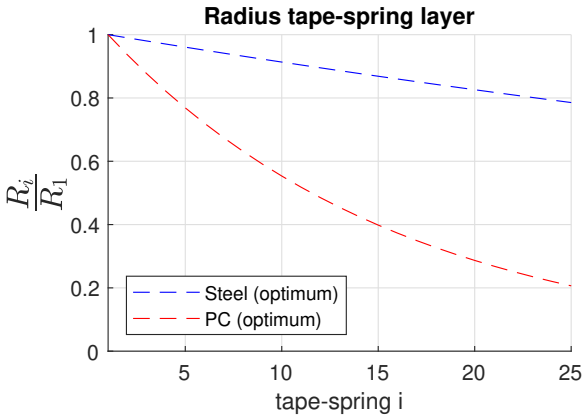

Fig. 3: The relative radius of tape-spring i compared to the outer tape-spring, $\frac{R_i}{R_1}$.

U_i of tape-springs $i = 1,...,n$. Lastly, R_i gives the radius of tape-spring i, so the outer tape-spring has the biggest radius R_1.

In figure 4a, it can be seen that the energy storage in a single tape-spring for spring steel is only 48% of the energy storage in a polycarbonate tape-spring for the outer tape-spring ($R_i = R_1$).

Figure 4b shows the total energy stored in a stack, normalized with the energy storage in the outer tape-spring for that specific material, as a function of the amount of tape-springs. It is clear that total amount of energy converges to a certain limit value. This value can be calculated with equation 9, and results in a 5.59 and 33.6 times higher energy storage for polycarbonate and steel, respectively, compared to the initial stored energy for the outer tape-spring. The solid lines, indicating the non-continuous thicknesses, have a lower limit value. These are 4.92 and 26.5 for polycarbonate and steel, respectively. This results in a ratio between the realistic stacking energy increase and the ideal stacking energy increase for polycarbonate and steel of $\frac{4.92}{5.59} = 0.88$ and $\frac{26.5}{33.6} = 0.79$, respectively.

4 Discussion

The maximum energy storage in a single-tape spring is higher for polycarbonate than for spring steel. The material index that has to be optimized to get the maximal energy storage U in a single tape-spring with a specific geometry can be derived from equation 2 and 3

$$\max\left(U(\sigma_y, E)\right) = \max\left(\frac{\sigma_y^3}{E^2}\right) \tag{10}$$

When maximizing energy storage in a stack of tape-springs, equation 9 has to be maximized. This results in the material index

$$\max\left(\sum_{i=1}^{n\to\infty} \frac{U_i(\sigma_y, E)}{U_1(\sigma_y, E)}\right) = \max\left(\frac{E}{\sigma_y}\right) \tag{11}$$

These two indices contradict each other. Therefore, polymers and elastomers are more suitable for maximizing energy storage in a single tape-spring, due to their relatively high yield strength and low Young's modulus, while spring steel is more suitable for maximizing energy storage in a stack of tape-springs, since they can be stacked more compactly.

The amount of steel tape-springs needed in a stack, in order to have a higher energy storage than a single polycarbonate tape-spring, is three. For three stacked steel tape-springs, the energy storage will be higher, but the overall thickness of the stack will be smaller than the single polycarbonate tape-spring. This shows, that if the space is limited, the energy storage capacity of a stack of spring steel tape-springs is more promising.

One major limitation in the approach is that no interaction between layers is assumed. Interactions could for example be sliding friction between layers or forces acting perpendicular to the tape-spring surfaces, due to unequal deformation. Currently, a constant fold radius is assumed, equal to the tape-spring radius. Besides the impact on the energy storage, this also could influence the force-deflection behaviour, which can be crucial in a force generator (e.g. in [5]). In the described case study, the subtended angle α is fixed at 180°. Bigger subtended angles are possible, but can result in self-contact during folding. Smaller subtended angles will work to some extent, but if made too small, the tape-spring will act more and more like a leaf spring, with a distributed deformation, as opposed to a locally deformed fold.

Regarding the unit volume, this is determined in the undeformed state to have a certain width. However, when the tape-springs deform, the width of the configuration will increase, as flattening will occur throughout the fold region. If the tape-spring becomes completely flat, the width would become the length of the arc, αR.

For determining the maximum energy storage increase, no limit is considered on the size of a tape-spring. This means that the radius of a tape-spring can be made arbitrary small in the optimal case. However, the smallest tape-springs would be very hard to produce, so the actual limit value of energy increase in stacks will be lower.

Lastly, the sliding boundary conditions for each separate layer in a stack are assumed to be possible. However, in reality it would be impossible to have a perfectly sliding end for each tape-spring layer. It is interesting to investigate what happens when the length change of one layer with respect to the other is not possible. This can be achieved by constraining all tape-spring ends in one (sliding) end-block, but it is also interesting to include a different, more elastic material in between the different layers, resulting in a sandwich composite sheet material. This could account for the length change, and subsequently store energy due to this longitudinal translation.

5 Conclusion

First, an overview of the theoretical descriptions of tape-spring behaviour is presented. Using this as a framework,

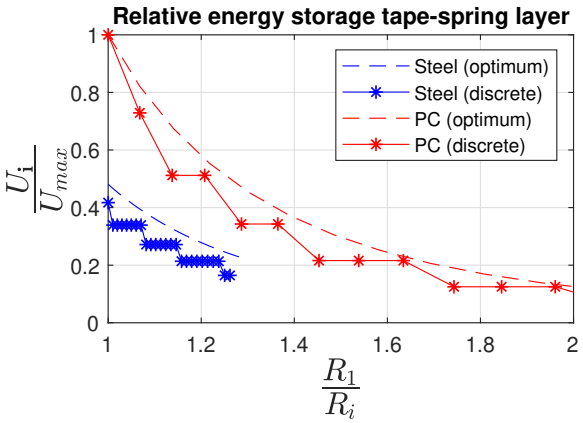

(a) The fraction of stored strain energy in a single tape-spring compared to the maximum stored energy in the outer tape-spring, (U_i/U_{max}), as a function of the radius of the tape-spring, (R_1/R_i).

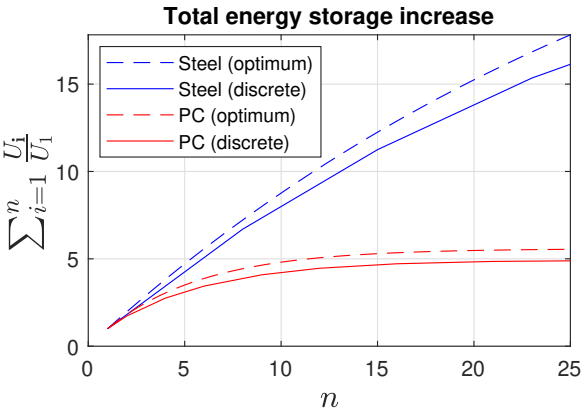

(b) The total stored energy in a stack of tape-springs as a fraction of the energy stored in the outer tape-spring, $\sum_{i=1}^{n}(U_i/U_1)$, as a function of the amount of tape-springs, n.

Fig. 4: The stored energy in single and stacked tape-springs are shown for both spring steel (blue) and polycarbonate (red). The dotted lines show the optimum, which can be achieved if all material thicknesses are considered. The solid lines indicates the energy storage in (the layers of) a stack of tape-springs when materials with discrete thicknesses are considered.

the theoretical energy increase in a stack of tape-springs is determined with respect to a single tape-spring. It was found that in an ideal situation an increase in energy storage of factor 5.59 is possible for polycarbonate and for spring steel an increase of factor 33.6. When considering discrete increments in material thicknesses, 88% and 79% of this ideal energy storage increase can be achieved, for polycarbonate and spring steel respectively. These results show that spring steel is more suitable for stacking than polycarbonate, and a general material index is derived which can be used to determine the most suitable material to maximize energy storage. This index is derived both for the situation of a stacked tape-springs as well as for a single tape-spring. These two indices contradict each other, implying that materials such as polymers and elastomers are more suitable for maximizing energy in a single tape-spring, while spring steel is more suitable for maximizing the energy storage in a stack of tape-springs.

References

[1] Howell, L. L., 2001. *Compliant Mechanisms*. John Wiley and Sons Inc., New York, US.

[2] Radaelli, G., 2017. "Synthesis of mechanisms with prescribed elastic load-displacement characteristics". Phd thesis, Delft University of Technology.

[3] Yang, H., Liu, R., Wang, Y., Deng, Z., and Guo, H., 2014. "Experiment and multiobjective optimization design of tape-spring hinges". *Structural and Multidisciplinary Optimization,* **51**, 12.

[4] Seffen, K. A., Pellegrino, S., and Parks, G. T., 2000. "Deployment of a panel by tape-spring hinges". In IUTAM-IASS Symposium on Deployable Structures: Theory and Applications, S. Pellegrino and S. D. Guest, eds., Springer Netherlands, pp. 355–364.

[5] De Jong, M., 2018. "Synthesis of a Force Generator using Two-Fold Tape Loops". Master's thesis, Delft University of Technology.

[6] Seffen, K. A., and Pellegrino, S., 1999. "Deployment dynamics of tape springs". *Proceedings: Mathematical, Physical and Engineering Sciences,* **455**(1983), pp. 1003–1048.

[7] Guinot, F., Bourgeois, S., Cochelin, B., and Blanchard, L., 2012. "A planar rod model with flexible thin-walled cross-sections. application to the folding of tape springs". *International Journal of Solids and Structures,* **49**(1), pp. 73 – 86.

[8] Bourgeois, S., Cochelin, B., Guinot, F., and Picault, E., 2012. "Buckling analysis of tape springs using a rod model with flexible cross-sections". *European Journal of Computational Mechanics,* **21**(3-6), pp. 184–194.

[9] de Jong, M. G., van de Sande, W. W. P. J., and Herder, J. L., 2019. "Properties of Twofold Tape Loops: The Influence of the Subtended Angle". *Journal of Mechanisms and Robotics,* **11**(2), feb, pp. 020912–020912–7.

[10] Seffen, K. A., 2001. "On the Behavior of Folded Tape-Springs". *Journal of Applied Mechanics,* **68**(3), p. 369.

[11] Walker, S. J., and Aglietti, G. S., 2007. "Modeling the hinge moment of skew-mounted tape spring folds". *Journal of Aerospace Engineering,* **20**(2), pp. 102–115.

[12] Lee, C.-H., Jeong, J.-W., Kim, Y.-J., and Lee, J.-J., 2016. "Deployment shock attenuation of a solar array tape hinge by means of the martensite detwinning of niti shape memory alloy". *Review of Scientific Instruments,* **87**(3), p. 035104.

[13] Hasberg-Schneider GmbH. Standard dimensions for precision gauge tape and reference sheets. https://www.hasberg-schneider.de/en/precision-thickness-gauge-strip-standard-dimensions.html.

Accessed: 2019-10-01.
[14] Goodfellow. Polycarbonate (pc) - sheet - material information. http://www.goodfellow.com/E/Polycarbonate-Sheet.html. Accessed: 2019-10-01.
[15] theplasticshop. Polycarbonate sheet: Lexan® exell® d - 2mm to 8mm thick. https://www.theplasticshop.co.uk/polycarbonate-sheet-2mm-3mm-4mm-5mm-6mm-8mm-thick.html. Accessed: 2019-10-01.

3

Paper: Increasing energy storage in tape-springs by stacking

Increasing energy storage in tape-springs by stacking

Jan Maarten Verzendaal
Department of BioMechanical Engineering
Delft University of Technology
Delft, 2628 CD, The Netherlands

Abstract

Tape-springs are single, constant curved thin-walled structures that exhibit interesting force-deflection behaviour when folded. This behaviour can be tailored, enabling the use of tape-springs as specific force generators. However, energy storage in a single tape-spring is limited, due to material yielding.

This study uses a simulation and experimental approach to investigate the potential for energy storage increase by stacking tape-springs, defined as the practice of placing tape-springs on top of each other in parallel. A practical configuration of a stack of tape-springs is considered, with the ends of each layer constrained with respect to each other. A simulation approach for parallel tape-springs based on the superposition principle is proposed and used to study the effect of stacking on the strain distribution.

The simulations show that the energy in a system of two closely placed tape-springs doubled, while only increasing the maximum strain concentration with 3.5%. For tape-springs placed further apart, the interaction between individual layers becomes more and more important, resulting in a higher strain energy in the system. The proposed superposition approach to simulate parallel tape-springs is experimentally tested and showed qualitatively comparable behaviour.

Nomenclature

α	subtended angle
ε_{vM}	Von Mises equivalent strain
ν	Poisson's ratio
σ_y	yield stress
θ	fold angle
E	Young's modulus
F_y	longitudinal compression/tension force
L	length tape-spring
R	fold radius
R_x	rotation around x-axis
r	radius tape-spring
t	thickness
U	potential strain energy
u_y, u_z	translation in y- and z-direction

1 Introduction

Compliant mechanisms are mechanisms that get their mobility from the elastic deformation of flexible segments. These compliant mechanisms are a promising alternative to rigid link mechanisms, since they experience less wear and backlash, and integrate functions in fewer parts, potentially saving costs [1]. Compliant shell mechanisms are a relatively new subset of this research area, which are compliant mechanisms consisting of a curved thin walled structure [2]. Possible applications of compliant shell mechanisms are collapsible walls [3], transmissions [4], gravity balancers [2], or human assistive devices [5]. A tape spring is a basic shape of such a shell geometry, being thin walled and having only one transverse curvature. Tape springs are used for different purposes, such as hinges in deployable structures [6–8], and also as force generators [9–11].

For tape-springs being used as force generators, the energy that can be stored in a single tape-spring is limited by material yielding, and therefore the force that can be generated by such a mechanism is limited. To increase energy storage in a force generator, such that the generated force is higher, or to increase energy release in a dynamic damping hinge application, multiple tape-springs can be combined next to each other [12, 13]. This method can be used in force generators as well, and besides placing several tape-springs next to each other, it is also possible to place the tape-springs on top of each other, which is referred to as stacking in this paper. By stacking the available space will be used more efficiently compared to tape-springs next to each other. Stacking is mentioned briefly in literature, but not as the main topic of study.

The opening moment of a tape-spring is the moment needed to keep a tape-spring in a folded position, and it changes with changing fold angles. Walker and Aglietti [14] tested multilayer tape-springs experimentally, and it was found that the opening moment of a folded multilayer tape-spring stack can be modelled as a summation of the individual tape-spring moments for sufficiently large separation dis-

tances, as for small separation distances the contact between the separate layers caused the opening moment to rise. Yang et al. [15] studied a tape-spring hinge combining opposite and equal sense bended tape-spring in a single layer tape-spring and a double tape-spring configuration. In this study it was found that the opening moment of a double layer tape-spring hinge is more than two times the opening moment of a single tape-spring, while the maximum stress in the double tape-spring configuration is less compared to a single tape-spring. Cook and Walker [16] mention a doubled tape-spring configuration, in which two tape-springs are placed on top of each other to strengthen a space inflatable structure. Lee et. al [17] studied the attenuation of the deployment of a tape-spring hinge, by adding a shape memory alloy layer between two stacked tape-springs. They found that the folding moment is proportional to the number of stacked tape-springs. However, this research is focused on the behaviour and stresses in the added shape memory alloy layer instead of the stacking of the tape-springs.

These studies show the possibilities of stacking for energy increase. However, a clear concise overview of the potential of this approach is lacking, as well as a clear simulation approach of parallel compliant shell mechanisms. The goal of this study is to show that stacking can be used to increase the total energy storage in a tape-spring assembly, without yielding the material. By using the principle of superposition in simulating the deformation behaviour, the complexity of the simulations are reduced. The resulting energy increase is relevant in force generators, since this would broaden the range of possible applications.

This paper starts with an introduction of the considered boundary conditions and tape-spring geometry, as well as an explanation of the simulation and experimental method in section 2. The resulting force-deflection behaviour and strain distribution from the simulations and the force-deflection behaviour found in the experiments are reported in sections 3.1 and 3.2, respectively. Subsequently, a discussion of the results is provided in section 4 in the same separation of simulations and experiments. Furthermore, the results of the experiments and the simulations are compared to each other and to the findings in existing literature. Lastly, a brief summary and general conclusion are given in section 5.

2 Method

2.1 Boundary conditions

The boundary conditions considered in this paper are derived from the potential application of a tape spring for an upper arm support system [11], as shown in figure 1. The approach to the arm is 2D, modelling the shoulder as a rotational joint around which the upper arm acts as a pendulum. The tape spring is fixed on one end (point 1) to the trunk, constraining two translations ($u_y = 0$, $u_z = 0$) and one rotation ($R_x = 0$). The other end (point 2) is connected to the arm using a slider, constraining one translation ($u_{z'} = 0$) and one rotation ($R_{x'} = 0$). The slider releases the shear forces from the arm, which could otherwise cause chafing.

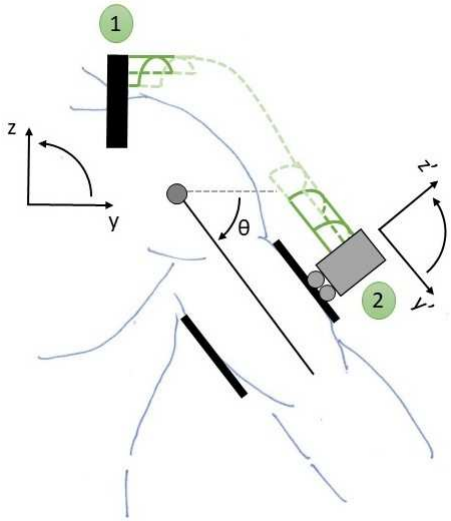

Fig. 1: The considered boundary conditions as derived from a potential upper arm support system. Endpoint 1 is fully constrained, while endpoint 2 is free to slide in the y'-direction.

2.2 Tape spring basics

A tape spring is a single-curved geometry, and is defined by the length L, thickness t, radius r, and subtended angle α. The geometry is shown in figure 2a. This tape spring can be folded in an equal sense manner - the concave sides facing towards each other [18]. Figure 2b shows the deformed geometry for fold angle θ, with the corresponding fold radius, R.

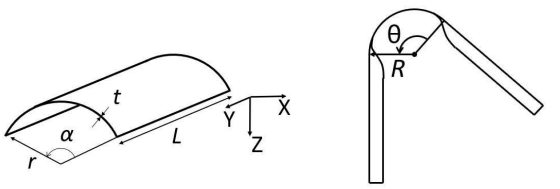

(a) Straight tape spring (b) Folded tape spring

Fig. 2: Parameters of a folded tape spring [19]

In this paper, the tape-spring is modeled with spring steel, the properties and dimensions of which are given in Table 1. The length is chosen considering the biometric data of an arm, while the thickness t and radius r are related using equation 1, derived by De Jong [19], in order to stay below the yield stress

$$t < \frac{2\sigma_y(1+\nu)}{E\sqrt{3}}r \tag{1}$$

L	t	r	E	ν	ρ
[mm]	[mm]	[mm]	[GPa]	[-]	[kg/m^3]
260	0.15	19.9	210	0.3	7900

Table 1: Dimension and material properties of tape spring

2.3 Stacking options

When stacking multiple tape spring, different constraints can be imposed on the individual tape springs with respect to each other. The translation degree of freedom at point 2 can be ensured by having a separate slider for each layer in the stack, or by constraining the separate layers into one end-block, which is free to slide.

In the first configuration, the endpoints of the individual layers do not interact longitudinally (y'-direction) with each other, while the endpoints' z'-translation and rotation are constrained similarly. When possible interaction throughout the length of the tape spring is not taken into account, the resulting behaviour of the stack would be just a summation of the behaviours of the individual tape springs, since they do not influence each other. This means that the peak stress in the material stays the same, while the total energy storage of the stack increases. This creates the opportunity to increase the energy storage in a tape spring configuration, while not plastically deforming the material.

Having separate sliders for each layer of a stack is not convenient for practical reasons (increased complexity, more parts, assembly, etc.). Therefore, the second configuration, in which the separate layers are all constrained into one end-block is considered. In this configuration, the translation along the arm is constrained for the individual layers, resulting in longitudinal forces at the tape springs ends. However, no shear forces are exerted on the arm since the end-block is mounted on a slider.

2.4 Superposition approach

The approach to the stacked configuration can be divided into four steps:

1. Simulate the translation-free bending ($\theta = 0, ..., \pi/2$) of a single tape-spring $i = 1, ..., n$.
2. Find the force-displacement relation in y'-direction for sliding endpoint for each rotation θ, by prescribing a y'-displacement, while constraining other movements.
3. (I) Use the principle of superposition on the axial forces to find the trajectory $y'(\theta)$ of a stack of n tape-springs, for which must hold:
   (a) $y'_1 = y'_2 = ... = y'_n$
   (b) $\sum_{i=1}^{n} F_{y',i} = 0$ for each θ

   or (II) use the principle of superposition on the strain energies U to find the trajectory $y'(\theta)$ for a stack of n tape-springs, for which must hold:
   (a) $y'_1 = y'_2 = ... = y'_n$
   (b) $\sum_{i=1}^{n} U_i(\theta, y') = min\,(U(\theta, y'))$ for each θ
4. Compare the peak strain and total strain energy of a stack of tape-springs to an unstacked tape-spring

The first step involves the simulation of an individual tape-spring, with one endpoint being rotated by θ with respect to the other endpoint around the x-axis, and a translational degree of freedom on the y'-axis (along the arm). The following step prescribes, for each of the solutions of rotation θ, a translation along the y-axis of one endpoint (along the arm), while the other translations and rotations are fixed. This results in a force field in the y-direction, which is a function of θ and y': $F_{y'}(\theta, y')$. Thirdly, the force fields of the individual tape-springs are used to find a solution for the trajectory along the arm $y'(\theta)$ of a combined stack. For this trajectory must hold that the y' positions of the endpoints of all individual layers are aligned ($y'_1 = y'_2 = ... = y'_n$), since they are in one end-block, and the forces in the y'-direction of all layers add up to zero ($\sum_{i=1}^{n} F_{y',i} = 0$), since the end-block is free to slide. An alternative method is to look at the summation of the strain energy fields of the tape-springs, $\sum_{i=1}^{n} U_i(\theta, y')$, and minimize this for each value of θ to find the trajectory, since the end-block follows the trajectory of minimum energy. Lastly, when the trajectory of the stack and corresponding deformations and forces of each contributing tape-spring are known, these sum up to the total behaviour of the stack, which can be used to determine the moment-rotation behaviour of the stack and the maximum strain and strain energy in the individual tape-springs and stack.

2.5 Simulation method

To study the strains in the different layers in the stack, a finite element model is created, based on isogeometric analysis (IGA) [20]. The geometry is defined by 15 evenly spaced points in the x-direction (the circular cross-section), and 130 points in the y-direction (the length of the tape spring), as shown in figure 3. Furthermore, at the ends of the tape spring so-called pilot points are defined halfway between the side edges. These are connected through stiff beams to the cross-section and the end. Constraints are applied at the pilot-points.

In order for the simulation to converge, an imperfection must be introduced to the geometry. It was chosen to change the subtended angle α of the cross-section throughout the length of the tape spring. The subtended angle was decreased linearly from 95.1° at the outer ends to 80.5° at $y = 0.15m$.

The rotation θ is divided in 100 steps between 0 and $\pi/2$ *rad*, with smaller spacing at the beginning and greater spacing at the end, based on the curve $y = 10^x$.

2.6 Experimental method

2.6.1 Production of tape-springs

The simulations are validated by experiments. The tape springs are produced from stainless steel 1.4310. This material is a common spring material with an ultimate tensile strength of 1500-1700 MPa, and does not suffer from creep and stress relaxation under normal conditions. The material for the tape-spring is laser cut from a flat sheet, including

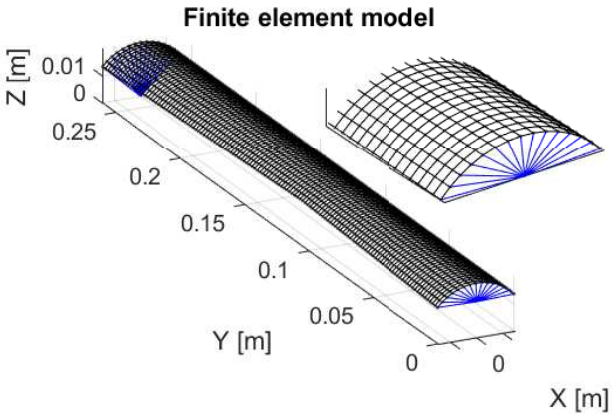

Fig. 3: The meshed finite element shell model. The points of the model are defined at the intersections of the black lines. The blue lines indicate the stiff beams that connect the edge of the shell to the so-called pilot points, at which the constraints are applied. The insert shows a close-up of one end of the tape-spring.

the previously described imperfection in the simulation. The transverse curvature is then rolled into this strip, resulting in the required tape-spring shape.

2.6.2 Measurement setup

The force-deflection behaviour of the produced tape-spring is tested in a measurement setup as shown in figure 4. The setup consist of one arm ('moment arm') on which a moment is exerted. One end of the tape-spring is fixed at the end of this arm, allowing no translations or rotations, while the other end is fixed on a slider, allowing longitudinal translation. The moment arm and slider are mounted on a base plate, and for the moment arm an extra bracket is introduced to improve the stiffness of the construction. An M6 shoulder bolt with 8 mm shaft is used as a shaft, and two EZO F608H ZZ ball bearings with flange are pressed in the moment arm to reduce friction. The moment arm is made by SLS of solid Nylon (PA12) and the clamps on the slider are 3D printed from PLA.

An Altmotion LT50-TR-G8-200 linear actuator is used to move a platform back and forth with a velocity of 1 mm/sec, on which a Micro-Epsilon optoNCDT ILD1420-20 distance sensor and a Futek LSB200 load cell are mounted, which have a measuring frequency of 20 Hz. A braided wire is used to attach the load cell to the moment arm at a distance of $0.030m$ from the rotational axis. This distance can be used to calculate the moment from the measured force, $M = 0.030\ F_{meas}$, as well as for determining the rotation of the mounting arm θ from the displacement δ measured by the laser distance sensor, $\theta = \delta/0.030$. The distance sensor and load cell have an uncertainty of $\pm 0.1\%$, and therefore, when multiplied with the distance from the rotational axis, an uncertainty of $\pm 7e^{-3} rad$ and $\pm 8e^{-4} Nm$, respectively.

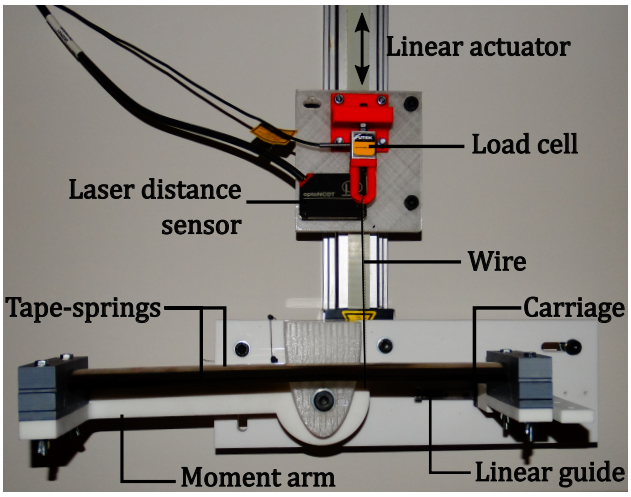

Fig. 4: Picture of the measurement setup

3 Results

3.1 Simulations

The tape-springs are simulated, using the four steps explained in section 2.4. The resulting force field $F(y,\theta)$ from the simulation for two tape-springs with an offset of 0 and 2 mm from their centre to the rotational joint are shown in figure 5a and 5b, respectively. The summation of these two fields, according to step 3 (I) of the superposition approach, is shown in figure 5c with the red line indicating the $y(\theta)$ trajectory of the stack for which holds $\sum_{i=1}^{n} F_{y,i} = 0$. The summation of the strain energy fields $U(y,\theta)$ of the same tape-springs is shown in figure 6, with the red line indicating the $y(\theta)$ trajectory of the stack for which holds $\sum_{i=1}^{n} U_i(\theta,y) = min\,(U(\theta,y))$ for each θ, according to step 3 (II) of the superposition approach. The two trajectories of the stack show good agreement with each other, with a RMSE of $6.3e^{-5}$ $[m]$, which gives a normalized RMSE (NRMSE) of 7.5% when normalized with the mean of $y - y_{inside}$.

Figure 7 shows the maximum Von Mises strain ε_{vM} in the tape-spring as a function of rotation θ, both of the inner and outer tape-spring when folded separately and together in a stack. During the buckling phase, from 0 to 0.35 $[rad]$, the highest strain concentration appears. For the stacked configuration, an increase in maximum strain concentration of $3.2e^{-4}$ or 5.4% is seen for the inner tape-spring, while a decrease of $2.1e^{-4}$ or 3.5% is seen for the outer tape-spring. When a separation distance of $1mm$ instead of $2mm$ between the tape-spring layers is assumed, an increase of 3.5% is seen for the inner tape-spring, while a decrease of 1.8% is seen for the outer tape-spring.

In figure 11 both the simulated strain energy of a stack (green, solid line), and the summation of the strain energies of the individual tape-springs (green, dashed line) are shown, for a separation distance of $2mm$. As can be seen, the difference between these two is marginally small. In figure 12 the percentage difference of the moment is shown, with a mean difference of 2.0%.

This superposition approach can also be applied to a

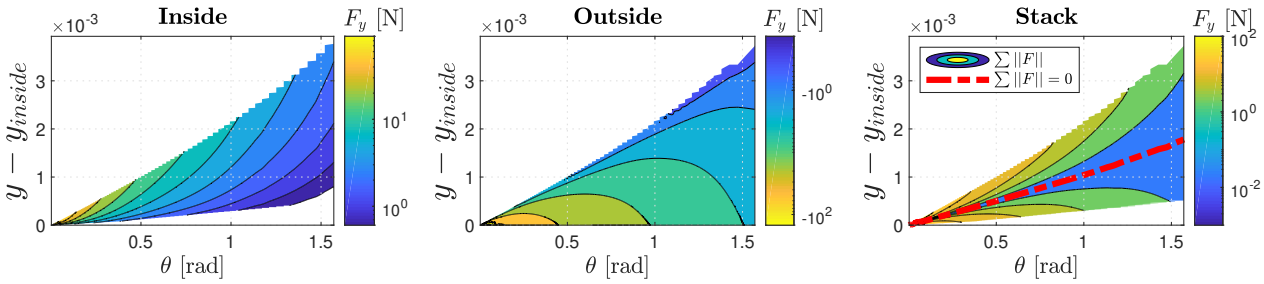

(a) Longitudinal force-displacement field of the inner tape-spring. The contours display the force in [N]

(b) Longitudinal force-displacement field of the outer tape-spring. The contours display the force in [N]

(c) Absolute value of the summation of the longitudinal force-displacement field of the inner and outer tape-spring. The red line indicates $\sum F_y = 0$.

Fig. 5: The longitudinal force-displacement fields for the separate tape-springs with their centre located at 0 mm (inner) and 2 mm (outer) offset of the rotational joint, and the combined force-displacement field. The displacement is plotted relative to the displacement of the inner tape-spring.

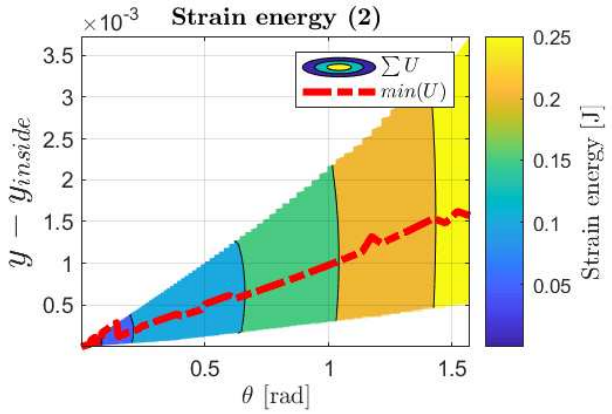

Fig. 6: Strain energy field of a stack of two tape-springs. The red line indicates the minimum strain energy for a specific rotation θ.

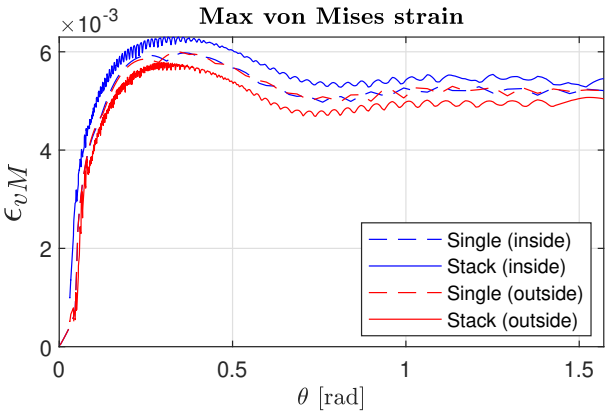

Fig. 7: Maximum Von Mises strain ε_{vM} in the material

stack of more than two tape-springs. In figure 8 the summed energy field and its minimum are shown for a stack of three tape-springs with an offset between their centre and the rotational joint of $0mm$, $1mm$, and $2mm$.

3.2 Measurements

The produced tape-springs are measured on the measurement setup and compared to the simulation results to verify the FE simulations. Three measurements are taken of each tape-spring configuration. The signal from the distance sensor is filtered with a moving average filter, using a window size of 30. Subsequently, the measured load is interpolated at 200 linearly spaced points between 0 and $\frac{\pi}{2}$ rad. In figure 9, the simulated (red) and measured (blue) force-deflection results for a single tape-spring with its centre aligned with the rotation point is shown, with the dashed line indicating the unloading step, showing the hysteresis of the measurement. The mean of the measurement is plotted in purple. The two results do not quantitatively agree with each other, as the simulation result gives higher values for the reaction moment, both for the peak moment during buckling, as well as for the opening moment post buckling. In black, the percentage difference between the simulation and the loading step of the measurement is shown, normalized with the mean of the simulation (red) and the mean of the measurement (purple).

The normalized root mean square error (NRMSE) is calculated for the moment-rotation behaviour and the strain energy as follows:

$$NRMSE(x) = \sqrt{\frac{\sum_{i=1}^{N} \left(\frac{M_{i,sim} - M_{i,meas(mean)}}{mean(M_{i,sim}, M_{i,meas(mean)}} \right)^2}{N}} \quad (2)$$

The NRMSE is calculated for two different intervals: $[0, \frac{\pi}{2}]$ $[rad]$ and $[0.35, \frac{\pi}{2}]$ $[rad]$. The second interval takes only the post-buckling behaviour into account. This resulted in an error in the moment of $NRMSE_1 = 39.8\%$ and $NRMSE_2 = 27.4\%$, and in the strain energy of $NRMSE_1 = 50.5\%$ and $NRMSE_2 = 36.0\%$ for the two intervals.

Besides the moment-rotation plot, a strain energy plot

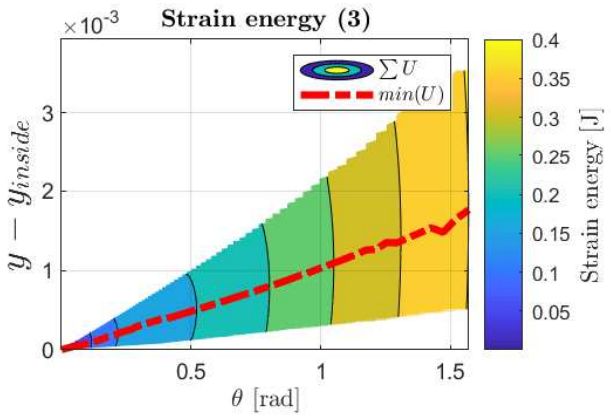

Fig. 8: Strain energy field of a stack of three tape-springs, with an offset between their centre and the rotational joint of 0, 1, and 2 $[mm]$. The red line indicates the minimum strain energy for a specific rotation θ.

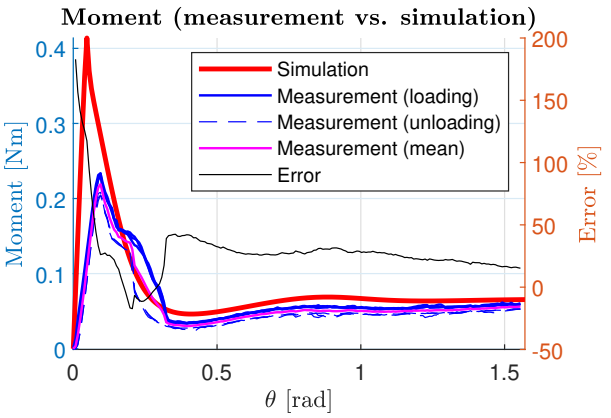

Fig. 9: Moment-rotation plot of both the simulation (red) and the measurements (blue). The dashed line indicates the unloading measurement, showing the hysteresis in the measurement. In black the percentage error is shown, calculated as $M_{sim} - M_{meas(mean)}$, normalized by the mean of M_{sim} and $M_{meas(mean)}$.

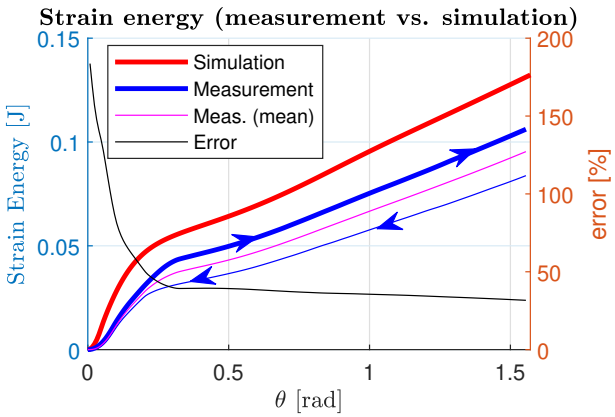

Fig. 10: Strain energy U plotted against rotation θ of both the simulation (red) and the measurements (blue). Tthe hysteresis in the measurement is indicated using the arrows. In black the percentage error is shown, calculated as $U_{sim} - U_{meas(mean)}$, normalized by the mean of U_{sim} and $U_{meas(mean)}$

Table 2: Measurement results for the stacked configuration

Separation distance [mm]		0	2	4
Strain RMSE [mJ]	Sum vs. stack	2.8	25.3	44.5
Peak moment [Nm]	Sum	0.44	0.41	0.37
	Stack	0.39	0.53	0.63
Mean moment difference [%]	Sum vs. stack $[0, \frac{\pi}{2}]$ *rad*	42	24	36
	Sum vs. stack $[0.35, \frac{\pi}{2}]$ *rad*	15	20	25

can also be made to compare the simulation to the measurements. In figure 10, the strain energy from the simulation and the measurement are shown. The strain energy from the measurement is taken by integrating the force-deflection curve from figure 9.

Measurements are taken of the stacked configuration as well. The strain energies of the measurements of the stacks are shown in figure 11 as solid lines, while the dashed lines indicate the summation of strain energies from the measurements of the free-sliding behaviours of the individual tape-springs. The values for the strain energy increases with the separation distance, which differs from the simulation results, which stay roughly the same and similar to the summation results. The RMSEs of the strain energy when comparing the summation of the individual tape-springs and the stack behaviour are given in Table 2. The main difference is due to the higher peak moment during the buckling phase, resulting in a higher energy storage. The higher the separation distance, the higher this peak moment is.

The percentage difference of the moment when comparing the summation of the individual tape-springs and the stack behaviour is shown in figure 12. Comparing different separation distances, the results of the moment summation of the individual tape-springs do not differ considerably, but the actual measured stack behaviours do. It can be seen that the moment differences increase with the separation distance, but qualitatively it shows the same behaviour. The means of the moment difference for the whole range of θ and the post-buckling phase are given in Table 2, showing the increasing difference between the summation and the stack behaviour for increasing separation distances.

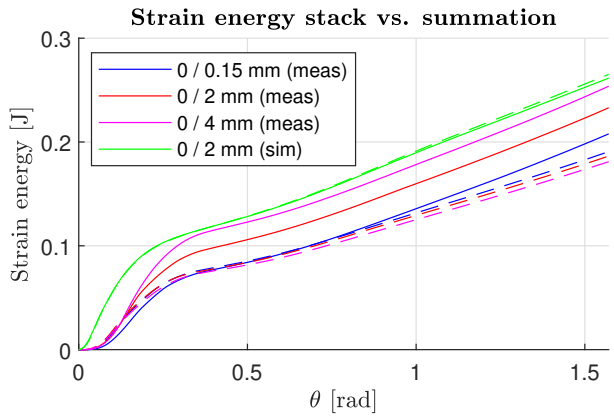

Fig. 11: The strain energy in the tape-spring is plotted against the rotation θ for both the simulation and the measurements. The solid lines indicate the strain energy as encountered in a stack including compression and tension forces, while the dashed lines show the summation of the individual free-sliding tape-springs.

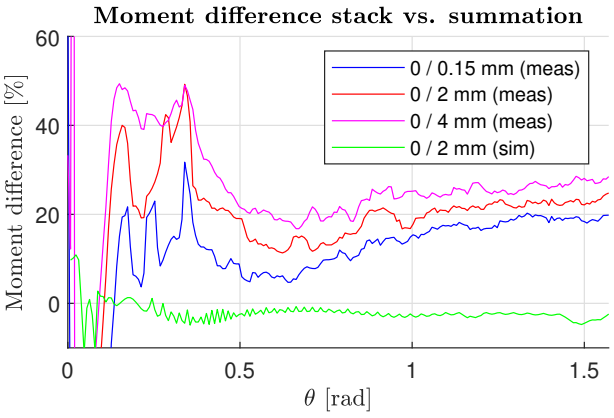

Fig. 12: The percentage difference in opening moment is shown, when comparing the behaviour of a stack of tape-springs, including compression and tension forces, to the summation of the individual free-sliding tape-spring behaviours. The difference is normalised using the moment of the stack of tape-springs.

4 Discussion

4.1 Simulations

The force displacement fields for the inner (compression) and outer (tension) tape-springs differ from each other. The inner tape-spring shows a stiffer behaviour than the outer tape-spring. This causes the trajectory of the stack to be closer to the free-sliding trajectory of the inner tape-spring. The stiffness difference agrees with the findings of Seffen [18], which show a more stiff relation for compression of a tape-spring than tension.

The resulting trajectory of the stack of tape-springs using the longitudinal forces as reference differs only slightly from the acquired trajectory using the strain energy. This difference can be attributed to the stored elastic energy in the stiff end-beams of the model, since the stiffness is only finite and some deformation takes place.

The maximum Von Mises strain ε_{vM} in a stacked configuration increases slightly in the inner tape-spring, while it decreases in the outer tape-spring. This corresponds to the findings of Seffen [18] regarding longitudinal curvature change for tape-springs under compression and tension, which show that for the former the deformation becomes larger, while for the latter the deformation becomes smaller, corresponding to higher and smaller peak strains in the material, respectively. If the increase of peak strain would cause material yielding, the radius could be made slightly bigger, such that the strain concentration will be lower. Still, the overall strain energy in the system will be roughly doubled in such a stack of two, without material yielding. When the separation distance between tape-spring layers increases, the maximum strain difference increases as well, since the longitudinal compression and tension forces increase.

The small difference between the strain energy of a stack including compression and tension forces at the ends and the summation of the individual free-sliding tape-spring behaviours shows that the additional forces do not change the force-deflection behaviour very much. So, when interaction forces between individual layers are not taking into account, the resulting behaviour is basically a summation of the individual tape-springs.

Lastly, Seffen [18] states a theoretic upper-bound estimate on the maximum load that can be carried without the forming of two distinct folds. This maximum load corresponds to a certain longitudinal displacement. As a formation of a second fold would not be possible for a single layer in a stack, significant contact forces are expected for the separation distance at which this maximum load appears. This gives a limit to the separation distance that can be studied with the current simulation approach.

4.2 Measurements

The simulations and measurements do not completely agree with each other. The overall shape show a similar shape, but the force magnitude differs significantly. The energy in the tape-spring can be approached by equation 3 [18, 19]. This equation shows that the energy in the system scales cubically with the thickness. According to the manufacturer the thickness of the tape-spring has an uncertainty of $\frac{0.005mm}{0.15mm} \approx 3.3\%$. Therefore, this gives an uncertainty in the strain energy of 10.3%. Furthermore, the Young's modulus E was simulated as $210GPa$, however, according to CES Edupack the value for 1.4310 annealed steel lies between 200 and $210GPa$. This accounts for an uncertainty of 5% in the strain energy. These sources of error can not completely explain the difference between the measurement and simulation. Another source of uncertainty can be found in the measurement setup, where the clamping of the tape-spring only frictionally constrains the torsional twisting of the tape-spring ends during the buckling, resulting in distorted peak buckling moments. Furthermore, there might be some uncertainty in the radius of the pulley around which the wire pulls.

$$U = \frac{Et^3}{12(1-v^2)}(1 \pm v)\alpha\theta \tag{3}$$

Since the simulations and measurements for single tape-springs do not agree, the simulations and measurements for the stack are not compared. Instead of a quantitative validation, these measurements can be used as a qualitative validation of the relation between behaviour of a single tape-spring and a stack of tape-springs.

The shape of the force-deflection curve of the tape-spring stack remains similar to the force-deflection shape of a single tape-spring, however, the magnitude of the peak moment and the post-buckling opening moment is increased for a stack. Figure 12 shows that the force-deflection curve of a stack of tape-springs does not agree with the summation of the individual tape-spring behaviours, which is in line with the findings of Yang et al. [15], but contradicts with Walker and Aglietti [14] and Lee et al. [17]. The reported value in Table 2 of the mean moment difference over the whole range of θ is surprisingly large for the separation distance of 0 *mm*. This indicates that the summation of individual tape-spring behaviours and stack behaviour do not agree well with each other. This is mainly due to the fact that the stack buckles at a slightly larger value of θ, resulting in a big offset between the two results and giving a distorted view. The post-buckling value behaves more as expected, and is lower for the smaller separation distance.

The amount of measurements taken in this study is too limited to extract a general correlation between the separation distance and the amount of strain energy in the stack of tape-springs, but it points to a positive correlation. The increase in strain energy is attributed to the interaction between the different layers, since the tape-spring geometries are in contact with each other during bending. These interaction forces increase with increasing separation distances, requiring an elaboration on the used model.

In section 3.1 the strain distribution and corresponding concentrations as found in the simulations, discarding interaction forces, are given. However, the total stored strain energy in the measurements of a stack, including interaction forces, is higher than the values found in the simulation. The implications of this increase in strain energy for the strain distribution is not completely clear, since this distribution cannot be measured easily. For a stack of tape-springs with 0 *mm* separation distance and a rotation of $\frac{\pi}{2}$, a difference of 8% is observed between the measurements with and without interaction forces. However, for a separation distance of 2 *mm*, the total strain energy at a rotation of $\frac{\pi}{2}$ is already increased by 20%. It is not clear whether the strain in this case is distributed more evenly throughout the material or if the strain concentrations become higher. This should be further investigated, in order to be able to design the tape-springs to be loaded up to their yield limit.

5 Conclusion

In this study, a superposition approach to simulate parallel tape-springs is proposed. This approach was experimentally tested and showed qualitatively comparable behaviour. The measurements show substantial quantitative differences, but can partially be explained by the manufacturing uncertainties and uncertainties in the measurement method.

Using the strain energy distributions from the simulations, it was found that the energy in a system of two closely placed equal tape-springs doubled, while only increasing the maximum strain concentration with 3.5%. This shows that energy storage increase is possible through stacking, without material yielding. For tape-springs placed further away from each other, the interaction between individual layers becomes more and more important, resulting in diverging results for simulation and experiment. Therefore, the proposed simulation approach only holds with limited interaction forces. The experimental results point to a positive correlation between the separation distance and the increase in opening moment and strain energy in the system.

References

[1] Howell, L. L., 2001. *Compliant Mechanisms*. John Wiley and Sons Inc., New York, US.

[2] Radaelli, G., and Herder, J., 2017. "Gravity balanced compliant shell mechanisms". *International Journal of Solids and Structures,* **118-119**, pp. 78 – 88.

[3] Alkisaei, H., 2016. "Statically Balanced Compliant Walls". Master's thesis, Delft University of Technology, February.

[4] Houwers, H., 2016. "Closed-loop two-fold tape spring transmissions". Master's thesis, Delft University of Technology, January.

[5] Nijssen, J., 2017. "A Type Synthesis Approach to Compliant Shell Mechanisms". Master's thesis, Delft University of Technology, January.

[6] Seffen, K. A., and Pellegrino, S., 1999. "Deployment dynamics of tape springs". *Proceedings: Mathematical, Physical and Engineering Sciences,* **455**(1983), pp. 1003–1048.

[7] Seffen, K. A., Pellegrino, S., and Parks, G. T., 2000. "Deployment of a panel by tape-spring hinges". In IUTAM-IASS Symposium on Deployable Structures: Theory and Applications, S. Pellegrino and S. D. Guest, eds., Springer Netherlands, pp. 355–364.

[8] Yang, H., Liu, R., Wang, Y., Deng, Z., and Guo, H., 2015. "Experiment and multiobjective optimization design of tape-spring hinges". *Structural and Multidisciplinary Optimization,* **51**, pp. 1373–1384.

[9] Radaelli, G., 2017. "Synthesis of mechanisms with prescribed elastic load-displacement characteristics". Phd thesis, Delft University of Technology.

[10] De Jong, M., 2018. "Synthesis of a Force Generator using Two-Fold Tape Loops". Master's thesis, Delft University of Technology.

[11] Van Der Kemp, S. J. M., 2018. "Design of a compact wearable arm support utilizing shape optimized com-

pliant shell mechanisms". Master's thesis, Delft University of Technology. Unpublished.

[12] Hoffait, S., Brüls, O., Granville, D., Cugnon, F., and Kerschen, G., 2010. "Dynamic analysis of the self-locking phenomenon in tape-spring hinges". *Acta Astronautica,* **66**(7), pp. 1125 – 1132.

[13] Ömer Soykasap, 2007. "Analysis of tape spring hinges". *International Journal of Mechanical Sciences,* **49**(7), pp. 853 – 860.

[14] Walker, S. J., and Aglietti, G. S., 2007. "Modeling the hinge moment of skew-mounted tape spring folds". *Journal of Aerospace Engineering,* **20**(2), pp. 102–115.

[15] Yang, H., Liu, R., Wang, Y., Deng, Z., and Guo, H., 2014. "Experiment and multiobjective optimization design of tape-spring hinges". *Structural and Multidisciplinary Optimization,* **51**, 12.

[16] Cook, A. J., and Walker, S. J., 2016. "Experimental research on tape spring supported space inflatable structures". *Acta Astronautica,* **118**, pp. 316 – 328.

[17] Lee, C.-H., Jeong, J.-W., Kim, Y.-J., and Lee, J.-J., 2016. "Deployment shock attenuation of a solar array tape hinge by means of the martensite detwinning of niti shape memory alloy". *Review of Scientific Instruments,* **87**(3), p. 035104.

[18] Seffen, K. A., 2001. "On the Behavior of Folded Tape-Springs". *Journal of Applied Mechanics,* **68**(3), p. 369.

[19] de Jong, M. G., van de Sande, W. W. P. J., and Herder, J. L., 2019. "Properties of Twofold Tape Loops: The Influence of the Subtended Angle". *Journal of Mechanisms and Robotics,* **11**(2), feb, pp. 020912–020912–7.

[20] Cottrell, J. A., Hughes, T. J., and Bazilevs, Y., 2009. *Isogeometric analysis: toward integration of CAD and FEA*. John Wiley & Sons.

4

Discussion

A clear overview of the potential of energy increase in tape-springs through stacking is currently lacking. Furthermore, the different stacking options and the resulting mechanics behind it are not explored explicitly. While the method of stacking tape-springs can be found in literature, it is not researched elaborately. Therefore, this thesis addresses these subjects.

This thesis begins in chapter 2 with an exploration of the method of stacking using a theoretical framework. A stack of concentric tape-springs with decreasing radii inward is considered, and a theoretical maximum value of energy increase in a unit volume is derived for different materials. This result is interesting for different tape-spring applications. First of all, larger forces can be produced in tape-spring force generators. Furthermore, it creates more context for tape-springs in a dynamic damping hinge application, as the energy release can be increased by combining the right materials and geometries, as shown by Lee et al. [11]. Besides for folding tape-springs, this result is also interesting for two-fold tape loops, as studied by De Jong [7]. A tape loop is a special subset of a tape-spring configuration, for which the rotation angle θ is fixed at $180°$. The stacking of tape-springs can be applied to this configuration as well, and since the rotation angle is constant the relative length change does not change during movement of the tape loop. This makes it possible to increase the force generated by the tape loop, according to the results found in this chapter.

In chapter 2, the relative length change between different layers of a stack is assumed to be possible. However, this is not a very practical assumption, since it is challenging to have several tape-spring ends sliding freely with respect to each other, while they are experiencing an end couple and radial forces. More information about the implications of a more practical implementation is needed. In the subsequent chapter, an additional constraint is imposed on the longitudinal translation of the tape-spring ends. This constraint results in compression and tension forces on the tape-springs, varying with rotation angle θ. The effects are studied in the next chapter, using a simulation and experimental approach.

Chapter 3 considers a stack of equal tape-springs with the previously described practical set of boundary conditions. A small overview of 2D stacking options and their length change is given in appendix C. The superposition principle is used in the simulation framework, and the different layers are simulated separately. Using this approach stacks of two and three tape-springs were simulated with different separation distances. The simulation approach is expected to be able to superpose more than three tape-springs as well.

The downside of the simulation approach is that only the interaction forces at the outer ends of the tape-spring are taken into account, while interaction forces throughout the shell are discarded. The divergence between the results of the simulation and the experiment for higher separation distances is attributed to these neglected interaction forces throughout the shell. The misalignment of the eigentwist of the stacked tape-springs increases with increasing separation distance. As a result, the additional forces on the tape-spring will increase. The resulting compression force on the inner tape-spring and the tension force on the outer tape-spring will lead to contact between the different layers throughout the shell. Since there is a positive correlation between the separation distance and the additional strain energy in the system, this interaction is assumed to be responsible for the additional stain energy. More research needs to be done on this correlation between separation distance

and strain energy, since the increase in strain energy might affect the strain distribution in the material. If the increased separation distance causes an increase in the maximum strain concentration, it could result in material yielding. If the maximum strain concentration would not increase, the increase of separation distance can be used to increase the energy storage of the system.

The experimental results from chapter 3 show an increasing difference between the strain energy of a stack and the summation of the strain energies of the individual tape-spring layers for increasing separation distances. The result that the stack behaviour is greater than the summation of the individual tape-springs agrees with the findings of Yang et al. [9], but contradicts with the findings of Walker and Aglietti [8] and Lee et al. [11]. The latter two state that the stack behaviour is equal to the summation of the individual tape-springs. For small separation distances this equality roughly holds, but for increasing separation distances these values diverge. The higher interaction forces for larger separation distances, as explained in the previous paragraph, are supposed to account for this divergence.

The proposed simulation approach, which is based on superposition, could possibly be used for other configurations of parallel tape-springs as well, as long as the interaction forces between the different layers can be discarded. For example, a pivot joint can be added to the sliding end block, giving the tape-spring assembly an extra rotational degree of freedom (DoF) ϕ, as shown in figure 4.1. An extra dimension ϕ should be added to the current (y, θ)-energy fields, giving the strain energies for different values ϕ as well. The resulting trajectory of the stack can be determined by the minimum strain energy for each position of θ. Subsequently, the force-deflection behaviour of the system can be determined. If this extra DoF would be introduced to a tape-spring with a constant cross-section, the fold region would be located closest to endpoint 1 as possible (until the tape-spring collides with the rotating arm, or the end effects of the clamp are limiting). This happens since the effective fold angle of the tape-spring becomes smaller as the fold moves towards endpoint 1, and hence the tape-spring obtains a lower energy state. The location of the fold along the tape-spring length can be controlled by introducing a subtended angle profile, such that the tape-spring folds at the location with the lowest subtended angle. This additional DoF ϕ would, however, completely change the resulting moment the tape-spring exerts around the joint, since now only the force perpendicular to the arm will contribute.

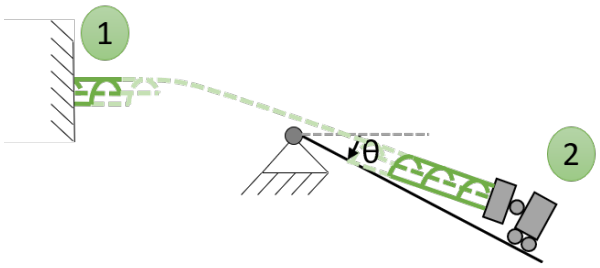

Figure 4.1: A tape-spring configuration with both a translational and a rotational degree of freedom at the arm.

Besides energy storage increase, stacking could open opportunities of modifying the force-deflection behaviour of a tape-spring in different ways. It is possible to introduce prestress to some layers of the stacked assembly. An example of the effect of prestress, added by the twisting of a tape-spring, is elaborated on in appendix B. Another interesting approach would be to stack tape-springs with different subtended angle profiles on top of each other. Since the tape-spring will likely buckle at the region with the smallest subtended angle, the interaction between the different layers can be tailored.

Another approach to increase the total energy storage in a tape-spring assembly besides stacking, could be introducing a variable cross-section, resulting in a better distributed strain energy. That way, the total energy storage could be increased, while maintaining a limited maximum strain value. This should be combined in an optimization problem, optimizing both for a specific force deflection profile as well as for maximum energy storage.

5

Conclusion

In this thesis, literature on stacking tape-springs is reviewed and the potential of energy increase by stacking tape-springs is explored. Furthermore, a description of different stacking options and the resulting mechanics behind them are given.

Two different methods of stacking are studied in this thesis. Firstly, a stack of concentric tape-springs with decreasing radii inward is studied. These tape-springs have a relative change in length between the different layers of $\Delta L = \theta(R_1^* - R_2^*)$ during folding, which is a function of rotation angle θ and fold radius R_i^*, and it is assumed they can freely translate. Secondly, a stack of equal tape-springs is studied, taking into account a practical set of boundary conditions. For this configuration the relative change of length is a function of the separation distance s of the tape-spring layers and the rotation angle θ, and can be defined as $\Delta L = 2\ s\ tan\frac{\theta}{2}$. In this second configuration, the longitudinal translation is constrained for the individual layers with respect to each other. The constrained relative length change results therefore in compression and tension forces on the tape-springs.

Starting point in chapter 2 is a theoretical exploration of the potential of stacking. The energy storage in a single tape-spring is compared to the energy storage in a stack of concentric tape-springs, with decreasing radii inward. A unit volume is studied and using analytical approximations for the energy storage of a tape-spring, a formula is derived for the maximum possible energy increase. This possible energy increase differs per material, so as an example the materials polycarbonate and spring steel are compared. It was found that in an ideal situation, with continuous increments in material thickness, an increase in energy storage of factor 5.59 is possible for polycarbonate and for spring steel an increase of factor 33.6. Subsequently, this possible energy increase is compared to the maximum possible energy increase when considering discrete increments in thickness. It was found that 88% and 79% of this ideal energy storage increase can be achieved for polycarbonate and spring steel, respectively. To generalize this, a material index for maximizing energy storage in a single shell was derived, $\max\left(\frac{\sigma_y^3}{E^2}\right)$, as well as a material index for maximizing energy storage in a stack of tape-springs, $\max\left(\frac{E}{\sigma_y}\right)$. These two indices imply that materials such as polymers and elastomers are more suitable for maximizing energy in a single tape-spring, while spring steel is more suitable for maximizing the energy storage in a stack of tape-springs.

In chapter 3, a simulation and experimental approach is used to study the energy increase in a stack of equal tape-springs. For the simulations of the parallel tape-springs, an approach based on the superposition principle is proposed. This approach is applied to a stack of both two and three tape-springs. The method is experimentally tested for a stack of two tape-springs and showed qualitatively comparable behaviour. The substantial quantitative differences can at least partially be explained by the manufacturing uncertainties and uncertainties in the measurement method. Using the strain energy distributions from the simulations, it was found that the energy in a system of two closely placed equal tape-springs with a separation distance of $1mm$ doubled, while only increasing the maximum strain concentration with 3.5%. This result shows that stacking is suitable to increase energy storage in a tape-spring assembly, without yielding the material. In these simulations the interaction between the layers throughout the shell is not incorporated, and as a result the stack behaviour is similar

to the summation of the individual tape-spring behaviours. However, the measurement results do not show the same behaviour. For a separation distance of $0mm$, when the tape-springs are placed directly on top of each other, 8% increase in strain energy is observed at a rotation of $\frac{\pi}{2}$, when comparing the summation of the individual tape-spring behaviours to the actual stack behaviour. For a separation distance of $2mm$, 20% increase in strain energy is observed at a rotation of $\frac{\pi}{2}$. This strain energy increase is attributed to the increase in interaction between the layers throughout the shell. These experimental results point to a positive correlation between the separation distance between the individual layers of the stack and the strain energy in the system.

Overall, stacking is beneficial for maximizing energy storage. A theoretical limit is derived for parallel concentric tape-springs, and experimentally it is shown that maximal energy storage can roughly be doubled in stack of two parallel equal tape-springs before material yielding occurs, when separation distance between individual layers is low.

Bibliography

[1] J. Herder, *Energy-free Systems; Theory, conception and design of statically balanced spring mechanisms*, Ph.D. thesis (2001).

[2] G. Radaelli, *Synthesis of mechanisms with prescribed elastic load-displacement characteristics*, Phd thesis, Delft University of Technology (2017).

[3] G. Radaelli and J. Herder, *Gravity balanced compliant shell mechanisms,* International Journal of Solids and Structures **118-119**, 78 (2017).

[4] J. Nijssen, G. Radaelli, J. Herder, C. Kim, and J. Ring, *Design and analysis of a shell mechanism based two-fold force controlled scoliosis brace,* (2017) p. V05AT08A014.

[5] S. J. M. Van Der Kemp, *Design of a compact wearable arm support utilizing shape optimized compliant shell mechanisms*, Master's thesis, Delft University of Technology (2018), unpublished.

[6] K. A. Seffen and S. Pellegrino, *Deployment dynamics of tape springs,* Proceedings: Mathematical, Physical and Engineering Sciences **455**, 1003 (1999).

[7] M. De Jong, *Synthesis of a Force Generator using Two-Fold Tape Loops*, Master's thesis, Delft University of Technology (2018).

[8] S. J. Walker and G. S. Aglietti, *Modeling the hinge moment of skew-mounted tape spring folds,* Journal of Aerospace Engineering **20**, 102 (2007).

[9] H. Yang, R. Liu, Y. Wang, Z. Deng, and H. Guo, *Experiment and multiobjective optimization design of tape-spring hinges,* Structural and Multidisciplinary Optimization **51** (2014), 10.1007/s00158-014-1205-9.

[10] A. J. Cook and S. J. Walker, *Experimental research on tape spring supported space inflatable structures,* Acta Astronautica **118**, 316 (2016).

[11] C.-H. Lee, J.-W. Jeong, Y.-J. Kim, and J.-J. Lee, *Deployment shock attenuation of a solar array tape hinge by means of the martensite detwinning of niti shape memory alloy,* Review of Scientific Instruments **87**, 035104 (2016).

[12] K. A. Seffen, *On the Behavior of Folded Tape-Springs,* Journal of Applied Mechanics **68**, 369 (2001).

A

Literature study: Comparison of manufacturing methods for decimeter-scale compliant shell mechanisms

Comparison of manufacturing methods for decimeter-scale compliant shell mechanisms

Jan Maarten Verzendaal
Department of BioMechanical Engineering
Delft University of Technology
Delft, 2628 CD, The Netherlands

Compliant shell mechanisms are produced using a wide range of manufacturing techniques and materials. This study provides a clear overview of the different manufacturing possibilities for compliant shell mechanisms, and their properties. This review paper presents an overview of manufacturing techniques and preforms a comparison study. Composite, polymer, and metal manufacturing techniques are studied on five performance metrics: productivity, economic batch size, geometric freedom, accuracy, and process robustness. The resulting overview will help designers to select the right manufacturing technique, tailored to their requirements, by enabling comparison of available processes on the five metrics. The study shows that for composite and polymer manufacturing, economic batch size is an useful criteria for choosing the ideal process, limiting the amount of suitable processes, while for metal manufacturing geometric freedom is a suitable criteria as well.

1 Introduction

An increasing amount of research is done on compliant shell mechanisms and understanding their specific force deflection curves [1–9]. Most of these studies start with a numerical model, that is optimized to achieve a specific behaviour. After obtaining the theoretically ideal design, it is generally manufactured and experimentally tested. In order to compare the numerical model and the experimental test, the manufactured part should be as close to the design as possible. Any small deviation might alter the behaviour, so a suitable manufacturing technique is essential.

In recent studies, there are different compliant shells being build to validate a numerical model, using a very broad range of methods, including drape forming [5, 6], vacuum-assisted resin transfer molding, vacuum forming [5], roller and press bending [7], wet hand lay-up [8], powder bed fusion [9]. There seems to be no agreement on the best suited production process.

All manufacturing processes have their own shortcomings, as well as their own potential, and there exists no perfect process. Furthermore, each application has its own requirements, resulting in a different ideal manufacturing process. Therefore, this study provides an overview of manufacturing techniques to aid in making a well-considered choice, discussing their properties.

A performance comparison of the manufacturing techniques is performed for a specific geometry and materials, based on five different performance metrics. This comparison forms a good starting point in choosing the ideal manufacturing technique, and can be expanded with other performance metrics or materials.

Section 2 introduces the scope of the paper, defining the different design parameters and the performance criteria. Section 3 contains the results of the literature research: a short description of the different manufacturing techniques, and their corresponding performances. These results are divided in different material groups: composite, polymer, and metal manufacturing techniques. Section 4 contains a discussion of the results, starting with some observations, followed by the limitations of the study. Lastly, a brief summary and general conclusion are given in section 5.

2 Method

2.1 Design parameters

The following three factors often play a role during product design: the geometry or shape of the product, the material and its properties, and the manufacturing process. All these three factors, determined by the intended application, influence each other, and therefore all have to be taken into account in an integrated manner. This means that design is an iterative process, consequently evaluating this interplay. In this research, the starting point is a geometry, and subsequently a limited set of materials is chosen, based on their promising properties. Lastly, the applicable manufacturing processes are determined.

2.1.1 Geometry

Compliant shell mechanisms are defined by Radaelli as "spatially curved thin-walled structures able to transfer or transform motion, force or energy through elastic deflection" [5]. This is quite a broad definition. In this study, a reference geometry is specified, with some minimal features.

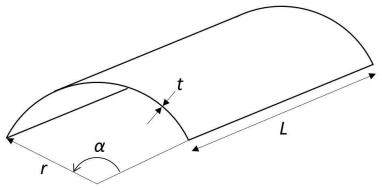

Fig. 1. The geometry of a tape spring with its specific parameters: radius r, thickness t, length l and subtended angle α.

Starting with the curvature, a minimum of one, transverse curvature is required, resulting in a tape-spring shape, as shown in Fig. 1. An optional extra could be another, longitudinal, curvature, resulting in a non-zero Gaussian curvature. A second optional geometry feature could be a non-constant cross-section, as studied by De Jong [10]. These extra geometry features result in more design freedom in the force-deflection behaviour of the mechanism.

The mechanism should be thin-walled, meaning that the thickness is small compared to the other dimensions. The absolute thickness, however, differs per material and design. The thickness is determined keeping the typical yield strengths for the material groups in mind, enabling large range of motion without plastically deforming [5–7]. For composites, a reference thickness t in the range of 1.0 - 3.0 mm is chosen, whereas for polymers, a reference thickness t in the range of 1.0 - 5.0 mm is specified. Regarding metals, a reference thickness t in the range of 0.1 - 0.3 mm is specified. The thickness is assumed to be constant throughout shell. The surface area of the compliant shell mechanisms is assumed to be in the range of 200 - 500 mm by 100 - 200 mm. All these measurements are taken, keeping an optional application of a human arm-balancer in mind.

2.1.2 Material

Following from the definition of a compliant shell mechanism, it should be able to elastically deform. This elastic behaviour is hugely dependent on the chosen material. This material choice, as one of the three factors in the design process, is mainly determined by the material properties. These properties can be selected based on the function of the product, but also on their processability, taking into account the geometry. Next to the material properties, costs and availability can play a role as well. Firstly, current research on compliant shells and their material choice is studied. Available materials can be categorized in the following four groups: ceramics, composites, polymers, and metals. As ceramics are not suitable for large elastic deformations, this group is left out of consideration. For the other groups, a selection of materials is considered in this study. This selection includes widely used materials, but do not contain the only suitable materials for compliant shell mechanisms.

Fiber-reinforced composites are a very promising group of materials. They combine the high stiffness of metals and the high deformability of polymers [11, 12]. Fiber reinforced composites create also more design freedom, compared to polymer and metal designs, as the fiber orientation and stacking can be altered, resulting in customized behaviour [13–16]. Different fibers can be used for reinforcement (e.g. carbon, glass, aramide). For high deformability, glass fibers are preferable, for their relative high strength and lower stiffness [17]. It has also been shown that, under pure bending, a fibre-reinforced polypropylene has fatigue-free operation up to three million load cycles [18]. A downside to glass-fiber reinforced composites (GF-RC) is the higher creep sensitivity compared to carbon-fiber reinforced composites (CF-RC) [19]. However, adding glass-fiber to a polymer, reduces the creep and stress-relaxation compared to unreinforced polymers [20]. Besides fiber reinforced composites, other composite materials are possible, such as laminated sheets or multi material molded parts [21]. However, this is left out of consideration in this overview.

Polymers play an important role in compliant mechanisms as well, because of their availability and ease of manufacturing [12, 20, 22]. A material often used in compliant shell mechanisms is polycarbonate (PC) [6, 12, 22]. Therefore, this material is included in the present study. Furthermore, polyurethane is a very promising material for complaint mechanisms, due to its high elastic energy storage and large elastic strain limit [6]. Polyurethane (PU) comes both as a thermosetting and as a thermoplastic polymer. In this study, the thermoplastic polymer (TPU) is studied, because of its better manufacturability.

Next to composites and polymers, metals are often used in compliant mechanisms, due to their high yield strength and their creep resistance. The ratio of the yield strength with respect to the Young's modulus should, however, be sufficient. Both stainless steel, especially spring steel with its high yield strength, is used for this application, as well as titanium, both in production and simulation [1,2,6,7,20,23–25]. The metals included in this study are therefore a (spring) steel and a titanium alloy.

2.1.3 Manufacturing process

Lastly, the applicable manufacturing techniques have to be determined. Starting point for the mapping of these techniques is a literature research on methods available for manufacturing shells, in the broadest sense. This research is conducted in Scopus, using the search queries shown in Table 1.

This search resulted in 674 documents. From this set, the irrelevant results are removed, firstly based on their title, and secondly looking at the abstract. In the search query, results containing 'Core shell' are already excluded, as these results contain manufacturing methods of a certain type of nanoparticles. Papers, regarding the following subjects, are excluded as well: joining techniques, in depth modelling (e.g. resin flow model, buckling prediction etc.), shells from nature (e.g. shrimp shell), non-structural shells (e.g. nanoparticles), shell mould casting, big, architectural building panels, LCD and other display panels, and design specific papers. Besides this, sandwich panels are left out of consideration, because these are primarily designed to be as rigid as possible, making them not suitable for compliant mecha-

Table 1. Search queries used in Scopus

Query	Search keywords	Search in
#1	Manufactur* Fabricat* Production	Title
AND		
#2	Shell (curved OR dished OR corrugated) sheet thin walled structure panel	Title
AND		
#3	Casting Deformation Moulding Molding Composite Powder Prototyping Forming Extrusion Shaping	Title-Abstract-Keywords
AND NOT		
#4	Core shell	Title-Abstract-Keywords

nisms. The remaining set consists of 98 search results. These papers were further studied, including relevant references.

The resulting manufacturing methods are presented in the following categories: Composites, Molding, Additive Manufacturing, Casting, Deformation, Deposition, Machining, and Powder methods, based on CES EduPack [26].

2.2 Performance Criteria

All manufacturing methods have their (dis)advantages, and therefore the best manufacturing method for each situation has to be determined separately. To make this choice, the different processes are evaluated on several performance criteria. Ideally, a fabrication process performs good on the following properties:

- **Productivity**: In order to increase productivity and decrease operating costs, production (cycle) time has to be as short as possible.
- **Economic batch size**: When choosing a manufacturing process, the desired batch size should be tailored to the economic batch size of the process, being the amount of products that can be produced for a reasonable price per product.
- **Geometric freedom**: Determining the solution space of a design, the geometric freedom has to be sufficient to be able to create the desired kinds of shapes. More freedom results in more design possibilities.
- **Accuracy**: The accuracy of the manufacturing process can be expressed as the deviation of the produced item with respect to the desired, designed item. As bending in compliant mechanisms plays a major role, the thickness is considered to be the most influential parameter of the design accuracy, because this influences the behaviour the most.
- **Process robustness**: The manufacturing process should be as robust as possible. Sensitivity for defects during manufacturing, such as voids, fibre misalignment, non-uniform fibre content, residual stress, springback, and warpage, influences the process in a negative way, resulting in decreased performance and need for (elaborate) modelling to prevent the defects.

The order of the above mentioned properties is not necessarily based on importance, but is arbitrarily chosen. The metrics are chosen to ensure that both the economical factors are taken into account (productivity, economic batch size), as well as the technical factors (geometric freedom, accuracy, process robustness).

To rank the different manufacturing methods with respect to each other, a metric is introduced for each of the properties. The metrics are divided into four different scores: '- -', '-', '+', and '++'. For most metrics, the higher score corresponds to good performance, however, for the metric of economic batch size, this doesn't hold. This metric represents the most feasible batch size for a certain manufacturing technique. For geometric freedom, the main focus is on the general shape of the shell, not necessarily on the design freedom in thickness variation for example. The metric for accuracy of the thickness of the shell is determined by the variation introduced during manufacturing. The last metric, process robustness, is a measure of how sensitive the process is to imperfections, such as voids, residual stress, warpage, spring back etc. Because all manufacturing techniques have different difficulties to cope with, there is not a clear a priori distinction within this metric. Instead, manufacturing techniques are evaluated on aspects like the amount of imperfections that play a significant role and the amount of modelling or other techniques needed to prevent such imperfections. The complete definition of the performance metrics are shown in Table 2.

3 Results

Most of the found manufacturing techniques were focused on applications in the automotive or aviation sector. This is explained by the frequent use of curved or complex shaped body panels. However, another interesting application found was the use in medical devices, both internal implants [27] as external body supports [28–33].

An overview of the manufacturing techniques will be given for each material group: firstly composites manufacturing techniques, secondly polymer manufacturing techniques, and lastly metal manufacturing techniques. In Fig. 2, all manufacturing methods discussed in this paper are shown.

3.1 Composite manufacturing techniques

Manufacturing techniques for composites materials are very specific, such that a special distinction is made in the manufacturing technique overview (see section 2.1.3). Composites consist of a polymer matrix, and particle, fiber, or

Table 2. Performance Metrics for manufacturing methods

Metric \Rank	- - (Very Low)	- (Low)	+ (Medium)	++ (High)
Productivity (cycle time)	>1 hour	10-60 min	1-10 min	<1 min
Economic batch size	Prototyping (<10)	Small (10 - 500)	Medium (500 - 10,000)	Large (>10,000)
Geometric freedom	Single curved sheet	Corrugations	Double curved sheet	Freeform surface
Accuracy (thickness deviation)	>30%	10-30%	2-10%	<2%
Process robustness	Very Low	Low	Medium	High

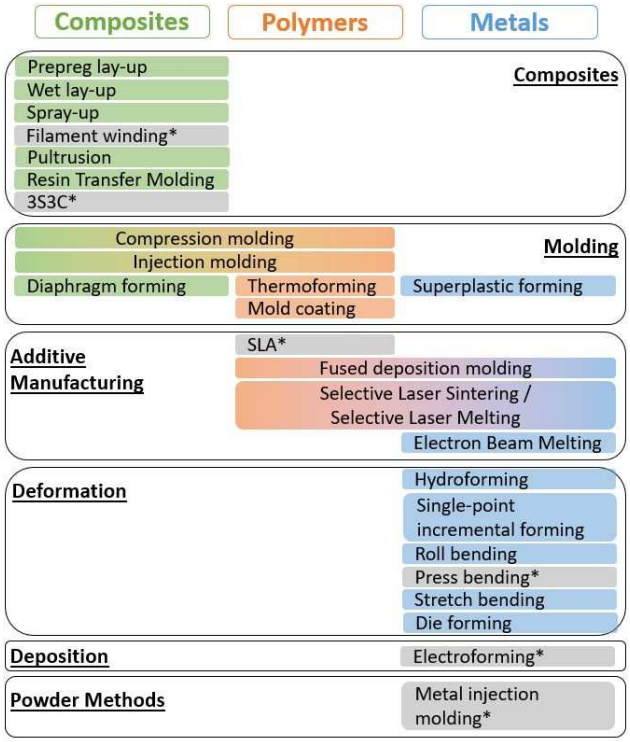

Fig. 2. An overview of the search result for composite, polymer, and metal manufacturing techniques, which can be used for the production of medium-sized compliant shell mechanisms. The manufacturing processes are categorized in composites, molding, additive manufacturing, deformation, deposition, and powder method techniques, according to [26]. The starred and grey boxed manufacturing techniques came up in the search results, but are not taken into account in the comparison, as they are not suitable for the chosen geometry and material or are still in the experimental phase.

some other kind of reinforcement. Most composite matrices are fabricated with thermosets, however, thermoplastic matrices are an option as well [34]. As most manufacturing techniques are focused on thermosets, the exceptions are mentioned in the description of the fabrication methods.

Prepreg Lay-up Prepreg lay-up is a manufacturing technique which uses polymer pre-impregnated (prepreg) fibres, which are placed into a mold and vacuum bagged, after which it is cured. This curing takes place in an autoclave. Therefore it is also known as autoclave processing or the vacuum bagging process [35]. An autoclave is an expensive tool for curing the composite under pressure and heat. However, a lot of research is done on out-of-autoclave curing of prepregs, showing promising results [36]. The prepregs can take several forms. Prepregs can come in the form of individual fibres, tapes, or complete sheets. When using individual fibres, it is possible to optimize the stress distribution, and a variable stiffness can be achieved [37]. It can also be in the form of tapes, as shown in [38]. The process for tape prepregs is very similar to fibre prepregs [39], and can be done manually (hand lay-up), or automatically.

Prepreg lay-up is highly labour intensive, with low production rates, and because it is an open mold process, it is less dimensionally stable than other, closed mold processes [40, 41]. Although there are some special prepregs with very short curing times [42], in general it takes several hours to manufacture a product. Besides this, other manufacturing challenges are maintaining accurate fibre orientations, especially in the case of manual lay-up, preventing entrapped air between layers, and warpage due to residual stresses [43]. An automated process reduces this variation, and can help overcome some of these challenges, but the process robustness is still quite low. The geometric freedom is very high using prepreg lay-up, but wrinkling might be an issue in complex shapes, as the prepreg has to be sheared to the correct position. Cutting the prepregs is also a possibility, but than the advantage of the continuous fibres is lost. The thickness variation in this process depends highly on the shape, as the thickness will change in corners/bends, causing "spring-in" effect, in which the product does not cool down evenly resulting in warpage [44]. The thickness variation can be of the order of 10% [45, 46].

Roll wrapping is considered a distinct production method by Mazumdar [35], but as it is very similar to prepreg lay-up, the only difference being the cylindrical or round tapered tool, this will not be considered separately.

Wet Lay-up Wet Lay-up uses, in contrast to prepreg lay-up, 'clean', dry fibres, without impregnation. The matrix material of the composite is first applied to the mold, after which the dry fibres are added to the resin and impregnated with the resin using a roller. This process is repeated, until the desired thickness is acquired. By placing the fibres, there is a lot of freedom in the process, just like the prepreg lay-up [35].

The manual placing and impregnation of the fibres make that this manufacturing process is even more sensitive to hu-

man variation, decreasing the repeatability of the process. Curing ussually takes place at ambient temperature and pressure, instead of in an autoclave. This reduces the capital costs of the process, but curing the resin at these conditions takes usually several hours [47]. Overall, the performance of this process is comparable to the prepreg lay-up.

Spray-up The spray-up process is very similar to the wet lay-up process, but applying the resin and fibres mixed together in a spraying manner on a mold, instead of placing them individually. This makes the process faster and less expensive. However, the fibre volume fraction and the thickness distribution is harder to control [35]. Another option would be spraying resin onto an edge-shaped textile formwork [48].

With respect to prepreg lay-up and wet lay-up, spray-up is more suitable for higher volume production [40]. The mechanical properties, are due to the chopped fibres, less than the fabrication methods using continuous fibres.

Filament winding Filament winding comes both in dry and wet filament winding [35, 49]. Because the shape of the product is round, closed (vessel) or open (pipe), it is not directly useful for the manufacturing of compliant shells, as a lot of post-processing is needed to get to the minimal required geometry of a tape spring. This method will therefore not be taken into account.

Pultrusion In the pultrusion process, prepreg fibres are pulled through a die to create a specific, continuous profile of constant cross-section. Due to the continuity of the process, it can produce high volumes for low costs [35]. To get to the final geometry, the profile has to be cut to the desired dimensions.

The geometric freedom is limited, as only a straight, corrugated profile is possible. The productivity, on the other hand, is high, as this is a continuous process, resulting also in a very constant quality [50]. The speed can be as high as 1 meter per minute, depending on the geometry, with a tolerance of a few percent [51]. There may be some defects present, for example residual stress due to unstable curing, or glass fibers on the surface of the profile [52].

Resin Transfer Molding The resin transfer molding (RTM) process is a process with a lot of variants. The standard RTM uses a closed mold, in which a continuous fibre preform is placed, which is filled with resin. This resin than cures, after which the product is removed from the mold. The RTM process results in high stiffness and strength, but has low production and surface quality [53].

The RTM process has cycle times of 10 - 15 minutes [54]. The typical production volumes is up top 10,000 units [55, 56]. The products can be complex shaped, but care has to be taken to the fibre placement. For complex shapes, 3D shaped preforms are preferred, in order to prevent the fibres from being displaced from their designed reinforcement pattern [57]. Also, one should be aware of dry spots in the preform, and make sure the resin is evenly distributed. RTM has an excellent thickness tolerance, as it has a two-sided mold. The accuracy is therefore much defined by the accuracy of the mold.

Next to the standard RTM process, the process variant high-pressure RTM (HP-RTM) exist as well. HP-RTM distinguishes itself by applying high pressure to the resin flow, in order to achieve higher productivity by shorter cycle times and better fibre impregnation. A disadvantage is that the equipment is much more expensive: the injector has to be able to inject faster, and the molds should be very precise to prevent leaking [53].

Another variant on the RTM process is vacuum-assisted RTM (VA-RTM). In this variant, the resin flows due to an applied vacuum, instead of heat or pressure. This process only uses a one-sided mold, as a vacuum bag is added on top. This reduces the costs of the process. The vacuum also helps to improve strength and reduce void contents [53, 58, 59]. The production volume is, however, somewhat lower than the standard RTM [60]. Also, the accuracy is less, as only a one-sided mold is used, resulting in a thickness deviation up to 10% [61, 62].

Other processes, such as liquid resin infusion (e.g. SCRIMP) [63], resin film infusion [64], and structural reaction injection molding [35] are all very similar to the RTM process or one of its variants. Therefore, these processes are not treated separately.

Single step sheet consolidation of curved composites (3S3C) Kazmi et al. introduces a new manufacturing method: single step sheet consolidation of curved composites (3S3C) [65]. This method is a combination of compression molding and resin infusion, and is able to fabricate curved thermoplastic composites. This process, however, is only described in that single paper, and is not evaluated further on a bigger scale. Therefore, by lack of sufficient literature, this manufacturing method is left out of consideration.

Compression molding For compression molding of composites, different types of raw material are sheet molding compound (SMC), bulk molding compound (BMC), glass mat thermoplastics (GMT), and prepregs [35, 53, 66]. Compression molding of composites is very similar to the compression molding of other materials, only containing reinforcement. The process has two molds, in between the material is placed, after which the molds are compressed.

Compression molding of SMC of BMC is very similar. SMC comes in the form of a sheet, while BMC comes in the form of a rope. BMC typically has a lower fiber volume fraction and shorter fiber length with respect to SMC, and therefore SMC, with better mechanical properties, is only considered in this study [35]. Compression molding of SMC begins with cutting the sheet into blanks, which can be molded. SMC can be molded in medium-high volumes, and has a short cycle time and good surface finish. GMT is similar to SMC, but is made from a thermoplastic matrix instead of a polymer matrix.

The cycle times for compression molding can be less than a minute [67]. This contributes to the fact that this

methods is very well suited for production quantities that exceed 10,000 parts [68]. It is possible to create both complex geometries as well as integrated functions, like inserts or colouring [69]. While cooling the molded product, non-uniform shrinkage can occur due to the complex geometry. The repeatability is very high, as the molds are of high quality, and accuracy of the compression molded product is high [70].

Compression molding of prepregs is done as well. The prepregs are compressed and cured between to heated molds, resulting in products of uniform thickness. This process has a cycle time of 5+ minutes, equipment costs [71]. The vacuum-assisted variant of this process performs better, as it has less defects in the final product [53]. A combination of PCM and SMC is also seen in literature, resulting in a complex-shaped product [69]. This method will, however, not be taken into account separately.

Injection Molding Injection molding thermosets can be done using BMC, but thermoplastic injection molding is possible as well [35]. The process, in which the feedstock material is heated and injected into a mold, has high-rate production, but has lower mechanical stiffness and strength, due to the shorter fibres in BMC [53].

With injection molding, almost every surface shape (e.g. diffractive, freeform, nano structure) becomes feasible without extra costs [72]. Cycle times range from 10 to 100 s and are controlled by the cooling time of the melted plastic [73]. The typical production volume for injection molding is very high, comparable to compression molding. High quality molds are required, resulting in good dimensional tolerance. Like in compression molding, one has to be aware of the possible shrinking, and take that into account when designing.

Diaphragm forming Lastly, diaphragm forming can be used to manufacture thermoplastic composites. This process is similar to the thermoforming technique for plastics, heating a sheet of material using a heated diaphragm, and then shaping it against a mold using air pressure. A design limitation of this method is the constant thickness of the sheet [35].

A main issue when using thermoforming is the non-uniformity in the part thickness. The thickness tolerance is typically 10 - 20% [74]. The uneven distribution is a result of the 'freezing' of the sheet thickness when it touches the cold mold [75]. A heated mold helps to prevent this. Prestretching the sheet minimizes the part non-uniformity as well [75]. Warpage can be an issue as well, as the sheet is not cooled evenly after the forming process. The cycle times of thermoforming are short compared to processes such as hand lay-up and autoclave consolidation [76]. The production volume is high, but for less quality molds a smaller batch size is possible as well. Complex shapes can be produced, but this will influence the thickness distribution over the product. If only drape forming is used, complex shapes with cavities need an extra forming step to get to the final shape.

Table 3. Performance comparison of different composite manufacturing techniques, based on the ranks shown in Table 2. The four different scores, '- -', '-', '+', and '++', indicate how good a production process scores on that metric. Economic batch size is an exception, as the scores for that metric indicate the most economical production size.

	Productivity	**Economic batch size**	**Geometric freedom**	**Accuracy**	**Process robustness**
Prepreg Lay-up	- -	- - / -	++	-	- - / -
Wet Lay-up	- -	- - / -	++	-	- -
Spray up	- -	-	++	-	- -
Pultrusion	++	++	-	+	++
Resin Transfer Molding	-	+ / ++	++	+	+
Compression molding	++	++	++	+	++
Injection molding	++	++	++	+	++
Diaphragm forming	-	- / +	+ / ++	-	+

3.2 Comparison composite processes

For composite manufacturing, the techniques are evaluated in Table 3. Seven out of the eight manufacturing techniques are capable of creating complex shaped geometries. The economic batch size, on the other hand, has a broad range of values, creating a good first step to choose the best suited process. The economic batch size is large for all the manufacturing techniques with high productivity. Furthermore, as the repeatability is higher for all the high volume production processes, the accuracy is in general higher. The manual techniques all perform worse than the automated processes regarding accuracy, as well as process robustness. This is due to the human variation factor that comes into play.

3.3 Polymer manufacuring techniques

3.3.1 Molding

Compression molding Polymers can be shaped using compression molding, as described in section 3.1 for composites manufacturing.

Injection molding Injection molding of polymers is possible, and is similar to the process of injection molding composites. A description of the process is given in section 3.1.

Thermoforming Thermoforming is a very diverse manufacturing technique, that has several variants. Throne makes a clear distinction between the different variants, divided in three categories: one-step, two-step, and three-step forming processes [77].

The one-step forming processes are drape forming, vacuum forming, free forming, matched mold forming, autoclave forming and diaphragm forming. In drape forming, a heated sheet is draped over a positive mold to get the required shape. Vacuum forming uses a negative mold and a vacuum pressure to shape the sheet to the mold. For free forming, no mold is necessary, as the sheet is heated and shaped using only pressure difference. Opposed to drape forming and vacuum forming, this method produces an uniform thickness shell. Matched mold forming uses two matched molds, between which the heated sheet is shaped. This method is only used for sheets too stiff to shape using the other techniques. An alternative thermoforming technique is autoclave forming, in which a sheet is pressed against an one-sided mold, which is placed in an autoclave. Lastly, diaphragm forming contains a heated diaphragm, that when in contact with the sheet, is pressed against a negative mold. This method is already explained in the composite section, section 3.1.

The two-step forming techniques combine one of the above mentioned forming technique with a preforming technique, either pneumatic of mechanic. This helps reducing the thickness variation in the product. Another two-step process is pressure forming, which combines a vacuum on one side of the sheet to draw it against the mold, after which a pressure is applied to finalize the shaping process. This can be useful for very stiff sheets.

The three-step forming processes are combinations of the different preforming and shaping techniques. Because these are not very distinct from the processes already mentioned, these will not be further discussed here.

The performance of thermoforming on the metrics listed in section 2.2 is already described in section 3.1, under diaphragm forming.

Mold coating As compression and injection molding are applicable only for mass production, there is also need for an adaptable and inexpensive manufacturing technique to produce prototypes. This need is identified by Lee et al. [78], in which a manufacturing technique is studied, that meets this need: mold coating. In this process, a curved surface is coated with a polymer solution, which is cured.

With mold coating, double curvature shells can be produced in very small batches. The production time of a single shell depends on the curing time, which is roughly 10 minutes, making the total production time high, compared to the previously described molding technologies. The mold coating process is based on draining the polymer under the effect of gravity, so a freeform surface can be difficult to manufacture, as the polymer solution can accumulate in cavities. The final, uniform, shell thickness can be tuned by delaying the moment of pouring the polymer solution on the mold, and experiments show that the thickness deviation can be up to 10%. As this process is very basic, not much defects will occur. But because it is a manual process, human variation will play a role in the production.

3.3.2 Additive Manufacturing

Following the example of [23], the additive manufacturing (AM) methods are divided into three categories: photopolymerization processes, extrusion-based systems, and powder bed fusion. From each of these categories, the basic working principle and an exemplary process will be discussed.

Photopolymerization process In the photopolymerization processes, polymerization and solidification takes place when a liquid polymer is exposed to UV-light, layer by layer. An example is stereolithography apparatus (SLA).

Photopolymers used in SLA are cross-linked, opposed to the branched molecular structure of injection molded thermoplastics for example. As a result, the photopolymers do not melt and exhibit much less creep and stress relaxation [79]. This is a good property for compliant mechanisms. The polymers used in SLA are thermosets, and a requirement for the material is that is has to be UV-curable [80]. Therefore, the thermoplastic polyurethane and polycarbonate are not suitable for this process. However, photocurable polyurethane is available for stereolithography [81], as well as polycarbonate-like materials [82]. As the material properties differ between the 'standard' polymer and the photopolymer, this process will not be taken into account in the overview.

Extrusion-based system The polymer is liquefied by heat, extruded through a nozzle, and deposited in the right place where it solidifies. An example of this is Fused Deposition Molding (FDM). An alternative to using heat is a chemical change that causes solidification. However, as this latter approach is less common, this study will focus on the former.

3D printing is known for its long building times. In the case of FDM, this also holds. A study on optimizing build speed shows that for different experiments, all buildings times were above 60 minutes [83]. The bigger the size of the product and the higher the accuracy and filling density, the longer the build time. Due to this slow production speed, the economic batch size is very small. This technique is mostly used for prototyping or highly customized designs. The geometric freedom in FDM is very high, as with support structures complex shapes can be made. This process deposits the material layer by layer, resulting in a non-smooth surface. Beside the smoothness of the surface, this also influences the properties, as they are anisotropic, which is a huge drawback of this production process. The orientation of the printed part is therefore crucial. The dimensional accuracy lies between 0.1 and 0.3 mm [84]. The process is sensitive for defects, mainly due to the cooling of the material after extrusion, causing warpage. Next to this, misalignments of print platform or nozzle can be a problem, as well as (partly) clogging of the nozzle [85]. Also the process parameters should be correctly adjusted to the material. The overall performance of the process highly depends on the machine and its settings.

Powder bed fusion In powder bed fusion, the raw material used is powder. The powder is placed layer by layer, which is than joined together by melting or sintering the particles or adding adhesive. Examples are Selective Laser Sintering (SLS) and Selective Laser Melting (SLM). In the former, the particles are not heated above melting temperature, but sintered together, while in the latter process the particles are heated above melting temperature, melting them together. When melting the material, a higher strength is achieved, but a downside is the increased heat affected zone around the product, which results in inaccuracies [79].

The building times are usually longer than an hour for this layer-wise process. Similar to FDM, this makes that the process is best suited for prototyping. However, when introducing line-wise heating with multiple lasers (instead of point-wise with a single laser), together with a batch of products combined in one powder bed, this can increase the productivity moderately [79]. The process is capable of producing complex shapes, as the powder bed is acting as support for the sintered/melted material. The resolution for powder bed fusion processes is better than for extrusion based systems, with a resolution of 40 - 120 μm, which is around 10% of the order of magnitude of the reference thickness. Defects to watch out for are once again the cooling related warpage and partly dense products.

3.4 Comparison polymer processes

For polymer manufacturing, the manufacturing techniques are evaluated in Table 4. For these six manufacturing techniques holds that only one process is not suitable for freeform surfaces, showing the good formability of polymers. Furthermore, the economic batch size has a broader range of values, creating a better starting point for the manufacturing choice. In that respect these two metrics are very similar to the composite manufacturing techniques. On top of this, the productivity is highly correlated tot the economic batch size, as low production time result in high economic batch sizes. The process robustness is best for the high production volume processes, as these processes have a high repeatability.

Table 4. Performance comparison of different polymer manufacturing techniques, based on the ranks shown in Table 2. The four different scores, '- -', '-', '+', and '++', indicate how good a production process scores on that metric. Economic batch size is an exception, as the scores for that metric indicate the most economical production size.

	Productivity	**Economic batch size**	**Geometric freedom**	**Accuracy**	**Process robustness**
Compression molding	++	++	++	+	++
Injection molding	++	++	++	+	++
Thermoforming	+	- / +	+ / ++	-	+
Mold coating	-	- -	+	+	+
FDM	- -	- -	++	-	- -
SLS / SLM	- -	- - / -	++	- / +	- -

3.5 Metal manufacuring techniques

3.5.1 Molding

Superplastic forming In superplastic forming (SPF), a superplastic metal sheet is heated to more than half of the melting temperature, after which it is possible to shape the sheet, using standard thermoforming techniques for polymers. In order for a metal sheet to be superplastic, there are three primary requirements: extremely fine grain size (less than 10 μm); high forming temperatures (greater than 0.4 T_{melt}); low strain rates [86]. SPF is based on sliding grains past each other, and the high forming temperatures are needed to allow diffusion in the material [87]. This makes the process only applicable to materials with specific superplastic microstructures, but titanium alloy sheets are available with the right properties [88]. SPF performs good on dimensional accuracy, surface finish and creating complex shapes, incorporating different functions [88].

One major disadvantage of SPF is the high cycle time, which can be 2 hours [89]. These high cycle times are caused by the low strain rates [86]. The economic batch size is small to medium [87], and according to Chatterjee et al. [88] roughly in the range of 100 to 10,000. Thinning occurs in this process in the same range as thermoforming, being more than 10% [88]. The geometric freedom and process robustness is good, just like the thermoforming techiniques.

A process variant name quick plastic forming (QPF), described by Guofeng et al. [89], is a superplastic forming technique, including an extra preforming step. It fits well in the two-step forming processes of thermoforming, as described in section 3.3.1. This process reduces the cycle time, as well as the costs, as this might include more ordinary sheet metals.

3.5.2 Additive Manufacturing

Similar to the approach in section 3.3.2, a categorization can be made for additive manufacturing of metals into categories. The categories 'extrusion based systems' and 'powder bed systems' are applicable in the case of metals, but in a slightly different manner. The basic principle as explained in section 3.3.2 is identical, so only the differences will be pointed out in this section.

Extrusion-based systems Metals can be shaped using FDM, similar to polymer. The difference in production is that, as the liquefaction of purely metal particles is hard, a polymer filament is used with metal particles in it. The polymer acts merely as a binder, and after printing the parts will get a heat treatment, in which the polymer is removed and the metal is sintered [90]. The filaments can have up to 85%

of metal in them, but are not usually on offer with titanium particles [91]. The properties of the process are similar to the polymer FDM process, but on top of this, the need to remove the binder and sinter the part might result in extra voids.

Powder bed fusion Powder bed fusion methods are more often used for metal printing than extrusion-based systems. For metal processing, there are even more powder bed fusion systems available, namely electron beam melting (EBM). EBM is very similar to SLM, only the method of energy absorption is different; instead of using a laser and material absorptivity, an electron beam and material conductivity is used [79]. As the working principle of EBM is based on material conductivity, this only works with metals. The resulting scanning speeds are very high, but the accuracy is worse with respect to SLM. An example of a titanium compliant mechanism produced by EBM can be found in the work of Merriam et al. [92]. The properties of the powder bed fusion process are mentioned in section 3.3.2.

3.5.3 Deformation

Hydroforming Hydroforming is a manufacturing method which uses a single die and hydraulic pressure to push a metal sheet into the mold, profitable for low-medium volume production [93, 94]. Forming a panel this way can take 5 to 15 minutes [93], and thinning can be up to 30% [95, 96]. Thinning can be reduced by lubrication, special materials, annealing and preforming, but it is never eliminated [97]. Complex shapes are possible with hydroforming, but complicates the selection of the appropriate loading path. Simulation techniques for determining the loading path are currently limited to simple shapes [94]. A suboptimal process can result in wrinkling, bursting or unexpected thinning. Besides this, one has to be aware of possible springback behaviour after the shaping process, which plays a bigger role in materials with a relatively high yield strength.

Other, slightly different versions of hydroforming, such as liquid impact forming and flexforming, are not discussed in this paper [94]. Also, explosive forming, where the hydraulic pressure is obtained with an explosion, is not discussed here.

Single point incremental forming Single point incremental forming (SPIF), dieless forming, or incremental sheet forming, is a manufacturing process in which a metal sheet is clamped at the sides, and a computerized rotating forming tool is deforming the sheet by locally pushing on the sheet in an incremental way. This process is developed for the production of prototypes or small batches [98–100]. A major limitation of the process is the high production time, making it unsuitable for mass production. In a case study for a metal sheet part in a door panel for an airplane, a production time of almost 2 hours is noted [101]. The geometries that can be produced can have double curvatures, however, corrugated structures are only possible if a backing plate is used. This backing plate is a rigid piece on the back side of the sheet that locally prevents deformations. Single-curved shapes are possible if the sheet is clamped only on the flat sides. Thinning in SPIF is very high and can be up to 70% [102]. The defects that occur in SPIF are threefold [103]. Firstly, there is sheet bending close to the major base of the part, which can be solved through the use of a backing plate. Secondly, elastic springback occurs after deformation, which can be reduced by optimizing the toolpath [99]. Thirdly, a so called "pillow" effect is present in the undeformed material on the minor base of the product, creating a concave curvature.

There are other variants on this process available, one of which is two point incremental forming (TPIF), in which a second tool or partial die is added at the other side of the sheet to improve the process performance [100]. In TPIF, springback can be reduced further by 'squeezing' and 'reverse bending' [104]. A combination of SPIF and stretch bending is also possible, which results in an improved geometrical accuracy and sheet thickness distribution, and enables changes in curvatures within one panel geometry [105].

Bending According to [93], bending can be achieved by roller bending, press bending, or stretch bending.

Roller bending uses two rollers, between which a sheet is rolled to the desired curvature. The thinning in roller bending is evenly distributed, resulting in a constant thickness sheet [106]. Roller bending is a continuous process with a very high production rate, typically running at speeds from 2 to 200 m/min, depending upon desired shape [107]. As the development and optimization of the process is time consuming and costly, it is best suited for large production volumes [108]. The geometry has generally only an one-way curvature. The curvature of this radius should be more than 200-300 mm, otherwise press bending should be used [93]. The production of a curved corrugated sheet is possible, when using specifically shaped rollers [109].

Press bending is the process of pushing and folding the sheet material. This process is typically used for one-way curvature geometries only [93]. However, the typical bends are very sharp, so this cannot achieve the tape-spring like geometry. Therefore this manufacturing process is left out of consideration.

Stretch bending can create geometries with a nonuniform one-way bent shape, in contrast with the roll bending and press bending processes. However, this process is also not suitable for double curved geometries. With prestretching the plate, net-thinning can be achieved, resulting in a constant thickness of the part [110]. According to Cooper [110], the productivity is typically in the range of 3-8 parts per hour, and the process is suitable for processing high volumes [93]. There may be some springback present in this process, but this is largely eliminated due to the relative uniform thinning and stress distribution [111].

A related process to roll bending is the English wheel. This wheeling machine uses two wheels, in between which a sheet is rolled back and forth to get the desired shape, enabling the production of double-curvature shapes. Conventional wheeling is not very common, but a new method has been developed [112]. However, this new method is still experimental, therefore this one is left out of consideration.

A process combination of roll bending and incremental sheet forming, called incremental roll bending, is described by Yoon and Yang [113, 114]. This process combines the flexibility of incremental forming and the continuous bending deformation of roller bending. This process is, however, not taken into account during this study.

Die forming Die forming, press forming, or stamping is a deformation technique, involving two dies: a negative and a positive one. These two dies are pressed together, shaping the metal sheet to the desired geometry. The major disadvantage is the cost of the dies, making the process only suitable for production of several thousands of parts [93]. The forming time for a single part, however, is very low, as it involves only one fast stamping action. It is possible to create complex shaped parts with die forming, but that could mean using a two-step stamping process, as shown for corrugated structures by Choi et al. [115]. The thinning that occurs during this process is highly dependent on the geometry, and can range from 15 to 40% [115, 116]. Besides thinning, springback can be an issue as well.

3.5.4 Deposition

Electroforming The technique of electroforming falls in the category of deposition. With this technique, very precise shells can be formed on wax models, having complex shapes [117]. However, this manufacturing technique is not applicable to either steel or titanium [118], and is therefore not considered.

3.5.5 Powder methods

Metal Injection Molding Metal can be injection molded on standard injection molding machines, but some changes have to be made to the process. A mixture of particles should be used, including metals and a binder, which after injection molding is sintered. However, manufacturing of the reference geometry (section 2.1.1) is not possible with metal injection molding: the maximum dimension in metal injection molding is 150 mm [119].

3.6 Comparison metal processes

For metal manufacturing, the different processes are evaluated in Table 5. The AM processes are best suited for small production volumes, as the production time is relatively high. Due to, among other things, the layered build-up, both processes perform very low on robustness. The geometric freedom of these AM processes are very high, so any desired shape can be build, within the building range of the used machine. The range in geometric freedom for the metal processes is broader, relative to the composite and polymer processes, making these metric values, together with the economic batch size, helpful in choosing a manufacturing technique.

Table 5. Performance comparison of different metal manufacturing techniques, based on the ranks shown in Table 2. The four different scores, '- -', '-', '+', and '++', indicate how good a production process scores on that metric. Economic batch size is an exception, as the scores for that metric indicate the most economical production size.

	Productivity	**Economic batch size**	**Geometric freedom**	**Accuracy**	**Process robustness**
Superplastic forming	- -	- / +	+ / ++	-	+
FDM	- -	- -	++	-	- -
SLS / SLM / EBM	- -	- - / -	++	- / +	- -
Hydroforming	- / +	- / +	++	-	+
Single point incremental forming	- -	- - / -	+	- -	-
Roll bending	++	++	- -	++	++
Stretch bending	- / +	++	- -	++	++
Die forming	++	++	++	- - / -	-

4 Discussion

The results of this study give a clear overview of the main manufacturing techniques available for shells. For each material group, a separate comparison is made between the different production processes. In all these comparisons, the repeatability for high volume productions is high, which results in good, constant accuracy. Economic batch size appears to be a good starting point for the selection of a production process for every material type. As this is very general for any kind of design, another metric should be taken into account for compliant mechanisms as well: accuracy of thickness distribution. This comes from the fact that for compliant mechanisms, bending behaviour is very important, and that is highly influenced by thickness deviation [5].

As the most used fabrication techniques are included in this study, it gives a global overview of the available options and their performance, and therefore creates a good first step in choosing the right manufacturing technique.

Interestingly, no manufacturing techniques showed up in the categories of Machining or Casting. For machining, this might be explained by the high costs due to the amount of waste material. Moreover, it is a technical challenge to use the technology of milling on a very thin plate, as the plate will be quite flexible. As regards casting, this technology is not well suited for thin sheets, due to problems with the material flow.

The results show that the economic batch size is highly correlated to the productivity. This shows that processes with high productivity are very well suited for high volume production. An exception in this is stretch bending of metal

sheets. For stretch bending holds that the productivity is not high, but it is still suited for high batch sizes. This is probably because stretch bending is often used for large curved panels that have a good accuracy, close and consistent tolerances, which are hard to manufacture using other techniques [111]. Furthermore, it can be seen that in general high volume production have a good repeatability, resulting in high process robustness. The possible defects are mostly getting rid of in the designing of the process and the part, so therefore during the process itself the parts will not be very sensitive for sudden defects. However, care should be taken in the designing of the process, because if the process is not correctly adjusted, it will result in low quality parts. This could mean, for example, that flow analysis might be needed for injection molding.

The scope of the project is defined by a certain geometry, a selection of materials, a limited amount of manufacturing techniques, and only five performance metrics. In further research, the study can be expanded in these areas.

Firstly, regarding the geometry, an optional extra that would be interesting is a non-uniform thickness. This non-constant cross-section would result in different force-deflection behaviour, but different from the change in subtended angle as described by De Jong [10].

Secondly, the material selection does not include all promising materials for compliant mechanisms. One promising set of materials for compliant mechanisms not yet mentioned are Bulk Metallic Glasses (BMG). These materials show a lot of potential, as they exhibit high yield strengths and strength-to-stiffness ratios of almost twice that of most high-performance crystalline titanium alloys [120]. However, they are not broadly available yet. These materials can be 3D-printed [121], injection casted [120], but can also be shaped with superplastic forming [122]. Furthermore, polyurethane can also be reinforced, offering more possibilities. Also, Neoprene might be an useful replacement for polyurethane, because of its high elasticity and high fracture toughness. PETG is sometimes used as well, as it is significantly easier to use in the thermoforming process due to its lower glass transition temperature [123].

Thirdly, the manufacturing techniques described are also limited, leaving several processes out of the overview. To show an example, practices of printing technology are applied to 3D printing, resulting in the promising technology of material jetting. This technology is not included in this study. Also the 3D printing technology of SLA is promising, but not included in the overview, due to the material selection in the beginning. This does not mean, however, that it is not suited for compliant shell mechanisms, made of other materials. Furthermore, the use of adaptable moulds, used in stretch bending [124] and multi-point forming, is not discussed. This technique would increase the customizability of the produced parts, but the accuracy of the mold goes down.

Lastly, the performance metrics used in this study are not adequate in every design process. One might be the absence of an explicit metric on costs. Currently, the costs are evaluated, only in an implicit manner using the metric Economic batch size. Moreover, as the metric Productivity is correlated to Economic batch size, this makes Productivity somewhat redundant. Furthermore, the metric Process robustness misses a clear definition, complicating the evaluation of the performance. An improvement could be to compare the processes on specific defects resulting in inaccuracies in relevant properties, such as stiffness, yield strength, or dimensional accuracy. For the metric of geometric freedom holds, that the distinction used does not make a sufficiently clear distinction between manufacturing techniques, as the range of values is not very diverse. An improvement could be to include the possibility of thickness variation in this metric, as that can be an interesting property for manufacturing processes. That way, thickness can be a design parameter in compliant shell mechanisms.

5 Conclusion

This paper presents an overview of manufacturing techniques that can be used for compliant shell mechanisms. The resulting overview will help designers to select the right manufacturing technique in each situation. The manufacturing techniques are presented in three different categories: composite manufacturing techniques, polymer manufacturing techniques, and metal manufacturing techniques. The manufacturing techniques in each category are evaluated on five different performance metrics: productivity, economic batch size, geometric freedom, accuracy, and process robustness. The starting point in selecting the best manufacturing technique in composite and polymer manufacturing is economic batch size, and for metal manufacturing both economic batch size and geometric freedom.

References

[1] Seffen, K. A., 2001. "On the Behavior of Folded Tape-Springs". *Journal of Applied Mechanics,* **68**(3), p. 369.

[2] Norman, A. D., Seffen, K. A., and Guest, S. D., 2008. "Multistable corrugated shells". *Proceedings of the Royal Society A: Mathematical, Physical and Engineering Sciences,* **464**(2095), pp. 1653–1672.

[3] Schenk, M., 2011. "Folded Shell Structures". Phd thesis, University of Cambridge.

[4] Seffen, K. A., 2012. "Compliant shell mechanisms". *Philosophical Transactions of the Royal Society A: Mathematical, Physical and Engineering Sciences,* **370**(1965), pp. 2010–2026.

[5] Radaelli, G., 2017. "Synthesis of mechanisms with prescribed elastic load-displacement characteristics". Phd thesis, Delft University of Technology.

[6] Van Der Kemp, S. J. M., 2018. "Design of a compact wearable arm support utilizing shape optimized compliant shell mechanisms". Master's thesis, Delft University of Technology. Unpublished.

[7] De Jong, M., 2018. "Synthesis of a Force Generator using Two-Fold Tape Loops". Master's thesis, Delft University of Technology.

[8] Kooistra, H., 2019. "Scoliosis brace design: Utilizing

compliant shell mechanisms and primary compliance vector path optimization". Master's thesis, Delft University of Technology. Unpublished.

[9] Broshuis, A. P. F., 2019. "Negative stiffness in compliant shell mechanisms". Master's thesis, Delft University of Technology. Unpublished.

[10] de Jong, M. G., van de Sande, W. W. P. J., and Herder, J. L., 2019. "Properties of Twofold Tape Loops: The Influence of the Subtended Angle". *Journal of Mechanisms and Robotics,* **11**(2), feb, pp. 020912–020912–7.

[11] Hufenbach, W. A., Gude, M., Adam, F., Modler, N., Heber, T., Renner, O., Körner, I., and Weck, D., 2011. "Experimental investigation of composite-based compliant structures". *Kompozyty,* **3**, pp. 187–191.

[12] Radaelli, G., and Herder, J., 2016. "A monolithic compliant large-range gravity balancer". *Mechanism and Machine Theory,* **102**, aug, pp. 55–67.

[13] Tong, X., Ge, W., Gao, X., and Li, Y., 2019. "Simultaneous optimization of fiber orientations and topology shape for composites compliant leading edge". *Journal of Reinforced Plastics and Composites*, apr.

[14] Tong, X., Ge, W., and Zhang, Y., 2016. "Topology optimization of compliant mechanisms with curvilinear fiber path laminated composites". *Proceedings of the Institution of Mechanical Engineers, Part C: Journal of Mechanical Engineering Science,* **230**(17), oct, pp. 3101–3110.

[15] Li, D., Zhang, X., Guan, Y., and Zhang, H., 2010. "Topology optimization of compliant mechanisms with anisotropic composite materials". In 2010 IEEE International Conference on Mechatronics and Automation, IEEE, pp. 416–421.

[16] Tong, X., Ge, W., Zhang, Y., and Zhao, Z., 2019. "Topology design and analysis of compliant mechanisms with composite laminated plates". *Journal of Mechanical Science and Technology,* **33**(2), feb, pp. 613–620.

[17] Koch, I., Zscheyge, M., Gottwald, R., Lange, M., Zichner, M., Böhm, R., Grüber, B., Lepper, M., Modler, N., and Gude, M., 2016. "Textile-Reinforced Thermoplastics for Compliant Mechanisms Application and Material Phenomena". *Advanced Engineering Materials,* **18**(3), pp. 427–436.

[18] Modler, N., Modler, K.-H., Hufenbach, W. A., Jaschinski, J., Zichner, M., Heber, T., and Winkler, A., 2011. "Static and Dynamic Testing of Textile-Reinforced Composite Compliant Structures Under Shear-Force-Free Bending Load". *Kompozyty,* **11**(4), pp. 352–356.

[19] Stacey, J. P., O'Donnell, M. P., and Schenk, M., 2019. "Thermal Prestress in Composite Compliant Shell Mechanisms". *Journal of Mechanisms and Robotics,* **11**(2), pp. 020908–1 – 020908–8.

[20] Howell, L. L., 2001. *Compliant Mechanisms*. John Wiley and Sons Inc., New York, US.

[21] Gouker, R. M., Gupta, S. K., Bruck, H. A., and Holzschuh, T., 2006. "Manufacturing of multi-material compliant mechanisms using multi-material molding". *International Journal of Advanced Manufacturing Technology,* **30**(11-12), pp. 1049–1075.

[22] Nijssen, J., 2016. "A Type Synthesis Approach to Compliant Shell Mechanisms". Master's thesis, Delft University of Technology.

[23] Diepens, T., 2015. "Optimizing Compliant Mechanisms for Sustainable Materials: A Case Study of a Compliant Grasper". Master's thesis, Delft University of Technology.

[24] Kebadze, E., Guest, S. D., and Pellegrino, S., 2004. "Bistable prestressed shell structures". *International Journal of Solids and Structures,* **41**(11-12), pp. 2801–2820.

[25] Seffen, K. A., You, Z., and Pellegrino, S., 2000. "Folding and deployment of curved tape springs". *International Journal of Mechanical Sciences,* **42**(10), pp. 2055–2073.

[26] CES EduPack software, Granta Design Limited, Cambridge, UK, 2018.

[27] Vanhove, H., Carette, Y., Vancleef, S., and Duflou, J. R., 2017. "Production of thin Shell Clavicle Implants through Single Point Incremental Forming". In 17th International Conference on Sheet Metal, SHEMET 2017, F. L., ed., Vol. 183, Elsevier Ltd, pp. 174–179.

[28] Mavroidis, C., Ranky, R. G., Sivak, M. L., Patritti, B. L., DiPisa, J., Caddle, A., Gilhooly, K., Govoni, L., Sivak, S., Lancia, M., Drillio, R., and Bonato, P., 2011. "Patient specific ankle-foot orthoses using rapid prototyping". *Journal of NeuroEngineering and Rehabilitation,* **8**(1), pp. 1–11.

[29] Kim, H., and Jeong, S., 2015. "Case study: Hybrid model for the customized wrist orthosis using 3D printing". *Journal of Mechanical Science and Technology,* **29**(12), pp. 5151–5156.

[30] Palousek, D., Rosicky, J., Koutny, D., Stoklásek, P., and Navrat, T., 2014. "Pilot study of the wrist orthosis design process". *Rapid Prototyping Journal,* **20**(1), pp. 27–32.

[31] Faustini, M. C., Neptune, R. R., Crawford, R. H., and Stanhope, S. J., 2008. "Manufacture of passive dynamic ankle-foot orthoses using selective laser sintering". *IEEE Transactions on Biomedical Engineering,* **55**(2), pp. 784–790.

[32] Paterson, A. M., Bibb, R., Campbell, R. I., and Bingham, G., 2015. "Comparing additive manufacturing technologies for customised wrist splints". *Rapid Prototyping Journal,* **21**(3), pp. 230–243.

[33] Cook, D., Gervasi, V., Rizza, R., Kamara, S., and Liu, X. C., 2010. "Additive fabrication of custom pedorthoses for clubfoot correction". *Rapid Prototyping Journal,* **16**(3), pp. 189–193.

[34] Brecher, C., Stimpfl, J., Dubratz, M., and Emonts, M., 2011. "Innovative manufacturing of 3D-lightweight components". *Laser Tech J,* **49**(5), pp. 36–40.

[35] Mazumdar, S. K., 2002. *Composites manufacturing: materials, product, and process engineering*. CRC

Press, Taylor & Francis Group.

[36] Centea, T., Grunenfelder, L., and Nutt, S., 2015. "A review of out-of-autoclave prepregs Material properties, process phenomena, and manufacturing considerations". *Composites Part A: Applied Science and Manufacturing,* **70**, mar, pp. 132–154.

[37] Khani, A., Abdalla, M. M., Gürdal, Z., Sinke, J., Buitenhuis, A., and Van Tooren, M. J. L., 2017. "Design, manufacturing and testing of a fibre steered panel with a large cut-out". *Composite Structures,* **180**, pp. 821–830.

[38] He, K., Nie, H., and Yan, C., 2016. "The Intelligent Composite Panels Manufacturing Technology Based on Tape-laying Automatic System". In 9th International Conference on Digital Enterprise Technology - Intelligent Manufacturing in the Knowledge Economy Era, DET 2016, L. Y., G. J., and M. P., eds., Vol. 56, Elsevier B.V., pp. 610–613.

[39] Compositence. Tape Laying. http://www.compositence.com/en/fiber-placement/tape-laying/. Accessed: 2019-06-25.

[40] Buragohain, M. K., 2017. *Composite Structures: Design, Mechanics, Analysis, Manufacturing, and Testing*. CRC Press, aug.

[41] Elkington, M., Bloom, D., Ward, C., Chatzimichali, A., and Potter, K., 2015. "Hand layup: understanding the manual process". *Advanced Manufacturing: Polymer & Composites Science,* **1**(3), jul, pp. 138–151.

[42] Malnati, P. Sub-8-minute cycle times on carbon/epoxy prepreg : CompositesWorld. https://www.compositesworld.com/articles/sub-8-minute-cycle-times-on-carbonepoxy-prepreg. Accessed: 2019-07-01.

[43] Manufacturing Processes Prepregs. http://www.fisica.unige.it/ rocca/Didattica/Material Science/SERP 13 - Composite Prepreg 09-12-13.pdf. Accessed: 2019-07-01.

[44] Aerospace Engineering Blog. Composite Manufacturing - Autoclave Variability. https://aerospaceengineeringblog.com/autoclave-variability/. Accessed: 2019-07-02.

[45] Brillant, M., and Hubert, P., 2011. "Modelling and Characterization of Thickness Variations in L-shape Out-Of-Autoclave Laminates". In 18th International Conference on Composite Materials.

[46] Koushyar, H., 2011. "Effects of variation in autoclave pressure, cure temperature, and vacuum-application time on the porosity and mechanical properties of a carbon/epoxy composite". Master's thesis, Wichita State University.

[47] Cripps, D., Searle, T., and Summerscales, J., 2000. "2.21 - open mold techniques for thermoset composites". In *Comprehensive Composite Materials*, A. Kelly and C. Zweben, eds. Pergamon, Oxford, pp. 737 – 761.

[48] Tan, Y. Y., and Lee, T. L., 2018. "The flexible textile mesh: Manufacture of curved perforated cladding panels". S. Alhadidi, T. Fukuda, W. Huang, P. Janssen, and K. Crolla, eds., Vol. 2, The Association for Computer-Aided Architectural Design Research in Asia (CAADRIA), pp. 349–358.

[49] Totaro, G., and De Nicola, F., 2012. "Recent advance on design and manufacturing of composite anisogrid structures for space launchers". *Acta Astronautica,* **81**(2), dec, pp. 570–577.

[50] Joshi, S., 2012. "12 - the pultrusion process for polymer matrix composites". In *Manufacturing Techniques for Polymer Matrix Composites (PMCs)*, S. G. Advani and K.-T. Hsiao, eds., Woodhead Publishing Series in Composites Science and Engineering. Woodhead Publishing, pp. 381 – 413.

[51] Lefteri, C., 2012. Benefits and drawbacks of Pultrusion. http://www.materialsforengineering.co.uk/engineering-materials-features/benefits-and-drawbacks-of-pultrusion/46801. Accessed: 2019-07-02.

[52] Common Pultruded Products Defects And Solutions - Unicomposite.com. http://www.unicomposite.com/news/common-pultruded-products-defects.html. Accessed: 2019-07-02.

[53] Lee, J., Kim, B., and Ko, D., 2019. "Development of vacuum-assisted prepreg compression molding for production of automotive roof panels". *Composite Structures,* **213**, pp. 144–152.

[54] Verrey, J., Wakeman, M., Michaud, V., and Mnson, J.-A., 2006. "Manufacturing cost comparison of thermoplastic and thermoset rtm for an automotive floor pan". *Composites Part A: Applied Science and Manufacturing,* **37**(1), pp. 9 – 22.

[55] Carruthers, J., 2018. What is Resin Transfer Moulding (RTM)? Coventive Composites. https://coventivecomposites.com/explainers/resin-transfer-moulding-rtm/. Accessed: 2019-07-03.

[56] Tempelman, E., Shercliff, H., and van Eyben, B. N., 2014. "Chapter 10 - resin transfer molding". In *Manufacturing and Design*, E. Tempelman, H. Shercliff, and B. N. van Eyben, eds. Butterworth-Heinemann, Boston, pp. 171 – 186.

[57] Cairns, D. S., and Shramstad, J. D., 2000. Evaluation of Hand Lay-Up and Resin Transfer Molding in Composite Wind Turbine Blade Manufacturing. Tech. rep., Sandia National Laboratories (SNL), jun.

[58] Shroff, S., Acar, E., and Kassapoglou, C., 2017. "Design, analysis, fabrication, and testing of composite grid-stiffened panels for aircraft structures". *Thin-Walled Structures,* **119**, pp. 235–246.

[59] Li, W., Krehl, J., Gillespie, J. W., Heider, D., Endrulat, M., Hochrein, K., Dunham, M. G., and Dubois, C. J., 2004. "Process and Performance Evaluation of the Vacuum-Assisted Process". *Journal of Composite Materials,* **38**(20), oct, pp. 1803–1814.

[60] EM-fiberglas. Resin Transfer Molding (RTM). https://www.em-fiberglas.dk/uk/the-advantages-of-composites/resin-transfer-molding-rtm.aspx. Accessed: 2019-07-03.

[61] Li, W., Krehl, J., J. W. Gillespie, J., Heider, D., Endrulat, M., Hochrein, K., Dunham, M. G., and Dubois, C. J., 2004. "Process and performance evaluation of the vacuum-assisted process". *Journal of Composite Materials,* **38**(20), pp. 1803–1814.

[62] Li, J., Zhang, C., Liang, R., Wang, B., and Walsh, S., 2008. "Modeling and analysis of thickness gradient and variations in vacuum-assisted resin transfer molding process". *Polymer Composites,* **29**(5), pp. 473–482.

[63] Kleineberg, M., Herbeck, L., and Schöppinger, C., 2002. "Advanced liquid resin infusion-A new perspective for space structures". In Toulouse, France: European Conference on Spacecraft Structures, Materials and Mechanical Testing, pp. 173–80.

[64] Volponi, R., Spena, P., De nicola, F., Guadagno, L., Raimondo, M., and Vietri, U., 2016. "Manufacturing process of a multifunctional composite panel with nanocharged matrix". A. D'Amore, L. Grassia, and D. Acierno, eds., Vol. 1736, American Institute of Physics Inc.

[65] Kazmi, S. M. R., Jayaraman, K., and Das, R., 2016. "Single-step manufacturing of curved polypropylene composites using a unique sheet consolidation method". *Journal of Materials Processing Technology,* **237**, pp. 96–112.

[66] Brooks, R., 2000. "Composites in Automotive Applications : Design". *Comprehensive Composite Materials*, pp. 341–363.

[67] Brooks, R., 2000. "6.16 - composites in automotive applications: Design". In *Comprehensive Composite Materials*, A. Kelly and C. Zweben, eds. Pergamon, Oxford, pp. 341 – 363.

[68] CompositesWorld, 2007. High-volume molding methods. https://www.compositesworld.com/columns/high-volume-molding-methods. Accessed: 2019-07-03.

[69] Wulfsberg, J., Herrmann, A., Ziegmann, G., Lonsdorfer, G., Stöß, N., and Fette, M., 2014. "Combination of Carbon Fibre Sheet Moulding Compound and Prepreg Compression Moulding in Aerospace Industry". *Procedia Engineering,* **81**, jan, pp. 1601–1607.

[70] TenCate, 2018. TenCate Advanced Composites Compression Molding datasheet. https://www.toraytac.com/media/feb88974-7d81-46f8-ad45-7960feaa1826/Z0IK5w/TAC/Documents/Product and application one pagers/Product 0Highlights Compression Molding.pdf. Accessed: 2019-07-03.

[71] Akiyama, K., 2011. "Development of Prepreg Compression Molding (PCM) technology". *SPE Automotive and Composites Divisions-11th Annual Automotive Composites Conference and Exhibition, ACCE 2011*.

[72] Mayer, R., 2007. "Precision Injection Molding: How to Make Polymer Optics for High Volume and High Precision Applications". *Optik & Photonik,* **2**(4), pp. 46–51.

[73] Liu, S.-J., 2012. "2 - injection molding in polymer matrix composites". In *Manufacturing Techniques for Polymer Matrix Composites (PMCs)*, S. G. Advani and K.-T. Hsiao, eds., Woodhead Publishing Series in Composites Science and Engineering. Woodhead Publishing, pp. 15 – 46.

[74] Throne, J. L., 2008. "Introduction to thermoforming". In *Understanding Thermoforming*, J. L. Throne, ed., second edition ed. Hanser, pp. 1 – 7.

[75] Ashter, S. A., 2014. "2 - the thermoforming process". In *Thermoforming of Single and Multilayer Laminates*, S. A. Ashter, ed. William Andrew Publishing, Oxford, pp. 13 – 38.

[76] Saraiva, F., 2017. "Development of press forming techniques for thermoplastic composites: Investigation of a multiple step approach". Master's thesis, Delft University of Technology.

[77] Throne, J. L., 2008. "General forming concepts". In *Understanding Thermoforming*, J. L. Throne, ed., second edition ed. Hanser, pp. 9 – 25.

[78] Lee, A., Brun, P.-T., Marthelot, J., Balestra, G., Gallaire, F., and Reis, P. M., 2016. "Fabrication of slender elastic shells by the coating of curved surfaces". *Nature Communications,* **7**.

[79] Gibson, I., Rosen, D. W., and Stucker, B., 2010. *Additive Manufacturing Technologies*. Springer US, Boston, MA.

[80] Kazmer, D., 2017. "28 - three-dimensional printing of plastics". In *Applied Plastics Engineering Handbook (Second Edition)*, M. Kutz, ed., second edition ed., Plastics Design Library. William Andrew Publishing, pp. 617 – 634.

[81] Hoang Sinh, L., Korhonen Harri, A., Marjo, L., Minna, M., Dang Luong, N., Torsten, W., Matthias, S., and Jukka, S., 2016. "Novel photo-curable polyurethane resin for stereolithography". *The Royal Society of Chemistry,* **6**.

[82] Proto Labs. An Overview of SLA Material Properties. https://www.protolabs.com/resources/design-tips/a-guide-to-stereolithography-3d-printing-materials/. Accessed: 2019-07-08.

[83] Gurrala, P. K., and Regalla, S. P., 2012. "Optimization of support material and build time in fused deposition modeling (fdm)". In Mechanical and Aerospace Engineering, ICMAE2011, Vol. 110 of *Applied Mechanics and Materials*, Trans Tech Publications Ltd, pp. 2245–2251.

[84] Capel, A. J., Edmondson, S., Christie, S. D. R., Goodridge, R. D., Bibb, R. J., and Thurstans, M., 2013. "Design and additive manufacture for flow chemistry". *Lab Chip,* **13**, pp. 4583–4590.

[85] Gunaydin, K., and S. Trkmen, H., 2018. "Common fdm 3d printing defects". In International Congress on 3D Printing (Additive Manufacturing) Technologies and Digital Industry.

[86] Hosford, W., and Caddell, R., 2011. *Metal forming: Mechanics and metallurgy*.

[87] Mouritz, A. P., 2012. *Introduction to aerospace ma-*

terials. American Institute of Aeronautics and Astronautics.

[88] Chatterjee, R., and Mukhopadhyay, J., 2018. "A Review of Super plastic forming". *Materials Today: Proceedings,* **5**(2), pp. 4452–4459.

[89] Guofeng, W., Chao, S., Shufen, L., and Mo, Y., 2014. "Research on quick superplastic forming technology of aluminum alloy complex components". *Materialwissenschaft und Werkstofftechnik,* **45**(9), pp. 854–859.

[90] 3D Print magazine. Markforged Metal X: metaalprinter op basis van FDM. https://3dprintmagazine.eu/markforged-metal-x-3d-metaalprinter-op-basis-fdm/. Accessed: 2019-07-11.

[91] Pires, R. Titanium 3D Printing - How to Get Titanium Parts 3D Printed — All3DP. https://all3dp.com/2/titanium-3d-printing-how-to-get-titanium-parts-3d-printed/. Accessed: 2019-07-11.

[92] Merriam, E. G., Jones, J. E., and Howell, L. L., 2014. "Design of 3D-Printed Titanium Compliant Mechanisms". In Proceedings of the 42nd Aerospace Mechanisms Symposium.

[93] Lee, G., and Kim, S., 2012. "Case Study of Mass Customization of Double-Curved Metal Façade Panels Using a New Hybrid Sheet Metal Processing Technique". *J. Constr. Eng. Manage,* **138**(November), pp. 1322–1330.

[94] Ko, M., and Cora, O., 2008. "1 - introduction and state of the art of hydroforming". In *Hydroforming for Advanced Manufacturing*, M. Ko, ed. Woodhead Publishing, pp. 1 – 29.

[95] Zhang, S. H., Wang, Z. R., Xu, Y., Wang, Z. T., and Zhou, L. X., 2004. "Recent developments in sheet hydroforming technology". *Journal of Materials Processing Technology,* **151**(1-3 SPEC. ISS.), pp. 237–241.

[96] Palumbo, G., Zhang, S. H., Tricarico, L., Xu, C., and Zhou, L. X., 2006. "Numerical/experimental investigations for enhancing the sheet hydroforming process". *International Journal of Machine Tools and Manufacture,* **46**(11 SPEC. ISS.), pp. 1212–1221.

[97] Morphy, G., 2008. "15 - hydroforming and its role in lightweighting automobiles". In *Hydroforming for Advanced Manufacturing*, M. Ko, ed. Woodhead Publishing, pp. 335 – 351.

[98] Kopac, J., and Kampus, Z., 2005. "Incremental sheet metal forming on cnc milling machine-tool". *Journal of Materials Processing Technology,* **162-163**, pp. 622 – 628.

[99] Giraud-Moreau, L., Belchior, J., Lafon, P., Lotoing, L., Cherouat, A., Courtielle, E., Guines, D., and Maurine, P., 2018. "Springback effects during single point incremental forming: Optimization of the tool path". *AIP Conference Proceedings,* **1960**(1), p. 160009.

[100] Trzepieciski, T., Krasowski, B., Kubit, A., and Wydrzyski, D., 2018. "Possibilities of application of incremental sheet-forming technique in aircraft industry". *Scientific Letters of Rzeszow University of Technology - Mechanics*, 04.

[101] Hirt, G., Bambach, M., Bleck, W., Prahl, U., and Stollenwerk, J., 2015. "The development of incremental sheet forming from flexible forming to fully integrated production of sheet metal parts". In Advances in Production Technology, C. Brecher, ed., Springer International Publishing, pp. 117–129.

[102] Salem, E., Shin, J., Nath, M., Banu, M., and Taub, A. I., 2016. "Investigation of Thickness Variation in Single Point Incremental Forming". *Procedia Manufacturing,* **5**, pp. 828–837.

[103] Micari, F., Ambrogio, G., and Filice, L., 2007. "Shape and dimensional accuracy in single point incremental forming: State of the art and future trends". *Journal of Materials Processing Technology,* **191**(1), pp. 390 – 395. Advances in Materials and Processing Technologies, July 30th - August 3rd 2006, Las Vegas, Nevada.

[104] Wang, H., Zhang, R., Zhang, H., Hu, Q., and Chen, J., 2018. "Novel strategies to reduce the springback for double-sided incremental forming". *The International Journal of Advanced Manufacturing Technology,* **96**(1), Apr, pp. 973–979.

[105] Bailly, D., Bambach, M., Hirt, G., Pofahl, T., Puppa, G., and Trautz, M., 2014. "Flexible manufacturing of double-curved sheet metalpanels for the realization of self-supporting freeform structures". *Key Engineering Materials,* **639**, 10, pp. 41–48.

[106] Montmitonnet, P., 2001. *Metal Working: Cold Rolling*. 12, pp. 5500–5506.

[107] Precision Metalforming Association, U. S., 1995. *PMA design guidelines for metal stampings and fabrications.* Precision Metalforming Association, Richmond Heights, OH.

[108] Ktari, A., Antar, Z., Haddar, N., and Elleuch, K., 2012. "Modeling and computation of the three-roller bending process of steel sheets". *Journal of Mechanical Science and Technology,* **26**(1), Jan, pp. 123–128.

[109] Corrugated sheet rolling. http://www.dupral.nl/profiled-sheets/corrugated-sheet-rolling/. Accessed: 2019-07-17.

[110] Cooper, D. Sheet Metal Forming. http://web.mit.edu/2.810/www/files/lectures/2015_lectures/lec6-sheet-metal-forming-2015.pdf. Accessed: 2019-07-17.

[111] Chang, K.-H., 2013. "Chapter 4 - sheet metal forming simulation". In *Product Manufacturing and Cost Estimating Using Cad/Cae*, K.-H. Chang, ed., The Computer Aided Engineering Design Series. Academic Press, Boston, pp. 133 – 190.

[112] Vazquez, E., and Coleman, J., 2017. Efficient Fabrication of Double Curves in Architecture Zahner. https://www.azahner.com/blog/efficient-fabrication-of-double-curves-in-architecture. Accessed: 2019-04-15.

[113] Yoon, S. J., and Yang, D. Y., 2003. "Development of a highly flexible incremental roll forming process for the manufacture of a doubly curved sheet

metal". *CIRP Annals - Manufacturing Technology,* **52**(1), pp. 201–204.

[114] Yoon, S. J., and Yang, D. Y., 2005. "An incremental roll forming process for manufacturing doubly curved sheets from general quadrilateral sheet blanks with enhanced process features". *CIRP Annals - Manufacturing Technology,* **54**(1), pp. 221–224.

[115] Choi, S.-W., Park, S. H., Jeong, H.-S., Cho, J., Park, S., and Ha, M. Y., 2012. "Improvement of formability for fabricating thin continuously corrugated structures in sheet metal forming process". *Journal of Mechanical Science and Technology,* **26**(8), Aug, pp. 2397–2403.

[116] Ingarao, G., Lorenzo, R. D., and Micari, F., 2009. "Analysis of stamping performances of dual phase steels: A multi-objective approach to reduce springback and thinning failure". *Materials & Design,* **30**(10), pp. 4421 – 4433.

[117] Bocking, C., Jacobson, D. M., and Rennie, A. E. W., 2002. "Rapid production of microwave packaging in silicon-aluminium by thin-shell electroforming". *Microelectronics International,* **19**(1), pp. 30–32.

[118] Nijland, M. What materials can be electroformed? https://insights.vecoprecision.com/what-materials-can-be-electroformed. Accessed: 2019-07-12.

[119] Heaney, D., 2019. "2 - designing for metal injection molding (mim)". In *Handbook of Metal Injection Molding (Second Edition)*, D. F. Heaney, ed., second edition ed., Woodhead Publishing Series in Metals and Surface Engineering. Woodhead Publishing, pp. 25 – 43.

[120] Homer, E. R., Harris, M. B., Zirbel, S. A., Kolodziejska, J. A., Kozachkov, H., Trease, B. P., Borgonia, J.-P. C., Agnes, G. S., Howell, L. L., and Hofmann, D. C., 2014. "New methods for developing and manufacturing compliant mechanisms utilizing bulk metallic glass". *Advanced Engineering Materials,* **16**(7), pp. 850–856.

[121] Shipman, M. Researchers Use 3-D Printing to Create Metallic Glass Alloys in Bulk. https://news.ncsu.edu/2018/03/metallic-glass-bulk-2018/. Accessed: 2019-07-19.

[122] Schroers, J., 2005. "The superplastic forming of bulk metallic glasses". *JOM,* **57**(5), May, pp. 35–39.

[123] Geerts, J., 2017. "Towards compliant and compact arm supports". Master's thesis, Delft University of Technology.

[124] Wang, S., Cai, Z., Li, M., and Lan, Y., 2012. "Numerical simulation on the local stress and local deformation in multi-point stretch forming process". *The International Journal of Advanced Manufacturing Technology,* **60**(9), Jun, pp. 901–911.

B

Twisted tape-spring

When taking a basic tape-spring, with a constant cross section, and no curvature added in the longitudinal direction, the negative stiffness behaviour of the tape spring during equal sense bending is only present on a very short interval. In order to elongate this negative stiffness, different possibilities are present. One is to introduce a varying subtended angle profile [7], another option is adding longitudinal curvature. Both of these methods result in a more complex geometry (with respect to the basic tape-spring). Another way of elongating this negative stiffness behaviour is by introducing extra boundary conditions. Next to the rotational constraint on the y-axis, a rotational constraint can be introduced in the x-axis (twisting of tape-spring before bending). The axis are shown in figure B.1.

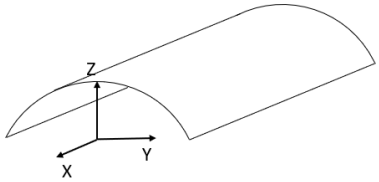

Figure B.1: Tape spring axes

This constraint will result in a twisted tape-spring. This tape spring has a longer range of negative stiffness, as can be seen in figure B.3a (for equal sense bending). The length of the tape spring is important to normalize the twist at the end of it. The parameters used in this example are:

- Length = 5e-2 [m]
- Radius = 2e-3 [m]
- Thickness = 5e-5 [m]
- Subtended angle profile = see figure B.2

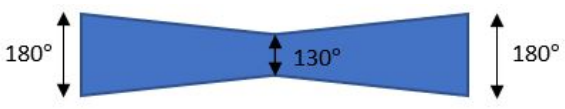

Figure B.2: Subtended angle geometry of simulated tape spring

The advantage of this approach for elongating the negative stiffness behaviour, is the basic geometry of the tape-spring. After forming the transversal curvature of the tape-spring, the shaping of the material is finished (no need to laser cut the geometry to get a varying subtended angle, or adding a longitudinal curvature).

If one side of the tape spring is considered being completely constraint, and attached to the earth, the twisting moment on the other end needs to be constraint by an applied moment. By combining two equally twisted tape-springs in a mirrored configuration, these twisting moments are cancelled out. This way, they can easily be combined, without the need of changing the design to account for this twisting moment.

The bending behaviour changes for different twist angles, resulting in a different negative stiffness profile. In figure B.3a, the force-deflection behaviour for three different twist angles are shown. As can be seen in this figure, the negative stiffness behaviour for larger twists is more gradual. What is also interesting, is that by increasing the twist angle from $\pi/10$ rad to $\pi/5$ rad, the peak moment goes down.

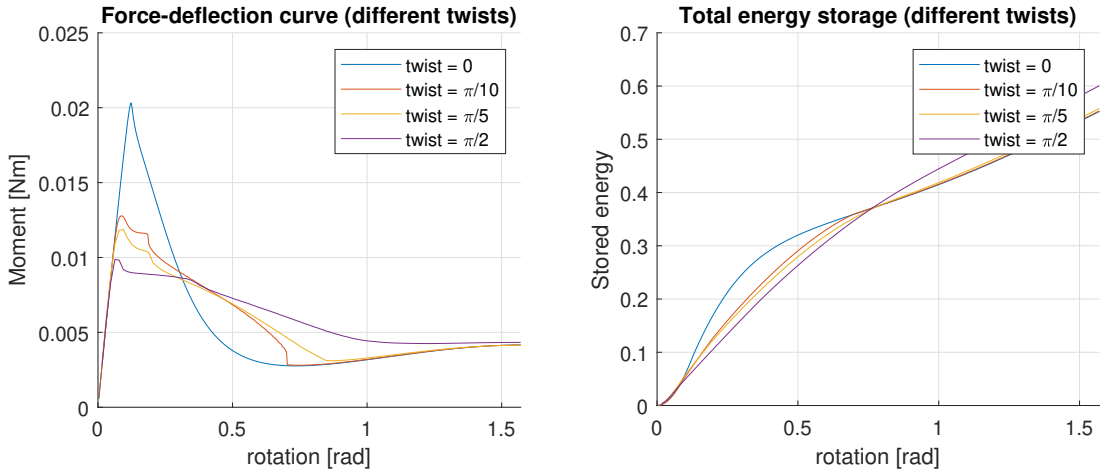

(a) Force-deflection curves of twisted tape springs for different twist

(b) Energy storage in twisted tape springs

Figure B.3: Force -deflection curves and energy storage of twisted tape springs

The area under the graph in figure B.3a is equal to the energy stored in the material. This total energy stored is shown in figure B.3b. As can be seen, the untwisted tape spring has initially more energy stored. For small twist angles, the difference in stored energy is, however, levelled, due to the elongated negative stiffness. For the case of twist angle being $\pi/2$ rad, the total energy stored is higher, as the residual moment at the rotation of $\pi/2$ rad is still higher than the others.

An interesting approach to these different force-deflection behaviours for the different twist angles, is to combine the different behaviours as building blocks, to generate another force-deflection behaviour, which is the sum of the individual tape-springs. An example is shown in figure B.4. In this figure, the curves of the $\pi/5$ rad and $\pi/2$ rad twists are added together, to form the new force-deflection curve, which has almost the same peak moment, but a longer range of negative stiffness.

Another approach can be to make the twist angle a function of the bending rotation, and in that way changing the shape of the force-deflection profile. This would, however, have several design challenges.

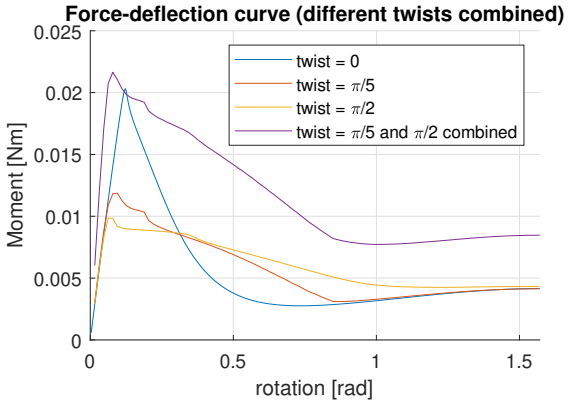

Figure B.4: Folding moment combined twisted tape springs

C

Stacking overview

Stacking options

In figure C.1, an overview is given of the different stacking options. A subdivision is made based on the radii of the tape-springs, with r_1 being the top tape-spring, and r_2 the bottom tape-spring.

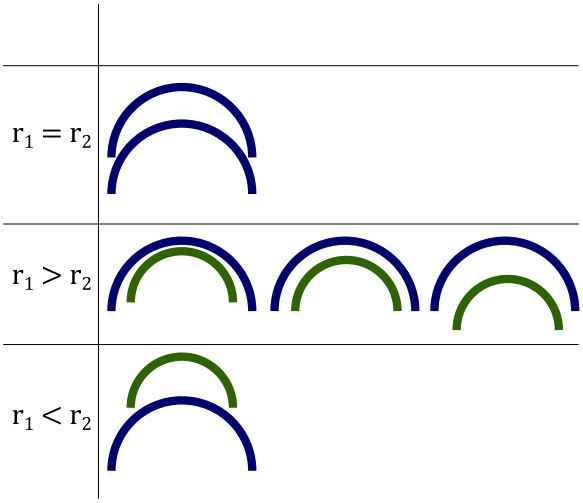

Figure C.1: Overview of stacking options, with r_1 as the radius of the top tape-spring and r_2 as the radius of the bottom tape-spring.

The configuration $r_1 = r_2$ is considered in chapter 3. This configuration is interesting, since this stack consists of equal tape-springs which might be beneficial from an economical production perspective.

In chapter 2 the configuration $r_1 > r_2$ is considered. The vertical placement of the tape-springs can be varied, as shown in the figure. The concentric configuration is studied in chapter 2, since this might have some advantages due to the aligned primary compliance vectors.

The last configuration, $r_1 < r_2$, is not considered in this thesis. It might not be a very efficient use of the available space.

Length change

When folding a stack of tape-springs, the endpoints of each layer are translating with respect to each other, as shown in figure C.2.

The different stacking options have all different relative length changes. Furthermore, the tape-springs can be placed at different separation distances Δs from each other, resulting in different relative length change during folding.

For the concentric configuration $r_1 > r_2$, the length change is explained in chapter 2. The resulting length change ΔL is $\Delta L = \theta(r_1 - r_2)$.

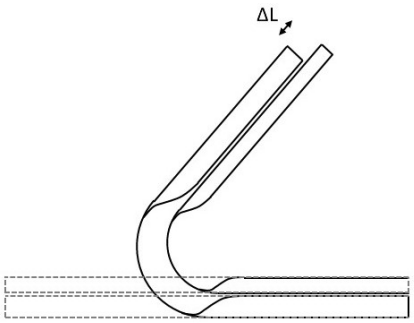

Figure C.2: Relative length change between layers of a stack of two tape-springs

For the configuration $r_1 = r_2$, the length change is derived below. In figure C.3 a schematic is shown of two tape-springs (in green and red) that are folded at an angle of θ. The green lines represent the straight parts of the tape-spring, while the red lines represent the folded region of the tape-spring. Using some goniometry, the relative length change ΔL can be approximated by $\Delta L = 2\Delta s \tan \frac{\theta}{2}$.

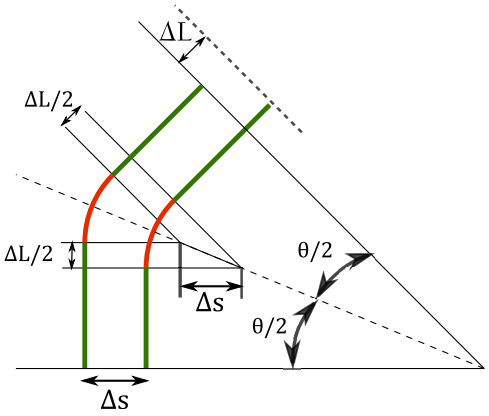

Figure C.3: Length change of parallel equal tape-spring.

In figure C.4 the length change divided by the separation distance, $\frac{\Delta L}{\Delta s}$, is shown. This function goes to infinity when it approaches a fold angle of 180 degrees.

In figure C.5 a photo is shown of two equal tape-springs stacked on top of each other, folded at 180 degrees. It is clear from this configuration that the fold radii of the tape-springs are not equal, and no relative length change can prevent this. The tape-springs are at this fold angle in a singularity position.

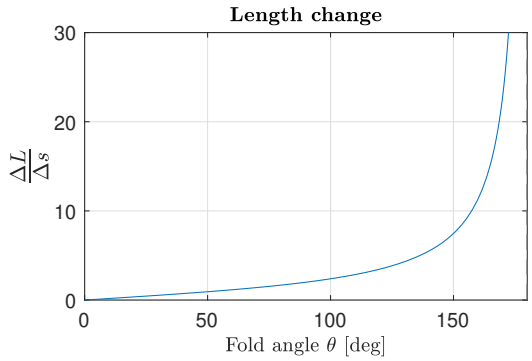

Figure C.4: Relative length change as function of fold angle θ.

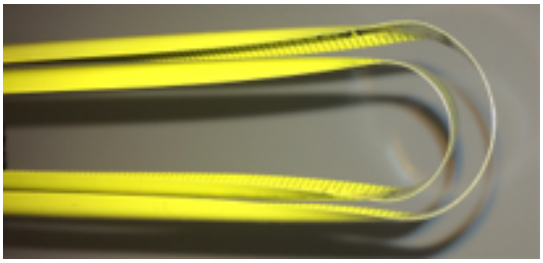

Figure C.5: Folded equal tape-spring in singularity position.

D

Simulations

D.1. Imperfection implementation

Introduction

In order for the simulation to converge, an imperfection has to be introduced. This imperfection should be large enough to ensure the simulation of converging, but as small as possible, to prevent other effects becoming dominant in the deformation behaviour. This chapter describes how the added imperfection to the simulation is determined.

The imperfection can be introduced locally on the geometry shape, the material properties or as an extra external force for example. Since a change in geometry is considered to be the easiest in the production of the tape spring, this approach is taken.

There are different options of changing the geometry locally and consequently creating a 'weak spot' which enables the simulation to converge. One could locally change the thickness, radius, or the subtended angle. It is chosen to change the subtended angle profile throughout the length of the tape-spring, as this can be achieved relatively easy compared to the other options.

Method

Two different methods of varying the subtended angle profile are tried, one using a defined linear subtended angle profile and the other using a random noise on the subtended angle profile.

Linear subtended angle profile

By changing the subtended angle throughout the length of the tape-spring, a weak spot is created. One end of the tape-spring is subjected to a rotation around a point halfway the tape-spring length, so the tape-spring is expected to buckle in the middle. By introducing the weak spot at this location, it enables the simulation to find a solution for the applied displacements. The subtended angle profile follows a linear profile from the ends to the middle, where it is the smallest. The geometry is defined by the subtended angle at the outer ends and the decrease in subtended angle in the middle, as shown in figure D.1.

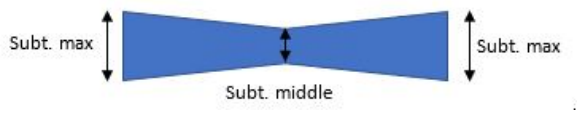

Figure D.1: Variables of the subtended angle profile of the simulated tape spring

The smallest possible imperfection while still converging is determined by running simulations for different values for the maximum subtended angle at the ends and the subtended angle in the middle. The maximum subtended angle values used are $[180°, 170°, 160°, 150°, 140°, 130°, 120°, 110°]$, and the subtended angle in the middle is reduced with respect to the maximum subtended angle with $[20°, 15°, 10°]$, resulting in 24 different combinations. Initially, a reduction of the subtended angle in

the middle of 5° was included as well, but since none of the '10° reduction'-simulations converged, this was left out later on.

This grid search is done for both a tape spring which is placed with the centre of the transverse curvature in line with the rotation point, as well as for a tape spring that is placed outward by $0.015m$. The step size used for the fold angle θ in the simulation is 1°, ranging from 0° up to 90°. If a displacement step does not converge, the step size is divided by two, up to a minimum size of $1/16^\circ$. The other parameters used are:

- length = 0.30 m
- radius = 0.02 m
- thickness = 2e-4 m

A schematic of the simulation is shown in figure D.2. In red the geometry is shown, the black line denotes the arm which rotates around the positive x-axis at point A, and the light blue line indicates the trajectory the second endpoint follows.

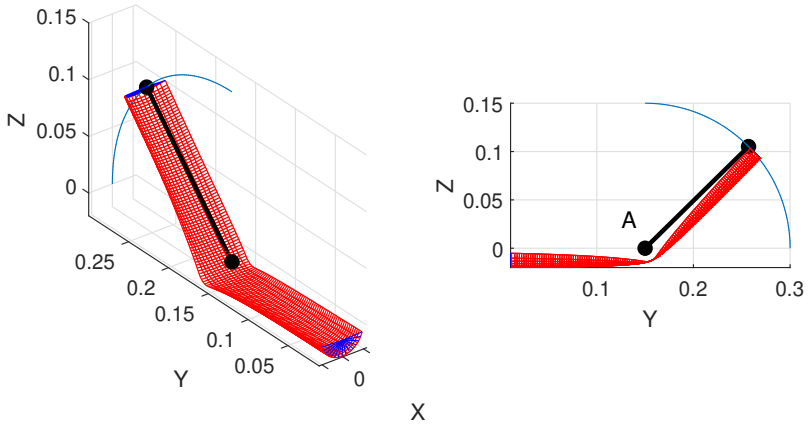

Figure D.2: Deformed geometry of a tape-spring with linear subtended angle profile.

Random noise subtended angle profile

In the second approach a random noise with varying amplitudes up to 5% was added to the subtended angle throughout the entire tape spring. The random noise ensured a varying subtended angle along the length of the tape-spring, while the symmetry in the Y, Z-plane was maintained.

Results

Linear subtended angle profile

The resulting moments around point A due to the folding of the inner tape-spring are shown in figure D.3. Eight out of the 32 simulations converges to 90 degrees, while the others fail to converge between a rotation of 10-20 degrees.

Two similar plots are made for the outer tape spring, shown in figure D.4. From the 24 different simulations, only three converge: $[130^\circ(20^\circ), 120^\circ(20^\circ), 110^\circ(20^\circ)]$ (the first number indicates the maximum subtended angle, while the second value between brackets denotes the reduction of the subtended angle in the middle).

Random noise subtended angle profile

The addition of the random noise enabled the simulation to converge to a solution as well. These solutions were highly dependent on the noise that was added to the initial geometry. For some configurations, the buckling occurred at one position in the middle around the rotation point, as shown in figure D.5a, while for other configurations the buckling appeared in two distinct regions on the tape

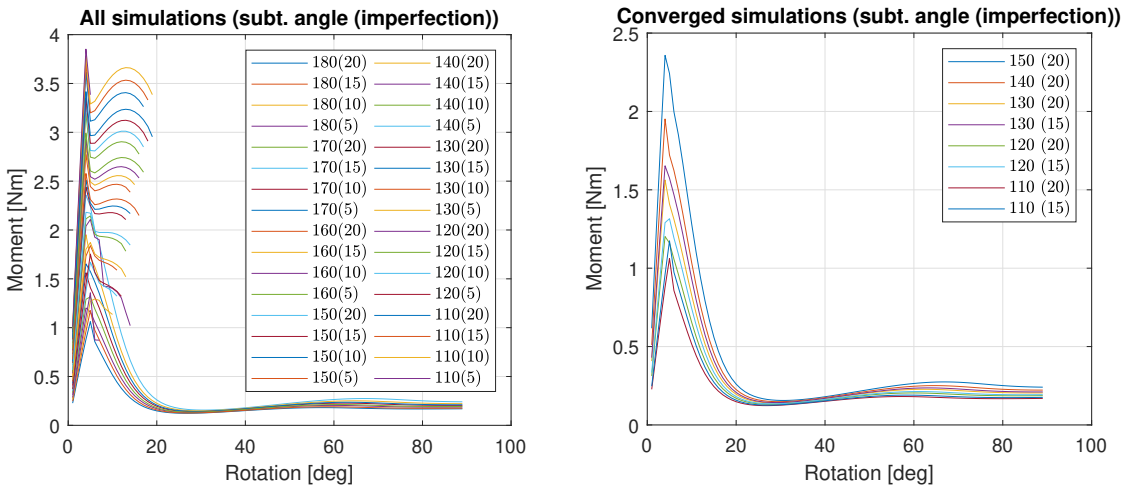

(a) All simulations (b) Converged simulations

Figure D.3: Resulting moment-rotation diagrams for the simulations of the inner tape-spring

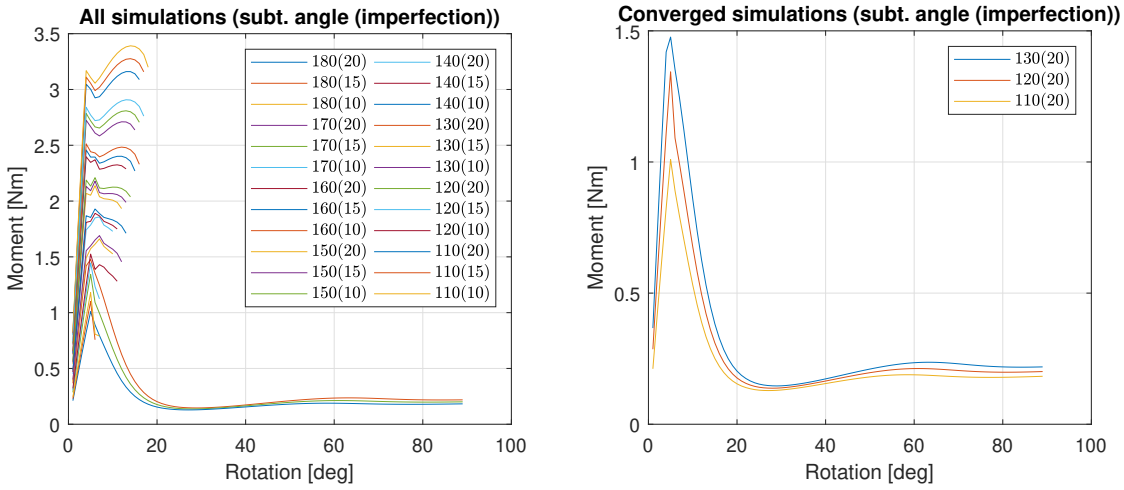

(a) All simulations (b) Converged simulations

Figure D.4: Resulting moment-rotation diagrams for the simulations of the outer tape-spring

spring, resulting in two completely different solutions, as shown in figure D.5b. This second deformation behaviour was never seen in experiments.

Furthermore, it was seen in some simulations, which initially formed two buckled regions close to each other, the two buckled regions merged into one around the rotation point. This transition resulted in a jump in the reaction forces/moments and endpoint displacements.

Discussion

Linear subtended angle profile

The simulations for the inner tape-spring seem to converge easier, so the simulation of the outer tape-spring is limiting to the imperfection that can be added. All three converged simulations of the outer tape-spring converge for the inner tape spring as well: $[130^\circ(20^\circ), 120^\circ(20^\circ), 110^\circ(20^\circ)]$. Since the first geometry $130^\circ(20^\circ)$ has the smallest relative difference in subtended angle, this one is most suitable for further analysis.

The moment-rotation diagram in figures D.3a and D.4a show a second moment peak/plateau for the non-converged simulations. This is behaviour is different from the other simulations. To get an idea of the source of this behaviour, the deformed geometry is studied for the different simulations.

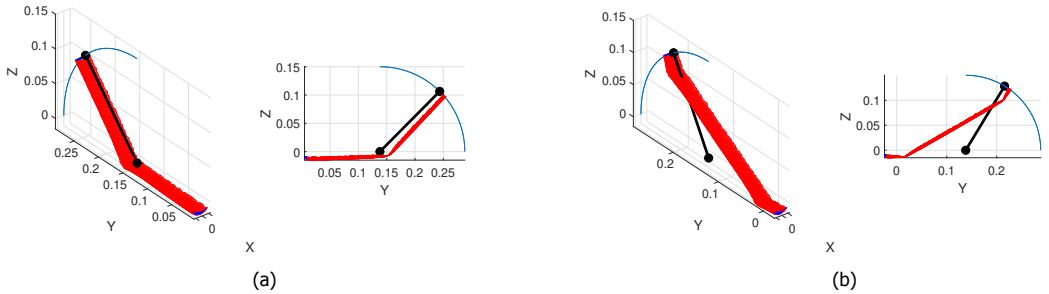

Figure D.5: Two different solutions for the deformed geometry of tape-springs with random noise on the subtended angle profile.

The deformed geometry of a non-converged simulation is shown in figure D.6. For the non-converged simulations, two instead of one buckled region is encountered at equal angles. From the converged simulations, it is seen that initially two small buckled regions join into one region. However, this does not happen for the more straight configurations. The imperfection added in the middle helps in forming this single fold.

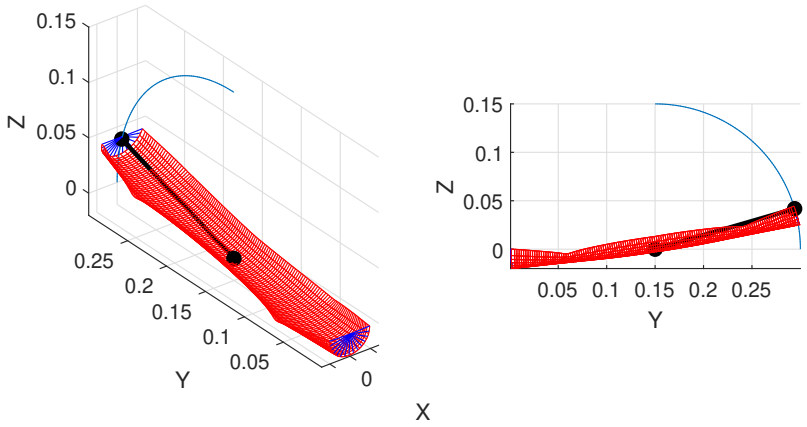

Figure D.6: Deformed geometry of a tape-spring which does not converge.

Besides determining the minimally needed imperfection of the tape-spring for convergence, the simulation data could possibly be used to determine the peak value for a perfectly straight tape-spring. The peak moment in the moment-rotation diagram becomes bigger for smaller imperfections, and extrapolation of the peak values of the converged simulations could be used to get an estimate of the peak value for a perfectly straight tape-spring.

Random noise subtended angle profile

The random noise is a possible source of the unpredictable deformation behaviour of the tape-spring, resulting in either one or two distinct fold regions. It is thought that the random noise can create some local minima throughout the tape spring, which are more likely to buckle. If these buckled regions are far away from each other, this could result in two distinct folds. Because merging these two folds in the middle to reach a lower energy state would mean going through an intermediate higher energy state, this solution is not found in many of the simulations.

Since the outcome of the simulations is highly dominated by the randomness of the noise, this approach is not preferred in the analysis of the folding behaviour of a tape-spring. The geometry with the linear subtended angle profile $130°(20°)$ is preferred.

Conclusion

Two ways of introducing an imperfection to the tape-spring geometry are explored: having a linearly decreasing subtended angle profile and a subtended angle profile with random noise. It was found that the random noise added onto the subtended angle profile resulted in different diverging deformation behaviours, making it unsuitable for determining the tape-spring behaviour. However, the linearly decreasing subtended angle profile with a minimum in the middle of the tape-spring gives consistent results, making it an useful approach to simulate a tape-spring. The smallest relative imperfection that was found to converge both in the inner and the outer tape-spring is 20° on a tape-spring of subtended angle 130°.

D.2. Force-deflection behaviour stack

Introduction

In this section, the different contributions of the layers in a stack are presented and compared to the behaviour of a single, free-sliding tape-spring. The tape-spring configuration and boundary conditions are shown in figure D.7.

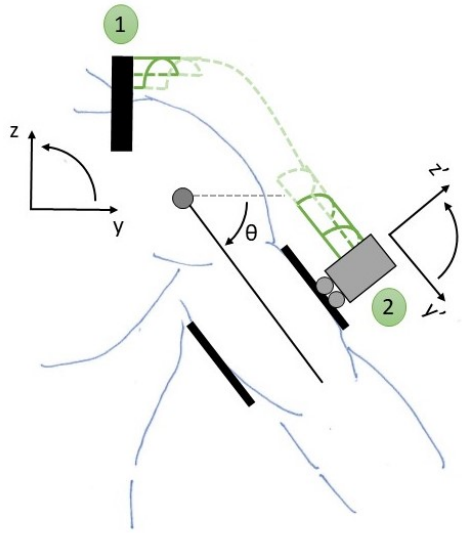

Figure D.7: The tape-spring configuration with its boundary conditions, as derived from a potential upper arm support system. Endpoint 1 is fully constrained, while endpoint 2 is free to slide in the y'-direction.

The tape-spring used in this section has the same geometry as the one considered in chapter 3. The geometric parameters and material properties are shown in Table D.1. The separation distance in the stack of two tape-springs is set to $2mm$.

L [mm]	t [mm]	r [mm]	E [GPa]	ν [-]	ρ [kg/m^3]
260	0.15	19.9	210	0.3	7900

Table D.1: Dimension and material properties of tape spring

Force contributions

The moment around the shoulder joint exerted by the folded tape-spring can be divided into three different contributions of endpoint 2:

1. $M_{x'}$, the moment around x'-axis;
2. $M_{Fy'}$, the moment exerted by the force in y'-direction, acting perpendicular to the arm;
3. $M_{Fz'}$, the moment exerted by the force in z'-direction, acting parallel to the arm at a small offset.

In figure D.8, the different contributions as well as the total moment are shown. The following data is shown:

- Blue, dashed: the behaviour of a single tape-spring, which is free to slide along the arm;
- Blue, solid: The summation of the behaviour of two single tape-springs that are free to slide along the arm;
- Red, dashed: the behaviour of the inner tape-spring of a stack, which is under compression;

- Purple, dashed: the behaviour of the outer tape-spring of a stack, which is under tension;
- Black, solid: The summation of the behaviour of the inner and outer tape-spring.

As shown in chapter 3, the summation of the free-sliding tape-springs is almost equal to the summation of the tape-springs in a stack that are under tension and compression. Furthermore, it can be seen that the moment contribution $M_{x'}$ of the inner tape-spring is negative, while the moment contribution $M_{x'}$ for the outer tape-spring is still positive. This agrees with the findings of Seffen [12], who states that the end couple ($M_{x'}$) of a tape-spring under compression (the inner tape-spring) reverses direction, leading to compression in the free edges of tape near the edge.

The contribution of the force in the y'-direction is zero for the single free-sliding tape-springs, as the tape-spring is free to translate in this direction. For the stacked tape-spring, these forces in the y'-direction are equal but opposite. Therefore, their contributions is very small. The little contribution is due to the extra distance from the outer tape-spring from the arm, resulting in a bigger moment contribution $M_{Fy'}$ from the outer tape-spring.

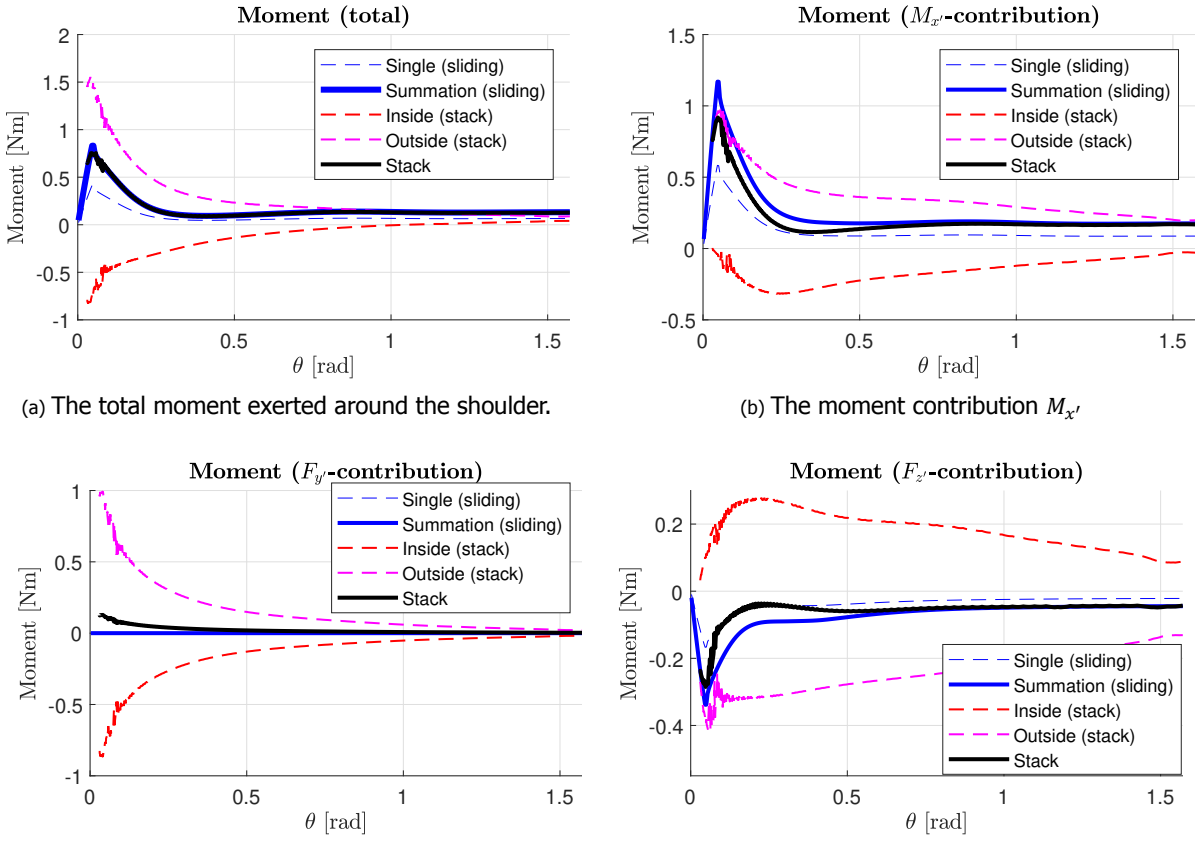

(a) The total moment exerted around the shoulder.

(b) The moment contribution $M_{x'}$

(c) The moment contribution $M_{Fy'}$

(d) The moment contribution $M_{Fz'}$

Figure D.8: The total exerted moment around the shoulder joint, and the different contributions.

E

Experiments

E.1. Production tape-springs

Introduction

This chapter describes the production process of the tape-springs that are studied in this thesis. It was chosen to fabricate the tape-springs out of stainless steel 1.4310, since it does not suffer from creep and stress relaxation under normal conditions. The thickness of the sheet was chosen to be $0.15mm$. The sheet can be cut to the right size quite well. However, it is challenge for a sheet of this material and thickness to shape it to a desired geometry, since it experiences high spring back behaviour. The production process can be divided into two discrete steps:

1. Cutting sheet to size
2. Shaping sheet

These two steps will now be discussed separately.

Cutting to size

The cutting of the material can be done in multiple ways. It can be done by hand using a simple pair of scissors, but to achieve more accurate results, a machine cutting process should be chosen, such as water jetting or laser cutting. Since a laser cutting machine is available at the 3mE workshop of the TU Delft, this process was chosen to cut the material to size. This process is very straight forward, but you should be aware of warping of the material if a batch of closely placed parts are cut at once.

First, the radius was determined of the tape-spring. Using this radius, the required arc length of the tape-spring was determined by multiplying the radius by the required subtended angle. This width should be cut from the sheet. Since in the simulations an imperfection on the subtended angle was introduced, this imperfection was also introduced in the geometry. The geometry is shown in figure E.1.

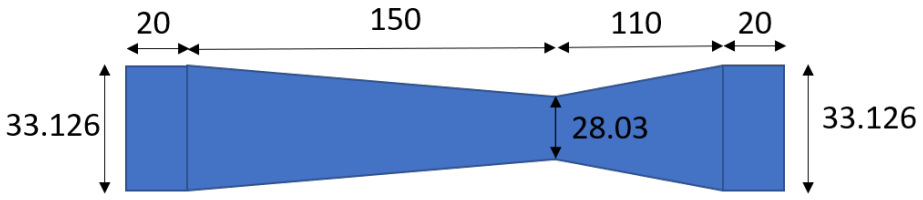

Figure E.1: The geometry lasercut from the sheet material. The dimensions are shown in mm.

The total length of the tape-spring was set to $300mm$. The last $20mm$ on each end of the tape-spring are cut at a constant width, since this part of the tape-spring would be inserted between the two clamps, and therefore the subtended angle does not matter. The moment arm of the measurement

setup was already constructed at a length of $150mm$, so in order to keep the smallest subtended angle at the rotational joint of the measurement setup (the location where the fold region will form), the imperfection is placed with a slight offset of the middle of the tape-spring at $150mm$ of the effective deformed length.

In figure E.2, a photo is shown of the lasercut sheet. The sheet is at this point still flat.

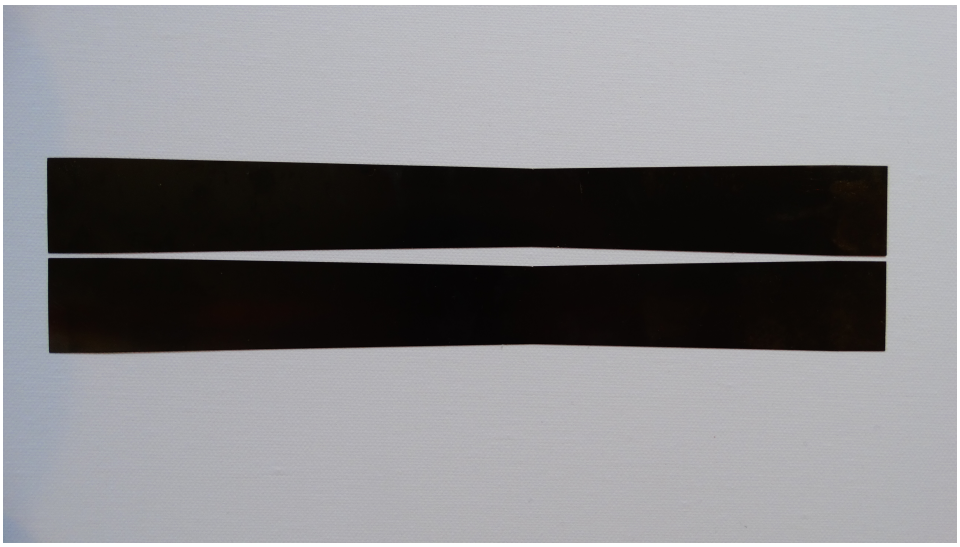

Figure E.2: The sheet as it comes out of the laser cutting machine.

The radius of the tape-spring was determined prior to the lasercutting process. However, the actual value of the radius after shaping the laser cut sheets was different, resulting in a actual subtended angle of $95.1°$ at the outer ends and $80.5°$ at the smallest point of the tape-spring.

Shaping sheet

For a tape-spring the material should be circular shaped along one axis. To bend a sheet, conventionally roll bending would be a useful method. However, due to the high spring back behaviour and the small radius that is required, this approach is not feasible. As an alternative, a rolamite is used to bend the material. A photo of the rolamite is shown in figure E.3.

The rolamite consists of one big roller and one small roller, held together with two sheets of stainless steel 1.4310 of $0.1mm$ thickness. The top and bottom plate are rigidly connected to each other. The small roller has a diameter of $10mm$. The flat tape-spring material is placed between the two sheets, parallel to the small roller, after which the rolamite is actuated by hand to move through the assembly. The tape-spring material is clamped between the two sheets, and is therefore forced around the small roller. As a result a constant curvature along the longitudinal axis is formed. The resulting radius with the roller of $10mm$ diameter is $19.9mm$.

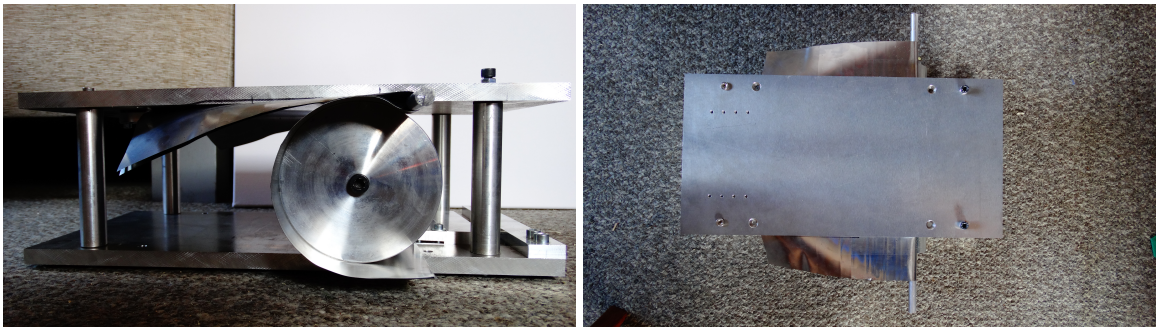

(a) Front view of the rolamite

(b) Top view of the rolamite

Figure E.3: Rolamite setup used for shaping the material.

As can be seen in figure E.3b, the width of the top and bottom plate is limited, and the rollers as well as the sheet materials stick out on both sides. The width of the top and bottom plate is $200mm$, the width of the big roller is $250mm$, the width of the sheet is $305mm$, and the width of the small roller is $380mm$. Not all the parts of the rolamite parts are wide enough to roll the tape-spring of $300mm$. This resulted in a small imperfection in the radius of the tape-spring. A little distortion could be felt at the location on the tape-spring that was aligned with the edge of the bottom and top plate. This is not considered a problem, because the ends of a tape-spring will not deform significantly during buckling.

The advantage of the used rolamite setup over a conventional roll bending machine is that the small roller, around which the material is deformed, is supported throughout its length instead of only at the ends. As a result, this roller can be made very small, while still capable of deforming the sheets without bending of the roller itself.

In figure E.4, two pictures are shown of a tape measure before and after it is rolled in the rolamite. An imprint of the cross-section in floral foam is shown in figure E.5. It can be seen that the cross-section before it is rolled is far from circular. The sides of the tape-spring are straight, while the middle has a curvature. However, after rolling, the cross-section has a constant curvature throughout the length of the tape-spring. The effect of this change in geometry is shown in appendix E.4. How the curvature can be determined is further explained in appendix E.2.

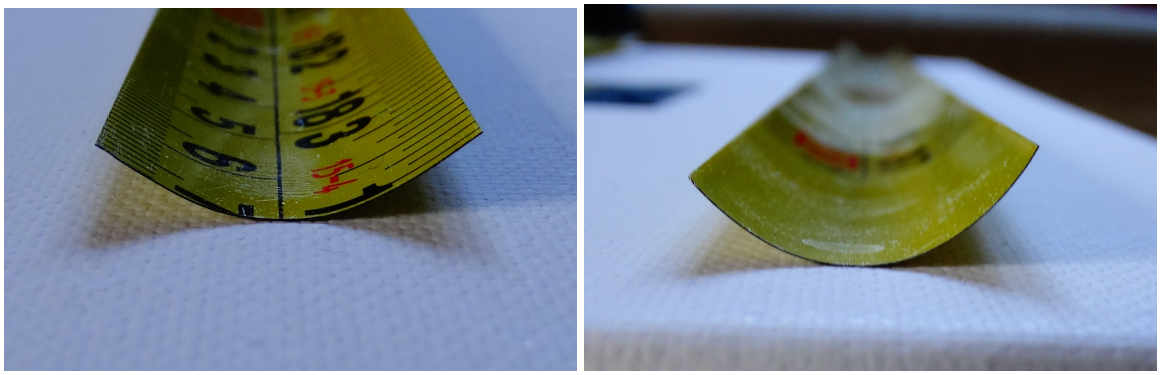

(a) Cross-section of an unrolled tape-measure.

(b) Cross-section of an rolled tape-measure.

Figure E.4: The resulting deformation of a rolled tape-measure.

Figure E.5: Cross-section imprint in floral foam of the tape-measure after rolling (left) and before rolling (right) in the rolamite.

E.2. Cross-section measuring

Introduction

The cross-section of the tape-spring has to be determined after it is rolled into shape. The approach that is taken to determine the curvature of the tape-spring is similar to the approach of De Jong [7] for determining the fold radius of a tape-spring. A photo of the imprint of a tape-spring in floral foam is analyzed using Matlab.

Process

The process can be divided in the following five steps:

1. Take a picture of the imprint cross-section of tape-spring in floral foam
2. Measure the width of the imprint
3. Perform the following image processing steps on the photo so only the imprint pixels remain:
   - Convert image to binary image (black and white), based on a threshold value (*im2bw*-function)
   - 2-D Gaussian filtering or blurring of image (*imgaussfilt*-function)
   - Remove small objects from binary image (*bwareaopen*-function)
   - Fill missed image regions and holes (*imfill*-function)
4. Fit circle on pixels
5. Scale circle to actual size, using the measured width of the imprint

Results

In figure E.6 the original photo taken of the floral foam after imprinting the cross-section is shown, as well as the processed photo with the fitted circle on it.

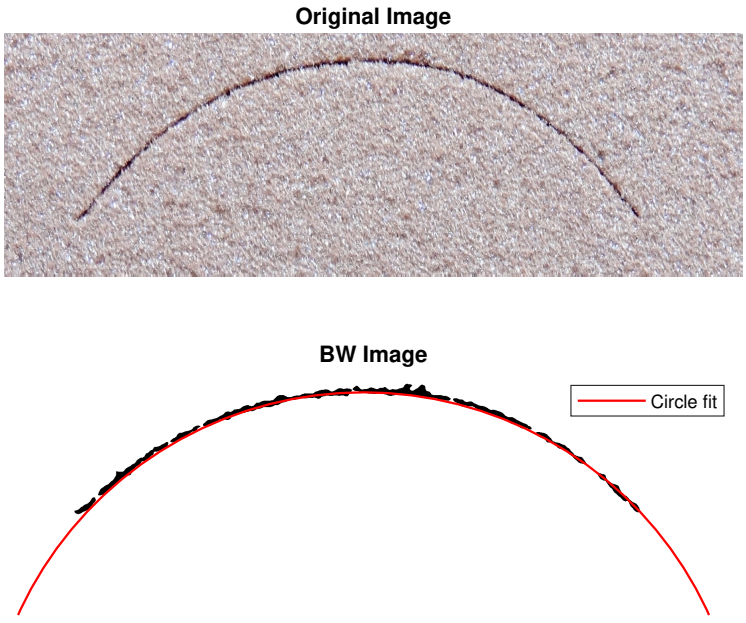

Figure E.6: The original photo of the imprint (top) and the black and white image after processing (bottom) are shown. In the bottom figure, the red line is a circle which is fitted to the imprint.

E.3. Measurement setup

Design

To measure the folding behaviour, a setup is needed to fold the tape-spring in a quasi-static manner, while measuring the required force for this deformation. A schematic drawing of the setup is shown in figure E.7a. The setup consist of one arm ('moment arm') on which a moment is exerted. At the end of this arm, the tape-spring is fixed (no rotation or translations allowed). The other end of the tape spring is attached to a slider, allowing for longitudinal translation of the tape spring during folding. A 3D CAD-design can be seen in figure E.7b. Both the slider and moment arm are attached to a base plate. For the moment arm, an extra bracket is introduced, to improve the stiffness of the axis.

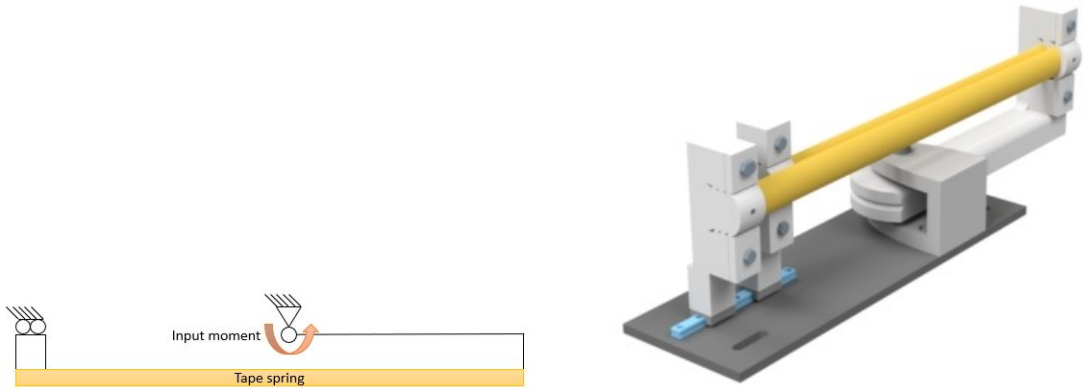

(a) Schematic drawing of measurement setup

(b) Design measurement setup

Figure E.7: Measurement setup

A more detailed view of the setup is shown in figure E.8. In this view, all the elements are included and indicated. The input of the system is a displacement of the Almotion linear actuator, using the Q Programmer control software. On this linear actuator, both a optoNCDT laser distance sensor and a Futek load cell is mounted. The laser distance sensor measures the distance the linear actuator moves backward, while the load cell is measuring the force in the wire. This wire is rotated around the axis of the mounting arm, at a distance of 0.030 m. This distance can be used to get from the measured force to the input moment on the moment arm (input moment = measured force x 0.030), as well as for determining the rotation of the mounting arm from the displacement measured by the laser distance sensor (rotation = measured displacement / 0.030).

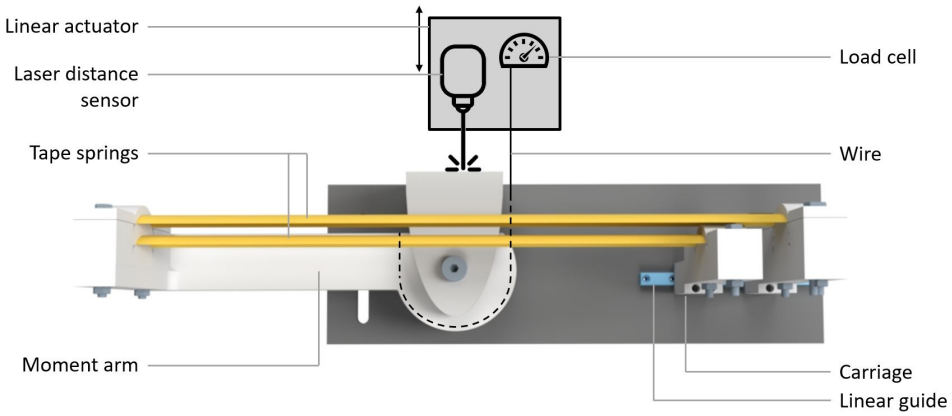

Figure E.8: Measurement setup - Top view

A short overview of the specifications of the different parts of the measurement setup is given below:

- Linear actuator: Altmotion LT50-TR-G8-200, with a maximum range of 200 mm and a loadbearing capability in the actuated direction of $1000N$;
- Laser distance sensor: Micro-Epsilon optoNCDT ILD1420-200, with a measuring range of 200 mm (from 60 mm to 260 mm), a linearity error of $\leq 0.08 - 0.1\%FSO$ (Full scale output) and a reproducability error of $8\mu m$;
- Load cell: Futek LSB200, with a maximum, measurable load of $45N$;
- Wire: Strategy stamina, braided fishing wire (25 lbs).
- Linear guide: THK LM guide model RSR-7Z, with a sliding range of ca. $90mm$

For the load cell, a Scaime CPJ Rail strain gauge conditioner is used as analog signal conditioner. Furthermore, for data acquisition a NI USB-6002 is used, together with a LabVIEW environment on the computer.

Construction

The moment arm and tape spring clamps at the linear carriages are 3d printed, by SLS of solid Nylon (PA12), ordered at RapidPrototyping.nl. The baseplate is lasercut at the faculty of 3mE at TU Delft from a white acrylic plate with a thickness of 6 mm. The bracket at the moment axis is 3d printed with an Ultimaker 3d printer at the faculty of 3mE of TU Delft as well, using transparant PLA with an infill of 20%. Two EZO F608H ZZ ball bearings with flange are pressed in the moment arm, one on top and one on the bottom. A M6 shoulder bolt with 8 mm shaft, tolerance e9, made from EN 1.7220 Equiv. alloy steel with an hardness of 33~38HRC, ordered at Misumi, is used as an axis in the moment arm.

Error analysis

Possible sources of error in the measurement setup are:

- sliding friction slider carriage
- strain in cable
- misalignment force sensor and force direction (both height and width)
- uncertainty radius of pulley
- play in carriage in z-direction
- slip in attachment point wire to moment arm
- geometric imperfections tape-measure
- Not perfect fit of clamp to tape-measure
- friction/backlash bearing

E.4. Measurements

In figure E.9 the difference can be seen of the force deflection behaviour of the buckling of a measurement tape before rolling it in the rolamite (green) and after rolling it in the rolamite (red).

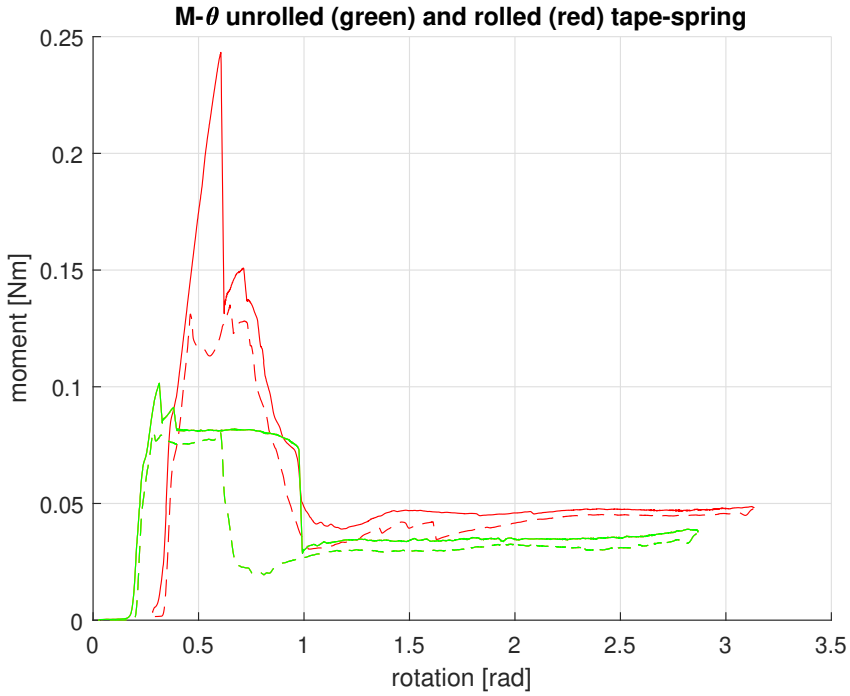

Figure E.9: M-θ curve unrolled non-circular tape-spring (green) and rolled circular tape-spring (red)

As can be seen, the peak value for the rolled tape-spring is much higher than for the unrolled tape-spring. This has probably to do with the initially straight sides of the tape-spring, that do not store any strain energy during folding. The flattening in the fold region stores the most elastic energy, but since the outer sides of the tape-spring already are flat, no deformation energy is stored in this part for the unrolled non-circular tape-spring. That is a possible explanation for the change in buckling stiffness.

Besides the higher peak value, the hysteresis is also decreased after rolling. This is apparently also an effect of the non-circular cross-section.